UTILISING THE CO-ANALYSIS OF EDM AND GPS DATA IN MODELLING SURFACE DEFORMATION AT THE SOUFRIÈRE HILLS VOLCANO, MONTSERRAT.

Submitted by Alexander Johnson to the University of Exeter

as a thesis for the degree of

Master of Science by Research in Geology

In September 2021

I certify that all material in this thesis which is not my own work has been identified and that no material has previously been submitted and approved for the award of a degree by this or any other University.

Signature: 

ABSTRACT

Greater understanding of volcanoes through monitoring and modelling of magmatic processes can help protect lives, communities, and economies at risk from volcanic activity. Ground deformation offers vital insight into the activity of volcanoes and associated magmatic systems, and can be monitored via geodetic methods. Each geodetic method has limitations, thus utilising multiple techniques provides better coverage of a volcano, but requires an understanding of how different methods respond to different changes in the magmatic system. This thesis investigates how EDM and GPS can be used in tandem to distinguish between shallow and mid-crustal magmatic processes. I focus on the Soufrière Hills Volcano (SHV), using ground deformation data collected by the Montserrat Volcano Observatory from 2010-2019. The SHV has been in an extended intra-eruptive pause since 2010, following 15 years of discontinuous effusive activity, and has a well-developed GPS and EDM monitoring network. I investigate how the two networks record ground deformation at the SHV, which parts of the magmatic system they respond to, and what they can tell us in tandem about the current status of the magmatic system. I also relate these investigations to the unusual behaviour of the GPS site HERM, relative to the rest of the GPS network. This study finds that the EDM network responds predominantly to changes in the shallow magmatic system, while the GPS network primarily responds to changes in the mid-crustal system. EDM line length change is mostly dictated by the relative horizontal movement of the reflector and base station; relative vertical displacement is less significant. I find that the behaviour of the EDM network from 2010-2019 can be explained by negative pressurisation in a shallow dyke conduit orientated NNW-SSE, while the deeper system is still undergoing pressurisation. The behaviour of HERM is also partially tied to the behaviour of the shallow system. Ultimately, monitoring multiple flanks of the volcano close to the vent is vital for both monitoring and modelling the shallow aspects of volcanic systems.

ACKNOWLEDGEMENTS

I start by thanking my primary supervisor, James Hickey, for his constant guidance and support throughout the Masters by Research Project; his supervision carried me through difficult moments of the project, especially with the impact of the Coronavirus pandemic. I am also grateful to Karen Pascal and the team at the Montserrat Volcano Observatory, for their information about the idiosyncrasies of the Soufrière Hills Volcano and its monitoring network, and for the comprehensive dataset of EDM and GPS data that made this project possible. I also thank them for providing the opportunity to travel to Montserrat and for their offered funding, even though this sadly fell through due to the pandemic. I also thank my third supervisor Ben Williamson for his supervision and support through the project.

I would like to thank the wider CSM community at the University of Exeter, especially the Postgraduate Researchers who created a welcoming environment in the first 6 months of my project, and somehow kept it going during the next 18 months of lockdowns and working from home. Special thanks for the research team I am lucky to be part of, comprising of Matthew Head, Rami Alshembari, and Rob Backhurst alongside James Hickey and Ben Williamson. I also wish to thank Chloe Young and Kieran Doyle, who as fellow PGR Course Representatives set up and ran the CSM Virtual Coffee mornings with me, which provided a much-needed tether to the wider PGR community during the pandemic.

Thanks must also go to my family, who were always on the end of the phone in difficult moments. Finally, I need to thank my wonderful partner Amy Bramble, for her constant support and unbreakable uplifting spirit.

TABLE OF CONTENTS

LIST OF FIGURES

-

LIST OF TABLES

-

Chapter 1

INTRODUCTION

-

1.1 Background

One of the main aims of volcanology is to continuously improve the forecasting of volcanic activity in order to inform decisions on protecting the people who live and work, and developing infrastructures, in the vicinity of dangerous volcanoes. Civil authorities and local communities ideally need to know when and where eruptions will occur, as well as the severity, nature, and length of eruptions, in order to effectively manage the potential hazard (Sparks, 2003). However, identification of precursory activity and eruption forecasting are still insufficient to reliably predict dangerous surface activity, making communication of volcanic hazards to communities at risk difficult (Segall, 2013).

Most volcanoes that pose significant risk to lives and livelihoods are continuously monitored by volcano observatories, who use a variety of methods to monitor the activity of volcanoes; including Electronic Distance Measurement (EDM), Global Positioning System (GPS), tiltmeters, Interferometric Synthetic Aperture Radar (InSAR), and strainmeters to measure deformation signals. Seismometers measure the seismic signals from fluid magma movement beneath the crust, as well as brittle fracturing of the surrounding rocks. Gas monitoring measures the volume and composition of gas emissions from the volcano, and fumarole temperatures are also monitored.

Volcanic deformation is primarily the surface inflation or deflation of a volcanic edifice and surroundings, caused by the movement of magma beneath the surface (Segall, 2013). Deformation sources can also include brittle crack extensions and hydrothermal sources. Changes in deformation signals may indicate volcanic unrest, a deviation from the background activity of a volcano towards a level of cause for concern (Dzurisin, 2007). When used in

combination with other monitoring methods, deformation measurements can provide essential insight into the status of active volcanoes (Sparks, 2003). Volcano deformation can be caused by magmatic sources such as overpressurization of a magma chamber, or magma movement such as sheet intrusions (Dzurisin, 2007). Deformation can also be caused by non-magmatic pressure sources such as hydrothermal systems (Fournier and Chardot, 2012), the loading of deposits on the volcanic edifice (Odbert *et al.*, 2015), flank collapse/instability (Bonaccorso *et al*., 2013), or the cooling of magma (Parker *et al.,* 2014). Magmatic causes of surface deformation are indications of active magmatism below the surface, and studies of the magnitude and pattern of surface deformation can allow the inference of subsurface magma system processes (Dzurisin, 2007). Exactly how the magmatic processes affect surface deformation can be examined via the use of computational models, which require assumptions and simplifications to be made about magma behaviour and crustal mechanics, but can be a useful tool in understanding subsurface processes.

1.1.1. Volcano-deformation monitoring

Deformation signals are monitored using a variety of methods, including Electronic Distance Measurement (EDM), Global Positioning System (GPS), tiltmeters, Interferometric Synthetic Aperture Radar (InSAR), gravity monitoring, and strainmeters.

EDM is the method of measuring the length of a baseline between two fixed points on the edifice (Odbert et al, 2014a). A reflector is installed at one end, and a fixed base station at the other. A total station is used to fire a laser at the reflector, and measures the two-way travel time to calculate the distance. The distance will change over time as the edifice deforms, and this can be used to infer subsurface behaviour (Ramírez-Ruiz et al, 2002). This technique requires a clear line of sight from base station to reflector, which can be affected by topography or vegetation. Base stations are installed on concrete columns, baseplates, or steel plates, ideally at a safe distance from the volcanic vent, while reflectors are installed by drilling into stable rock or lava flows (Battalglia et al, 2019). EDM monitoring is a cheaper method of monitoring ground

deformation than most other methods, and a single total station can be used to measure multiple EDM lines. Depending on the volcano, EDM monitoring can be a safer technique than most, as the installation and maintenance of reflectors close to the vent is a much quicker process than with GPS stations. However, unlike GPS monitoring, data collection has to be undertaken in the field.

GPS is a worldwide navigational and surveying tool that uses satellites to locate a point. GPS stations are installed in secure bedrock on the volcanic edifice, and record X, Y and Z coordinates (Odbert et al, 2014a). Continuous GPS monitoring uses permanent GPS stations installed in stable bedrock, which broadcast data back to the monitoring observatory. Campaign GPS sites are baseplates upon which a tripod is set up, and data collection can only be undertaken in the field. GPS monitoring, especially continuous GPS monitoring, is expensive, and the deformation data is spatially limited compared to InSAR. However, unlike InSAR, GPS is not affected by atmospheric factors. GPS is also not reliant on line of sight, giving it an advantage over EDM. With the exception of campaign GPS, and the installation and maintenance of continuous GPS sites, no fieldwork is required (Battalglia et al, 2019).

Tiltmeters measure angular movement by two different methods, borehole bi-axial electronic sensors, and long-base devices. Borehole tiltmeters use electrolytic bubble sensors, while long-base devices use fluid filled tubes whereby the tilt is calculated by measuring the fluid levels at each end of the tube (Gambino et al, 2014). InSAR measures land surface altitude by reflecting radar signals off the edifice and measuring the two-way travel time back to the satellite (Amelung et al, 1999). Strainmeters measure the deformation in a borehole to record the near-surface strain (Linde and Sacks, 1995).

1.1.2. Volcano-deformation modelling

Deformation modelling is the application of analytical or numerical methods to simulate the volcanic processes (such as dyke opening/closing, or pressurisation of a magma reservoir) occurring at depth, on the assumption that the effect of these processes are transmitted through the crust producing surface deformation (Dzurisin, 2003).

Analytical volcanic deformation modelling has been used since the publication of the spherical-sourced Mogi model in 1958 (Mogi, 1958), and provides a rapid and simple way of modelling volcanic inflation or deflation. Analytical models simplify the equations of elasticity, by satisfying a significant set of assumptions: the crustal rheology is usually defined as a homogenous isotropic, elastic half space with a flat, free surface, and the source shapes are often simple. Later analytical models incorporate source shape variation, such as rectangular dyke sources (Okada, 1985), sill-like sources modelled as horizontal circular crack (Fialko et al, 2001), and prolate spheroids (Battaglia et al, 2013). Viscoelastic behaviour is also incorporated, either through a viscoelastic half-space (Bonafede et al, 1986) or a viscoelastic shell surrounding the magma chamber (Del Negro et al, 2009; Bonafede and Ferrari, 2009; Delgado et al, 2018; Galgana et al, 2014; Newman et al, 2001; Segall, 2019). However, the predictive abilities of these models are limited by their simplifications and assumptions. For example, the Mogi model assumes an infinitely small 'point' source in a homogenous rheology and a flat surface (Dzurisin, 2007). The source radius-to-depth ratio is also a key limit on the Mogi model, with an operational limit source radius-to-depth ratio of < 0.37 found for the Mogi model (Taylor et al, 2021). It also fails to take into account the effect of topography (Cayol and Cornet, 1998), which interacts with the vertical deformation profile of sources to produce local variations in recorded deformation (Johnson et al, 2019). Including topography in models is therefore essential for the proper modelling of volcanic sources, and is especially important when modelling EDM in order to recreate proper line-of-sight measurements on the edifice.

Later analytical models work around some of these limitations, such as the McTigue model (McTigue, 1987), which updates the Mogi model to model a finite sphere, rather than a point source, to remove source radius to depth ratio limitations. Basic topography can also be included (Williams and Wadge, 2000), but these analytical approaches are somewhat inflexible. Analytical models remain extremely useful in situations where computing capacities are limited and where speed is of the essence, such as the monitoring of a new or rapidly evolving deformation problem, or as a quick first order benchmark for more detailed models (Hickey and Gottsmann, 2014). Simple analytical models can also provide with a calibration of more complex FE models when modelling

scenarios within their limits, and where the deformation response is broadly symmetrical. Analytical models are also still the preferred option for situations where the additional complexity offered by FE models cannot be justified, such as scenarios with limited data availability.

Advanced numerical modelling removes some of the disadvantages of analytical models by removing or relaxing some of the assumptions they require. One such numerical modelling method is Finite Element Modelling (FEM), the utility and accessibility of which has improved rapidly in recent years with increases in computer power (Hickey and Gottsmann, 2014). FEM has the ability to solve for factors such as irregular source geometries (Hickey et al, 2015b; Albino et al, 2017), complex topography (Trasatti et al, 2003; Johnson et al, 2019), and heterogeneous rheologies (Geyer and Gottsmann, 2010; Hickey et al, 2017). Justification for such additional complexity is afforded through a variety of advances in the understanding of volcanic systems. For example, FE models are able to simulate pressurised magma chambers embedded within heterogeneous domains containing a range of material properties (Masterlark et al, 2012) that better reflects the complex subsurface factors observed around active magmatic systems. These factors include magma migration; areas of brittle or ductile rheology and associated temperature variation, and variations in melt fractions (Magee et al, 2018). Petrological inferences into the behaviour of magmatic systems also show a complex history of magma crystallisation, and by proxy physical behaviour, during ascent (Cimarelli et al, 2011). FE modelling allows for the incorporation of these complex behaviours where they are thought to have a significant impact on the observed deformation, and especially when multiple complex factors interact, such as incorporating complex topography, multiple sources of varying geometries to model complex reservoir geometries, and a heterogeneous medium, in a high heat flow setting where viscoelasticity is appropriate. Simplifications and assumptions still underpin numerical modelling approaches, with approximations of environmental conditions for media and pressure sources commonly used (Kavanagh et al, 2018). Analytical modelling can approximate each individual characteristic, and possibly stretch to some simple combinations (e.g. Mogi source with viscoelastic shell and simplified topography), but cannot replicate the layering of multiple complex factors that FEM offers.

1.1.3. Soufriere Hills Volcano, Montserrat

Since 2010, the Soufrière Hills Volcano (SHV) has been in an elongated intra-eruptive pause state of an anomalously lengthy eruption, which has been ongoing since 1995 (Odbert et al, 2014a; Sheldrake et al, 2017). A number of volcanic deformation modelling studies have focused on constraining the parameters of the magmatic plumbing system controlling the eruption of the volcano, using both analytical and numerical models (Voight et al, 1997; Voight et al, 1999; Shepherd et al, 1998; Melnik & Sparks, 2002; Wadge et al, 2006; Voight et al, 2010a; Loughlin et al, 2006; Mattioli et al, 1998; Costa et al, 2007; Hautmann et al, 2009; Linde et al, 2010; Young and Gottsmann, 2015; Widiwijayanti et al, 2005; Elsworth et al, 2008; Foroozan et al, 2010; Hautmann et al, 2010; Hautmann et al, 2013; Gottsmann et al, 2020).

1.2 Motivation and Aims

The majority of studies undertaken for the SHV use GPS or strain deformation data from 1995-2010, usually focusing on short to medium term deformation patterns. GPS-led studies usually focus on deformation patterns over the course of eruptive phases which last one or two years, while strain data studies focus on short-term deformation patterns of minutes or even seconds. The GPS network on the island is extensive, but efforts to monitor deformation using GPS stations close to the vent have proven difficult, with destruction of equipment due to volcanic activity common (Odbert et al, 2014a), and in general difficult access for the maintenance of the sites. Currently, the only GPS station incorporated into the daily monitoring within 1.5 km of the vent is HERM, which displays unusual deformation behaviour when compared with the rest of the GPS network. As a result, previous GPS-led studies may be inhibited by the limitations of the spatial distribution of the GPS network, especially with inferences about the shallow part of the magmatic system due to the lack of GPS stations in close proximity to the vent.

In contrast, this study combines for the first time the recent 2010-2019 dataset of both GPS and EDM data to examine long-term patterns of deformation at SHV. The EDM network includes 6 reflectors which are, relative to the GPS network, much closer to the vent and therefore theoretically better placed to

respond to the shallow magmatic system. This makes the SHV deformation network ideal for interrogating the hypothesis that GPS and EDM record the same deformation source differently, and that by utilising both in co-analysis we can model in greater detail the behaviour of the magmatic system. We therefore aim to explore the differences in how GPS and EDM record deformation, both generally and at SHV, before utilising the co-analysis of these two monitoring techniques to investigate the geometry and behaviour of magmatic system, including the shallow part(s) of the system. By using the 2010-2019 dataset, we also interrogate the hypothesis that the SHV is currently building to another eruptive phase.

1.3 Thesis Structure

This thesis begins with a brief introduction to the background of numerical and analytical modelling used in the study of volcanic deformation, as well as an overview of the history of the Soufrière Hills Volcano and its monitoring network. Chapter 2 is a literature review of work relating to volcanic deformation, volcanic deformation modelling, and the SHV. Chapter 3 is a preliminary study into the effect of surface deformation on combined EDM and GPS measurements in a simple 2D axisymmetric model, and provides a basic framework upon which Chapter 4 can build from. Chapter 4 comprises the bulk of the original project research, presented in a research paper format. This paper examines in detail how GPS and EDM can be used to distinguish between deep source and shallow system processes at the SHV by utilising Finite Element Modelling, with implications for the future interpretation of deformation monitoring data at the SHV, a potential explanation for the deformation behaviour of GPS site HERM, and an investigation of how the MVO EDM network could be developed.. A set of conclusions and take home messages is presented in Chapter 5, and supplementary materials for Chapter 4 are provided in Appendices.

Chapter 2

VOLCANO DEFORMATION MODELLING AND THE SOUFRIÈRE HILLS VOLCANO

-

This literature review will cover the background of volcano deformation modelling, exploring both analytical and numerical modelling techniques. Next, the review will cover the background of the SHV, exploring its historical evolution before examining the 1995-2021 eruption period in detail. These aspects are then brought together in a review of modelling studies into the SHV.

2.1 Volcanic Deformation Modelling

Modelling volcanic deformation encompasses a range of techniques from simple analytical models to utilising multi-physics simulation software for finite element modelling. While the modern approaches are vastly more advanced due to the improvements in computational ability, there are still limitations around the non-uniqueness of results. Deformation modelling aims to replicate observed deformation data in order to better understand subsurface processes and aid with prediction of eruptive episodes. With the development of space-geodesy in the 20th century, GPS and InSAR data have become routinely used in modelling, with strain, tilt, and EDM data also being used.

2.1.1 Analytical Models

Analytical models are mathematical models with a closed form solution. In the context of volcano deformation modelling, this means results are obtained from sets of equations representing simplified source and medium properties (Pascal, 2013).

Widely regarded as the genesis of analytical volcano deformation modelling, the Mogi model was developed in 1958 (Mogi, 1958; Lisowski, 2007), and is still widely used to model surface deformation of volcanoes induced by a spherical magma chamber. The assumptions in the Mogi model include:

- The medium is an elastic, isotropic, homogenous
- The surface is assumed flat or negligible.
- The depth of the source must be at least 5 times greater than the radius of the source.
- The source shape is spherical.
- The fluid (magma or gas) causing the change in stress in considered incompressible

The fact that the Mogi model is still in common usage shows that as an approximate indicator of magma chamber depth and/or pressure it remains a useful tool in deformation modelling (Hickey and Gottsmann, 2014; Taylor et al, 2021).

While later analytical models began to increase in complexity (while remaining relatively simple) in terms of source geometries and/or medium and magma properties, analytical models of surface deformation now include diverse source geometries, such as rectangular dyke sources (Okada, 1985), sill-like sources modelled as a horizontal circular crack (Fialko et al, 2001), and prolate spheroids representing magma chambers (Yang et al, 1988; Battaglia et al, 2013). However, these analytical representations are mostly still simple source shapes, and more complex geometries are not always possible to be modelled by analytical approaches.

Other analytical models can include simplified 2D topographical effects (Williams and Wadge, 2000), but most analytical models do not account for topography, which can have a significant impact on deformation behaviour (Trasatti et al, 2003; Johnson et al, 2019) and is important for accurately representing monitoring techniques such as EDM (Hickey, 2015b).

While early volcanic deformation models all use homogenous media required by their analytical formulation, the approach is largely unreflective of how rocks

exist at depth (Ranalli and Rybach, 2005). Homogenous model domains can underestimate both the depth of pressure sources, and the overpressure required to produce the measured deformation (Foroozan et al, 2010). Other studies have found that heterogeneous models usually have lower overpressure requirements (Hickey et al, 2013; Manconi et al, 2007; Geyer and Gottsmann, 2010; Hautmann et al, 2010).

Most analytical models of deformation available consider the crust has an elastic behaviour, which, using Hooke's Law, states that any stress produces an instantaneous strain. Consequently, this means surface deformation is instantaneously produced from source pressurisation. However, rocks are believed to only behave elastically at depths shallower than the brittle-ductile transition zone, which is closer to the surface in the areas of high heat flow associated with volcanic activity (Ranalli, 1995). Purely elastic models also often require unrealistic pressures which exceed the tensile strength of crustal rocks (Gudmundsson, 2006; Hickey and Gottsmann, 2014). As a result, purely elastic rheologies are not always accurate representations of the behaviour of rocks in volcanic regions, and sometimes more complex rheological representations such as viscoelasticity produce more realistic results. Various mathematical models for viscoelastic rheologies are used, all allowing for a viscous creep following instantaneous elastic deformation (Christensen, 1982; Crawford, 1998). There are three commonly used models of viscoelastic behaviour: the Maxwell model, the Kelvin-Voigt model, and the Standard Linear model (Head et al, 2019). Each model of viscoelastic deformation produces a slightly different deformation response (Christensen, 1982; Crawford, 1998). The Maxwell model can produce unrealistic deformation patterns as the deformation increases linearly with time, without limit, under the application of constant stress. It also produces unrealistic recovery behaviour, as it can remain in a permanently deformed state once the initial stress is removed (Head et al, 2019). Analytical models, which incorporate viscoelastic behaviours (Bonafede et al, 1986; Dragoni and Magnanensi, 1989; Bonafede and Ferrari, 2009; Del Negro et al, 2009), are usually restricted to simplified source geometries. Homogenous viscoelastic models, such as Bonafede et al (1986), fail to account for the effects of varying temperature on the viscoelastic behaviour of rocks. A means of incorporating nonhomogeneous viscoelastic

behaviour is the use of viscoelastic shells (Bonafede and Ferrari, 2009), whereby viscoelastic properties are only assigned to a small spherical volume surrounding the deformation source, which is embedded in an elastic medium. This is designed to simulate the temperature halo surrounding magma bodies, which changes the Young's Modulus and resultant stress/strain behaviour of surrounding rocks.

2.1.2 Numerical Models

Numerical models are an interpretation of a real world system via the combination of a large number of mathematical equations which are analysed by a computer. Numerical modelling has become an increasingly common method of modelling volcanic deformation as computing power becomes more readily accessible. While they are not as quick as analytical models, numerical models are often more realistic and allow for the simultaneous integration of multiple physical processes (Pascal, 2013).

One method of incorporating heterogeneous media into numerical models is to create a layered anisotropic medium with varying elastic moduli, based on density variations derived from seismic P-wave velocities (Foroozan et al, 2010). The Young's Modulus of material properties can also be varied to reflect the degree of fracturing in the area (Gudmundsson, 2011). A numerical modelling approach allows for more complex heterogeneity, with localised fracturing, faulting, and interactions with caldera/edifice structure and their effects on the deformation response taken into account (Di Natale et al, 1997; Folch and Gottsmann, 2006; Geyer and Martí, 2009; Bonaccorso et al., 2013; Holden et al., 2017; Zhan et al., 2019).

Spatially varying, temperature dependency can also be derived from a variable Young's modulus. A 1D-temperature distribution vertical profile is used, assuming a heterogeneous geothermal gradient, using seismic data (Foroozan et al, 2010; Hickey and Gottsmann, 2016; Tammaro et al, 2021). A combined effect of the background geotherm interacting with the local heating effects of the magma source can be calculated and fed into the viscoelastic model, as well as introducing time-dependent behaviours.

Numerical models are not without their limitations. Computing power restricts mesh density, especially in 3D modelling, which can introduce numerical errors and limit the accuracy of model outputs. If initial conditions or boundary conditions are poorly formulated, or inherent assumptions in the numerical equations used to simulate physical behaviours are incorrect, then these errors will affect the model output (Carmo, 2020).

2.2 The Eruptive History of the Soufrière Hills Volcano

The earliest inferred eruption of the SHV is recorded in radiocarbon dating as ~450 ka (Hatter et al, 2018), with evidence for other historical eruptive events in 8050 BCE ±2000, 4050 BCE, 2460 BCE ±70, 1180, 1480 ±50, and 1550 ±50 (Le Friant et al., 2008; Smith et al., 2007). Non-eruptive volcanoseismic swarms have been detected on an approximately 30-year timescale (Elsworth et al, 2008; Odbert et al, 2014b), with volcanoseismic crises in the 1890s, 1930s, and 1960s interpreted as aborted eruptions before one developed into a full eruption in 1995. The most recent period of activity stretches from 1995 to present (Roobol and Smith, 1998), and includes eruptive phases in 1995, 1999, 2004, 2008, and 2009 (Odbert et al, 2014a).

Contemporary eruptive activity began in July 1995 with phreatic eruptions followed by effusive activity and lava dome growth in November 1995 (Wadge et al, 2014). The subsequent collapse of lava dome structures lead to large-scale pyroclastic flows, the main volcanic hazard on Montserrat (Young et at, 1998) alongside lahars. Pyroclastic flows affected much of the southern half of the island, triggering the mass evacuation of the area; in 1997, the capital city of Plymouth was hit by a pyroclastic flow (Cole et al, 1998) and later buried. The eruptive activity at the SHV has been discontinuous since 1995, broken up into a series of extrusive ‘phases’ and inter-eruptive ‘pauses’ in extrusion (Odbert et al, 2014a). In total, there have been 5 eruptive phases with the most recent being in 2010 (Figure 2.1). The initial eruption from 1995 to 1998 was characterised by lava extrusion, cyclical dome growth and collapse and subsequent triggering of pyroclastic flows, alongside repeated Vulcanian eruptions and lahars (Wadge et al, 2014). Phase 2 began with the resumption

of lava extrusion in November 1999 and marked the start of near-constant volcanic activity until 2003. Three large dome-collapse events occurred in Phase 2, alongside sub-daily cyclic behaviours of magma and gas flux (Young et al, 2003). Phase 3 stretched from 2005-2007, and began with new lava dome growth on August 1st (Loughlin et al, 2010). Dome growth was slower than previous eruptive phases initially, but the extrusion rate increased rapidly by late December 2005 (Ryan et al, 2010). This phase involved significant intra-crater fracturing and associated ash and steam emissions from the northern vent, and by mid-February lava extrusion was occurring at a rate of >6 m^3/s, well above average (Loughlin et al, 2010), eventually leading to a single major dome collapse and pyroclastic flows, although smaller pyroclastic flows did occur throughout. Phase 3 was less explosive and contained less major dome collapse events than the previous two phases (Wadge et al, 2014). Phase 4 began with a major seismic crisis, followed by an explosion in July 2008 (Wadge et al, 2014). Pumice-rich pyroclastic density currents and lava extrusion were associated with these early explosive eruptions (Komorowski et al, 2010), but lava extrusion slowed and stopped altogether by September (Wadge et al, 2014). Similar to Phase 3, significant fracturing of the lava dome occurred during Phase 4 seismic activity, as surface volcanic activity receded between September and December 2008 (Wadge et al, 2014). Phase 4 concluded with a small dome collapse and subsequent explosive eruption in December, followed by rapid lava extrusion, and major pyroclastic flows. Phase 4 marked a different pattern of volcanic activity to previous phases, with a much shorter duration and high degree of explosivity (Wadge et al, 2014). The end of the 4th phase showed very high extrusion rates, and strong cyclic behaviour on hourly timescales. The most recent period of activity was Phase 5, lasting from October 2009 to February 2010. The behaviour of Phase 5 is similar to the end of Phase 4, with a short burst of explosive activity, rapid lava extrusion, dome collapse, and pyroclastic flows (Wadge et al, 2014). Since the termination of phase 5 in 2010, the volcano has been in an elongated pause state, with no magma extrusion (Harnett et al, 2019), reduced seismic activity (with the exception of intermittent volcanotectonic earthquake swarms) and reduced gas emissions (Stinton et al, MVO OFR 20-05).

GPS data shows steady inflation of the volcano (Figure 2.3) (Stinton et al, MVO OFR 20-05). The current EDM network is younger than the GPS network (early sites were destroyed), but the EDM data available from 2005 onwards shows a similar pattern, with line contraction associated with deflationary eruptive phases and line lengthening with the post-2010 inflationary pause (Figure 2.2). Pause 5 has also seen multiple strong volcanotectonic events in October 2010 (MVO OFR 13-03), March 2012 (Šindija et al, 2021) and March 2014 (Stinton et al, MVO OFR 20-05), the deformation response of which has been detected by GPS sites close to the vent and parts of the EDM monitoring network. In relation to the ground deformation data, eruptive phases are marked by deflationary episodes, while pauses are characterised by inflation of the volcanic edifice (Odbert et al, 2014a).

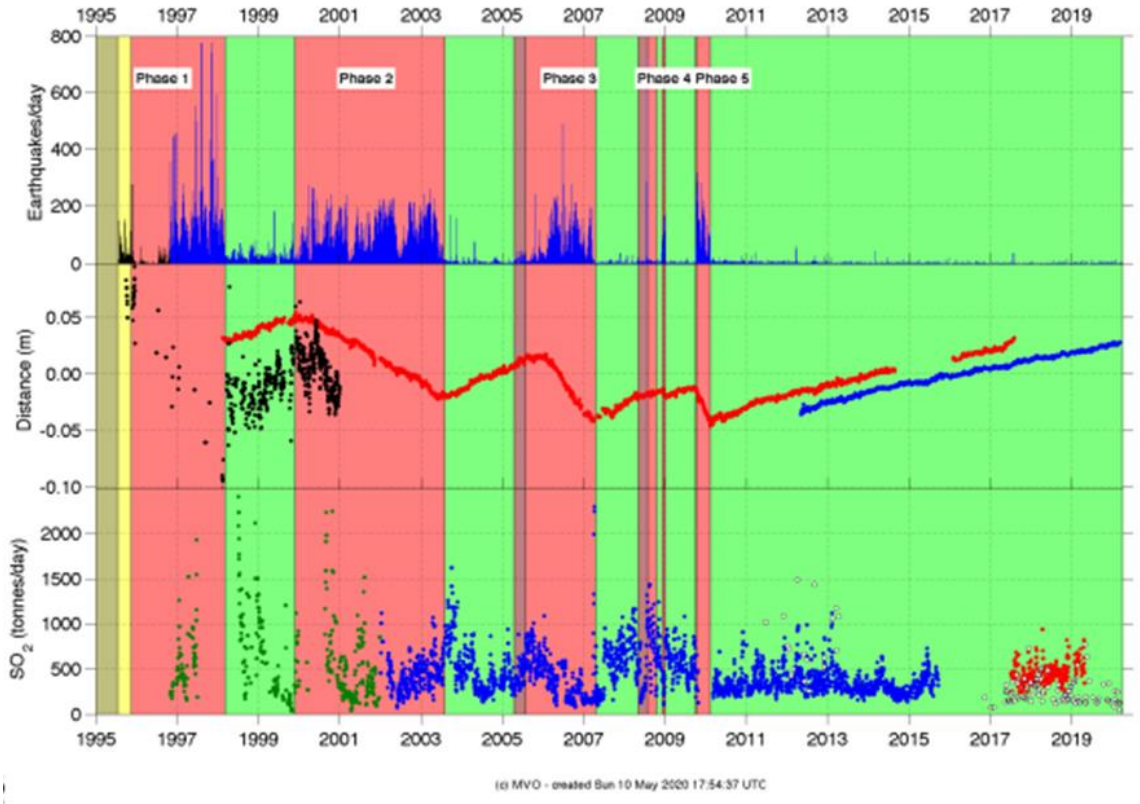

Figure 2.1- Summary of all monitoring data for the entire eruption of the Soufriere Hills volcano between 1995 and March 2020. Extrusive phases and pauses are shown in red and green respectively. Top: Number of seismic events detected and identified by the seismic system. Middle: Radial displacement of cGPS stations MVO1 (red) and NWBL (blue) smoothed with 7-day running mean filter, Black: GPS Height of HARR. Bottom: Measured daily SO2 flux, filtered with 7-day running median filter. Green: COSPEC, Blue: old DOAS, Red: new DOAS, White: Traverse data (Stinton et al, MVO OFR 20-05).

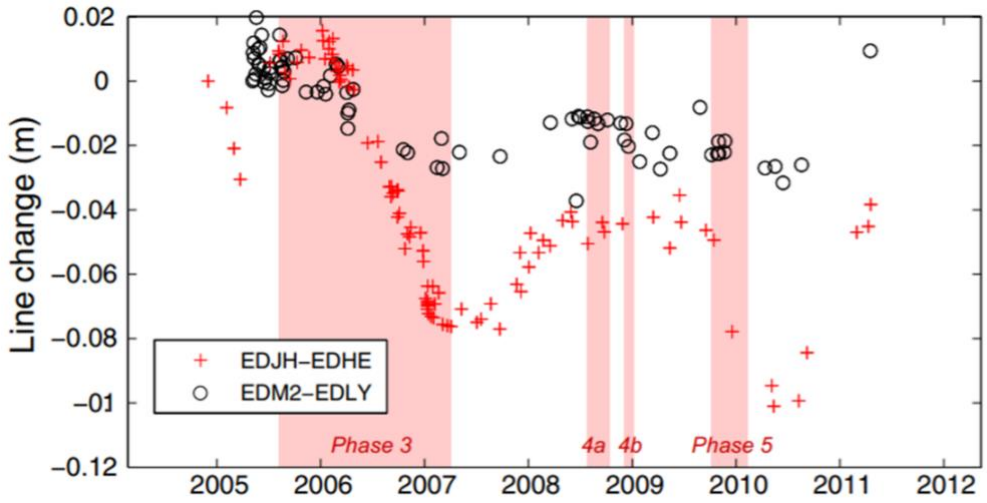

Figure 2.2 – EDM data documenting ground deformation at the SHV between 2005-2012. Line lengthening is associated with inflationary pauses, and shortening with deflationary eruptive phases. EDJH-EDHE appears to be more sensitive to changes in the behaviour of the volcano than EDM2-EDLY (Odbert et al, 2014a).

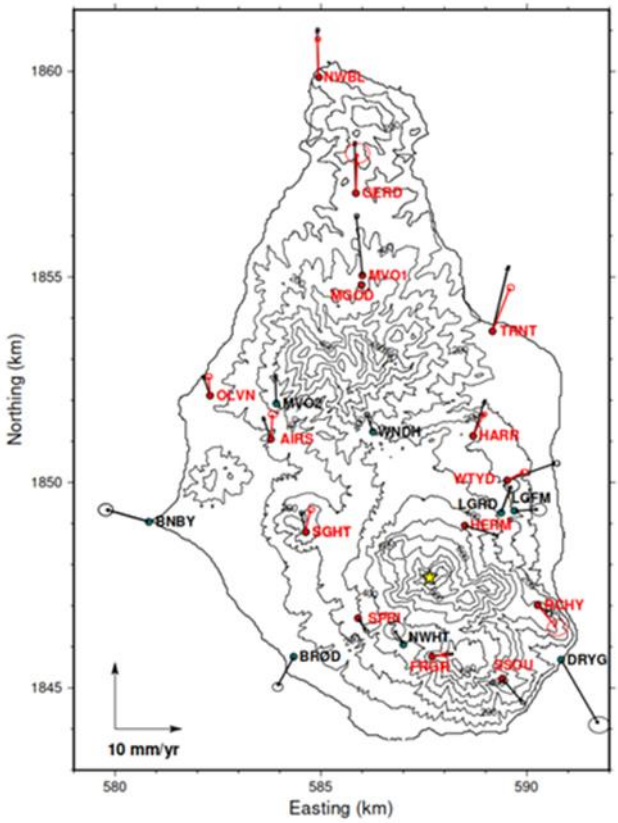

Figure 2.3 –SHV GPS Horizontal Deformation 2010-2019 .Calculated relative to the Caribbean tectonic plate velocity model. The vent is marked with a yellow star, Black arrows show the average velocities for 2010-2019. Red arrows show velocity vectors for the Oct 2018-Mar 2020 period. The length of the arrow = magnitude of deformation, and the size of the circle = 95% error. Continuous and campaign GPS sites are marked in red and black respectively. [Stinton et al, MVO OFR 20-05].

2.3 Modelling the Soufriere Hills Volcano Magmatic System

The common interpretation of the magmatic system at the SHV is split into multiple sections: the near-surface magma conduit (0-1 km below the vent, which is approximately 950 m above sea level), the shallow conduit-dyke system (1-5 km), the upper mid-crustal magma chamber (~6 km), and the deeper mid-crustal magma system (~13 km) (Figure 2.4). Consequently, this section is structured using a similar breakdown, with the exception of examining the two parts of the mid-crustal system together.

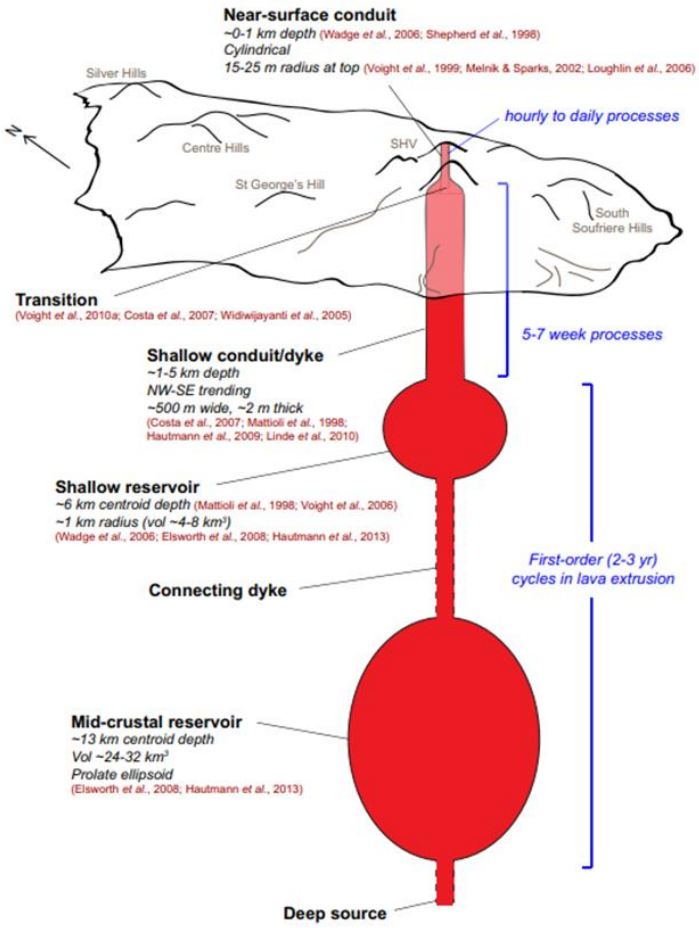

Figure 2.4- A simplified illustration of the geodetically constrained geometry of the SHV magmatic system. Inferred timescales of deformation are labelled (Odbert et al, 2014a).

2.3.1 Near-Surface Magma Conduit

Processes in the near-surface magma conduit (NSMC) have been inferred to operate on hourly to daily timeframes (Odbert et al, 2014a; Voight et al, 1999). Early inferences of the near-surface magma conduit found a conduit of approximately cylindrical geometry, with a radius of about 15 m (Voight et al, 1999; Melnik & Sparks, 2002). These studies utilised early measurements of lava spine dimensions, magma ascent rates, and volume extrusion rates, in order to examine the short-term cyclic deformation patterns that enable short-term forecasting.

Examining the 1996-1998 period of activity at the SHV in particular, with repeated dome growth and flow-producing collapse, Voight et al (1999) inferred the cause of cyclic behaviour being: i.) the degassing and crystallisation of magma in the upper conduit, creating a plug; and ii.) the overpressurization of magma beneath that plug. This process creates a valve system, proposed to be driven by viscosity changes in the magma due to the degassing and crystallisation, which controls the cyclicity of surface magma extrusion. The valve system was mathematically modelled by Melnik and Sparks (2002), who account for gas loss and crystallization kinetics by utilising variable permeable flow and Avrami equations, respectively. Their findings similarly constrain the NSMC to a radius of 15 m. Melnik & Sparks (2002) also found a magma overpressure maximum at depths of a few hundred metres, which potentially could mark the location of the magma plug hypothesised by Voight et al (1999).

A potential problem with any early inferences of the NSMC reliant on spatially limited ground deformation data (such as GPS, strain, tilt, or EDM) is that a cylindrical conduit so close to the surface is unlikely to produce measurable ground deformation beyond a 1 km radius of the vent, making measurements difficult due to access issues and destruction of equipment. This issue limited any ground deformation data applicable to the NSMC to campaign GPS surveys, which carry a greater error than permanently installed GPS stations. Additionally, the small volume of the NSMC means its deformation signal could be easily dominated by the higher magnitude deeper system signal (Odbert et al, 2014a), making it difficult to interpret the shallow system. Some GPS data were obtained from within a 1 km radius of the vent via the campaign GPS survey detailed in Shepherd et al (1998), who found the rate of variation of

strain with distance from the vent indicated a centre of pressure at a depth shallower than 750 m below the summit. Shepherd et al (1998) used a simple cylindrical model to interpret their GPS observations. A similar result was found in Wadge et al (2006), who used InSAR data moderated by GPS measurements to examine deformation between 1998 and 2000. The model utilised a simple heterogeneous medium, with varying Young's Modulus values and densities, and concluded that processes occurring in a conduit at a depth of between 200 and 800 m below the dome surface were driving surface deformation patterns during phase 2 dome growth. It was also observed that geodesy measurements at the SHV are affected by the subsidence of fresh pyroclastic material as it settles and cools, distorting InSAR measurements in particular (Wadge et al, 2006; Odbert et al, 2015).

A strain data-led study was undertaken by Voight et al (2010a) to estimate the size of the NSMC. This study explored explosive Vulcanian eruptions in 2003, which triggered lava dome collapse and pyroclastic flows (Herd et al, 2005), to determine the duration of intense eruptive activity and inferred conduit emptying. Strain data was also used to infer the pressurisation of the NSMC immediately before Vulcanian eruptions and gas emissions events was generated from the contraction of the mid-crustal system (Hautmann et al, 2014). The study then calculated the volume of the erupted material from the corresponding plume heights. The strain records contained no apparent contribution from a dyke-like pressure source during the Phase 2 explosive eruptions (Voight et al, 2010a), therefore the volume of erupted material could be assumed to equate to the volume of the NSMC. Assuming a 15 m radius for the conduit (Melnik & Sparks, 2002), this equated to a cylindrical conduit drawdown of approximately 2 km. An apparent problem with this calculation is the strong dependency on the radius figure. More recent estimates of conduit width based on magma spine observations of 50 m (Loughlin et al, 2006) would result in a drawdown depth of about 720 m, less than half of the original estimation.

2.3.2 Shallow Conduit/Dyke

Initial GPS investigations of Phase 1 lava extrusion indicated the shallow feeder system was composed of a vertical dyke orientated NW-SE (Mattioli et al, 1998). Tilt signal data collected in 1997 (Voight et al, 1997) recorded

deformation signals both radially and tangentially to the vent, which could not be reconciled with a vertically axisymmetric source, but could be attributed to the dilation or contraction of a NW-SE orientated dyke (Costa et al, 2007; Hautmann et al, 2009). The approximate maximum depth of the dyke conduit can also be constrained by petrological estimations of the depth of magma storage, estimated at 5-6 km (Barclay et al, 1998) and this is also backed up by independent seismological data (Aspinall et al, 1998).

A proposed geometry is one of a cylindrical conduit extending from the NSMC to the magma chamber/deeper magmatic system (Figure 2.5). This geometry was used to develop a model of magma flow in dykes that produced pulses of magma extrusion, matching the SHV cyclic lava extrusions on timescales of 5-7 weeks with a dyke 300-500 m long and 3-6 m wide (Costa et al, 2007). The cause of a 5-7 week periodicity in the tilt cycles was attributed to pressure variations in the dyke conduit (Hautmann et al, 2009).

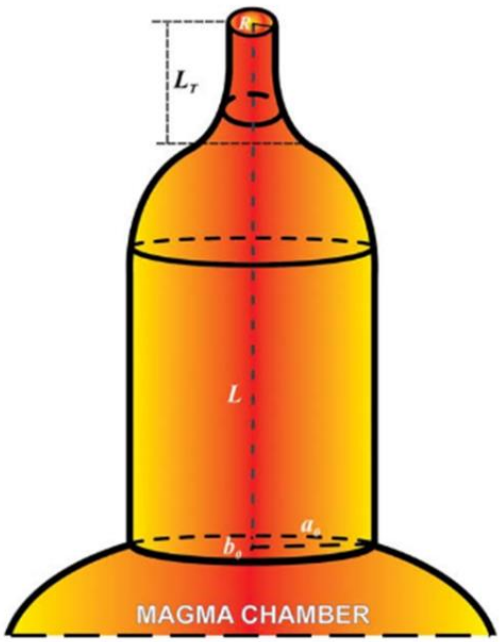

Figure 2.5- Shallow magma system model geometry. L = 5km (Length of dyke system). The transition from an elliptical dyke to a cylindrical conduit occurs at a depth of approximately 1.2 km below the vent. L_T = Length of the conduit = 1.2 km, L = Length of the dyke system = 5 km. R = Conduit Radius = 15 m. The variation with depth of semi-axis lengths, a0 and b0, are defined using arctangent functions (Costa et al, 2007; Hautmann et al, 2009).

A proposed geometry for the conduit/dyke system is an elliptical dyke transitioning to a conduit at a depth of 1.2 km (Hautmann et al, 2009); found using a 3-D Finite Element Model (FEM) with a Digital Elevation Model (DEM) of Montserrat. A potential limitation of the geometry used is that the near surface magma conduit is given a radius of 15 m, which contradicts magma spine observations that indicate a diameter of approximately 50 m (Loughlin et al, 2006). However, this study does manage to include the effects of the DEM and a degree of crustal heterogeneity, both steps forward in the accuracy of modelling of volcanic systems. The recorded tilt data could be explained by pressure changes in an elliptical dyke 5 km long, with the dyke-conduit system orientated NNW-SSE (Hautmann et al, 2009). This is complementary with seismic data and displays a similar strike to tectonic faulting on the island, and matches with the local stress fields generated by the subduction of the Atlantic plate under the Caribbean plate (Wadge et al, 2014). This inference of a roughly NW-SE orientated dyke conduit (Mattioli et al, 1998; Hautmann et al, 2009) is further supported by a strain data study of the Vulcanian eruption of the 3rd March 2004 (Linde et al, 2010). This study used Mogi source in combination with an Okada style dyke model. Later strain data studies investigating the 29th July 2008 Vulcanian eruption found the conduit was much larger than previous estimates, with a radius of approximately 40 m, narrowing to a radius of 15 m close to the surface (Young and Gottsmann, 2015). In addition, they inferred that the conduit was surrounded by a halo of highly compliant rock with a Young's Modulus of 1 GPa (compared with 10 GPa for the main edifice and shallow crust at depths of approximately 1000 m and higher) with a radius of approximately 250 m, creating a shallow system ~600 m wide. The conduit was only partially emptied in the eruption of 2008 (Young and Gottsmann, 2015). Tilt changes from Phase 2 (1997) activity originated from a spherical source at a depth of 0.75-1 km depth, with a radius of 200-340 m (Widiwijayanti et al, 2005). These findings were based on a modelled shallow system of a simple Mogi point source and conduit. Treating this pressure source as the dyke-conduit transition zone could explain the large horizontal source pressurization identified by Widiwijayanti et al (2005).

2.3.3 Mid-Crustal Magmatic System

Modelling studies into the mid-crustal magmatic system are partially limited by the footprint of the island (and by proxy the extent of the monitoring network). A commonly modelled structure for the magmatic system feeding the SHV is two vertically stacked magma chambers, connected via a conduit. The basis for this double chamber system comes from the analysis of cGPS data (Elsworth et al, 2008, 2014; Foroozan et al, 2010; Hautmann et al, 2010).

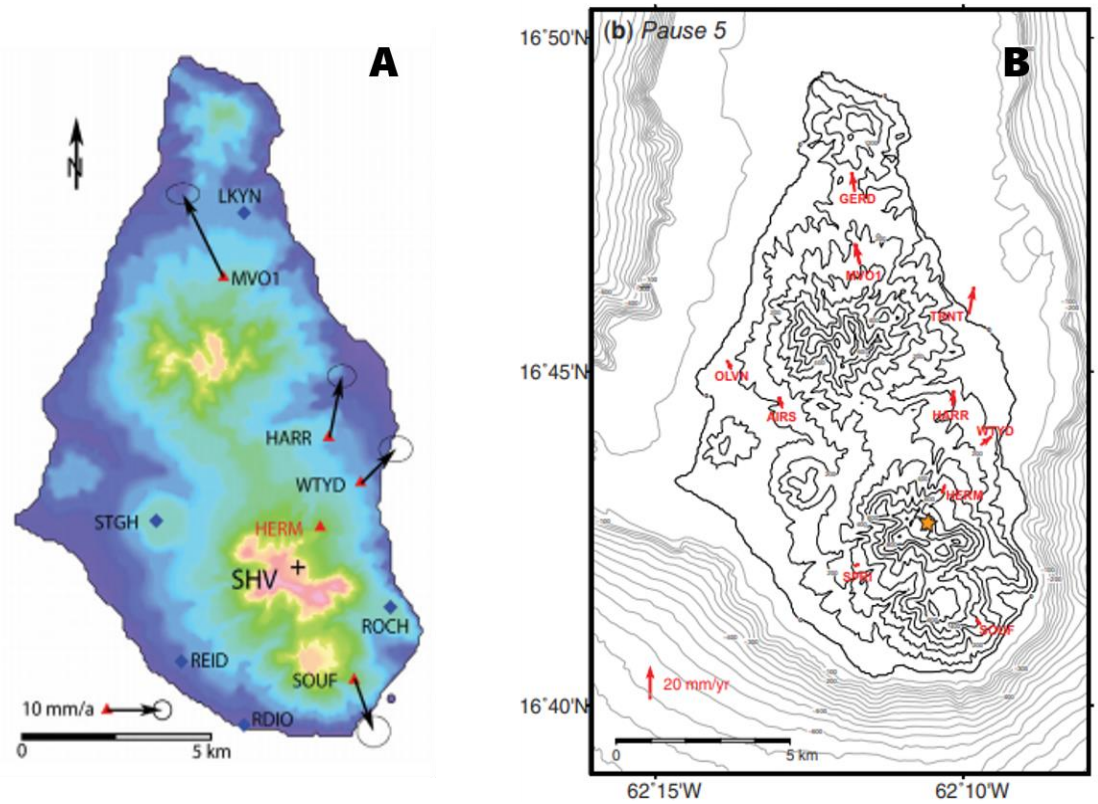

Figure 2.6 –Comparison of radial displacement as measured by the continuous GPS network on Montserrat. A.) Horizontal deformation velocities recorded between July 2003 and November 2005 (the intra-eruptive pause between Phase 2 and Phase 3), displaying a strong radial deformation pattern. Vent marked with a black cross (Elsworth et al, 2008). B.) Horizontal ground deformation measured between February 2010 and December 2011, during the still-ongoing inflation episode. Note the increase in the number of cGPS stations and the change in movement patterns to the south and south-west of the vent. The SOUF and SPRI stations show minimal movement, in comparison to the significant velocity of SOUF recorded in Phase 1. Vent marked with orange star (Odbert et al, 2014a).

Elsworth et al (2008) used an inversion of the 1995-97 campaign GPS data to determine the depth of a shallow chamber at 5-6 km, and inferred a deeper chamber at 10-12 km from crystal phases in erupted magmas and post-1997 geodetic data. This study only used deformation data was recorded by 4 GPS sites at the time (the GPS site HERM was excluded for its anomalous readings) (Elsworth et al, 2008). Radial deformation recorded by the continuous GPS network (Figure 2.6) continues to be the primary indicator of deep magmatic system behaviour at SHV.

The overall structure of the magmatic system first proposed by Elsworth et al (2008) is largely supported by subsequent literature. Foroozan et al (2010) suggests a greater source depth of 17 km for the deeper source based upon cGPS data from Pause 2 inflation and Phase 3 deflation; they accounted for crustal mechanical heterogeneity by adopting P-wave velocity profiles from Paulatto et al (2010) to produce a layered crustal rheology with variation of the Young's Modulus with depth.

The introduction of the FEM method allowed the introduction of a basic DEM of Montserrat into the modelling, accounting for the effect of topography on surface deformation, as well as allowing for the testing of different source shapes. Using the same cGPS data from Pause 2 inflation and Phase 3 deflation, and the same model of crustal heterogeneity as Foroozan et al (2010), the FEM approach yielded a new result; a single vertically prolate source (with a horizontal: vertical axis of 0.6) centred at a depth of 13 km (Hautmann et al, 2010). This study highlighted how incorporating magma compressibility and/or visco-elasticity of host rocks in areas of high heat flow impact the estimates of source dimensions and source pressurisation when modelling surface deformation at SHV. This alternative model for the lower magmatic system is best represented as a prolate ellipsoid magma reservoir with an estimated a volume of 32 km^3 (Gottsmann et al, 2020; Hautmann et al, 2010). This single magma reservoir model was first presented with internal stratification, centred at 10 km depth, extending from 14 km up to 6 km and connecting directly to a shallow conduit system (Voight et al, 2010b). A single prolate source as a proxy for the magmatic system was the best fit for the 2003-2005 GPS intraeruptive period when modelled using 3D inversions (Gottsmann et al, 2020), in this case extending from the base of the dyke-conduit system at

4.34 km below sea level, to a depth of 15 km. This proposed reservoir geometry also tilts towards the NW at an angle of 9.3°.

Confidently distinguishing between the single-source (Voight et al, 2010b) and dual-source (Elsworth et al, 2008) models using the best fit of deformation data alone is extremely difficult (Mattioli et al, 2010). The temperature distribution caused by the heat flux of two stacked magma chambers is very similar to that of a single prolate source, so viscoelastic temperature-dependent models also show difficulty in distinguishing between the two proposed magmatic system structures (Gottsmann and Odbert, 2014). However, more recent studies (Gottsmann et al, 2020) lean more towards the single prolate source model, as it more accurately reflects the modern understanding of trans-crustal magmatic systems (Cashman and Sparks, 2017; Christopher et al, 2014).

Chapter 3

EXPLORATORY ANALYSIS OF HOW EDM AND GPS JOINTLY RECORD SURFACE DEFORMATION

-

3.1 Background and Motivation

The way GPS records volcanic surface deformation has been widely documented in a variety of GPS data-based modelling studies, with limited spatial coverage of the edifice (Mattioli et al, 1998; Shepherd et al, 1998; Melnik and Sparks, 2002; Costa et al;, 2007; Hautmann et al, 2009; Foroozan et al, 2010; Hickey et al, 2016; Gottsmann et al, 2020). EDM modelling has to date been a rarer method of anchoring the results of modelling studies (Hickey et al, 2015b), and co-analysis of both rarer still (Bonaccorso et al, 2005). The SHV has a well-developed network of both GPS stations and EDM stations/reflectors, making it an ideal candidate to explore utilising both in tandem to model the magmatic system, which to date has never been done before. In order to explore how EDM records deformation compared to GPS, a first-order study was undertaken comparing how the two geodetic techniques record the same deformation event in a synthetic 2D axisymmetric model with a simple volcanic edifice. By modelling and comparing the response of a diverse range of EDM baselines, and synthetic GPS receivers (the end points of the EDM lines) to changing deformation source characteristics, this initial study will aid the interpretation of EDM measurements moving forward in this thesis.

3.2 Methods

3.2.1 Model Setup

The Finite Element Modelling (FEM) approach is used in this study for the ease of source parameter changes, especially source shape. The Structural Mechanics module of COMSOL Multiphysics v5.4 software is used for all FEMs. A 2-D axisymmetric homogeneous elastic half-space forms the 50 km x 50 km model space. This size was chosen to avoid boundary effects affecting the interior and results. A simple volcanic edifice was added to the top of the model space using a right-angled triangle, the dimensions of which are approximately equal to the Soufriere Hills Volcano, with the same rheological and mechanical properties as the rest of the elastic medium (Table 3.1). The bottom surface of the model is fixed, with a free top surface, rollers on the lateral surfaces, and an Infinite Element Domain (IED) that surrounds the model geometry to help shield the interior of the model from boundary effects (Figure 3.1). Points were placed at regular intervals along the simple edifice to simulate EDM reflectors close to the vent, and two points away from the edifice to simulate EDM base stations (Figure 3.2). The source is formed of a hollow semi-ellipsoid, with a boundary load applied to the outer edge to simulate pressurisation of the source.

3.2.2 Modelling Approach

This study experimented with varying source pressure between 2 and 10 MPa, source depth between 4000 and 12000 m, and prolate, spherical, and oblate source shapes (achieved with the variation of the X-axis to Y-axis ratio while maintaining a consistent source volume; table 3.2). It was then observed how the changing parameters affected the simulated EDM line-length and 3-component ‘GPS’ on a simple volcanic edifice. Table 3.1 provides a list of the parameters varied and the ranges experimented with. EDM line lengths were calculated prior to and after the application of an instantaneous source pressure to extract the modelled line length change. A percentage line length change was used to correct for variations in starting length and to allow for like-for-like comparison between EDM lines, as otherwise shorter lines would show a lower deformation response as a consequence of their original starting length being shorter.

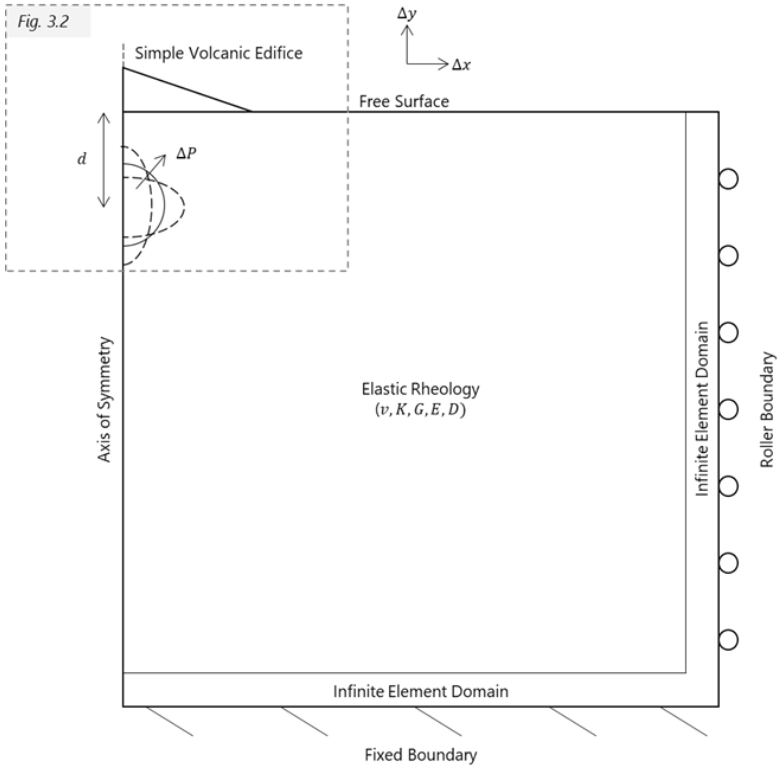

Figure 3.1 – Schematic diagram of 2D model setup (full model). Model geometry and boundary conditions of preliminary study comparing GPS and EDM measurement of elastic deformation of a simple volcanic edifice.

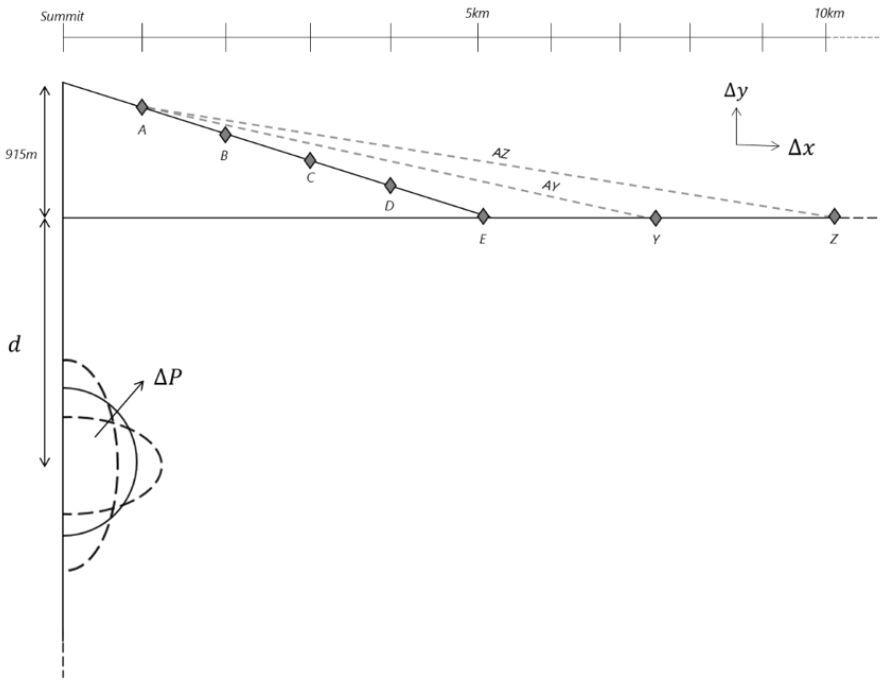

Figure 3.2 – Schematic diagram of 2D model setup (edifice and source). Zoomed model geometry of volcanic edifice, positioning of EDM base stations (Y and Z) and reflectors (A-E), drawing of EDM lines (dashed), and variation in pressure and geometry of pressure source.

Table 3.1 – 2D Model parameters. Parameters varied in the experiment with source variation, and the values used.

Variable	Definition	Dimensions	Value (Start, Finish, Interval)
	Source Parameters		
d	Depth	m	4000, 12000, 1000
A:B	Source Shape	-	*see table 3.2
ΔP	Pressure Change	MPa	2, 10, 2
	Mechanical Characteristics		
v	Poisson's Ratio	-	0.25
E	Young's Modulus	Pa	5.00E+10
D	Density	kg/m^3	0.25

Table 3.2 –Source shape parameters. The X-axis and Y-axis were modified at a constant rate of change and adjusted to maintain a constant source volume. The ratio of A-axis length to B-axis length is then used to describe the source shape

X-axis (m)	Y-axis (m)	Volume (km^3)	A:B Ratio	Shape
677.00	1477.11	4188.8	0.46	Prolate
744.05	1344.00	4188.8	0.55	Prolate
820.01	1219.50	4188.8	0.67	Prolate
905.02	1104.95	4188.8	0.82	Prolate
1000.00	1000.00	4188.8	1.00	Spherical
1104.95	905.02	4188.8	1.22	Oblate
1219.50	820.01	4188.8	1.49	Oblate
1344.00	744.05	4188.8	1.81	Oblate
1477.11	677.00	4188.8	2.18	Oblate

An analytical solution for this problem could not be used for a comparison, as analytical models cannot model a slope, and the purpose of this exercise was to observe how modelled points on a sloping edifice deform.

3.3 Results

Results show that at shallow source depths, EDM line length shortening occurred, while deeper source depths produced line lengthening (Figure 3.3). At a source depth of 4000 m, Points B, C, D, and E all displayed greater radial deformation (around 3-4 mm) than the EDM base station proxies Y and Z, which deformed by 1-2mm, generating the line length shortening. At deeper

source depths, the radial deformation response decreased for points A-E on the edifice. Line lengthening was generated instead by the increased vertical deformation response of the points on the edifice (around 2 mm of uplift average across points A-E at source depths greater 6000 m) relative to the EDM base station proxies, which only experienced 0-1 mm of uplift at all source depths.

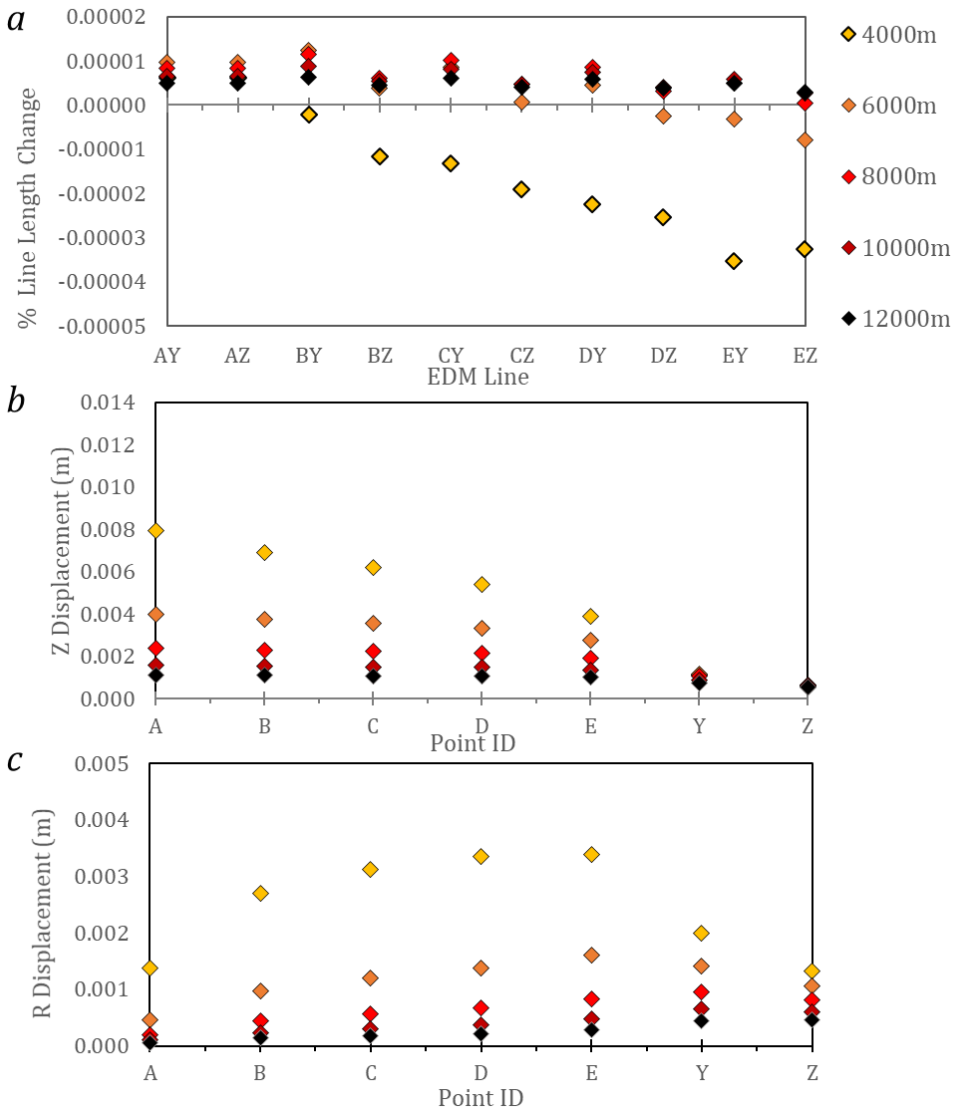

Figure 3.3 – Impact of changing source depth of a spherical source. The source is pressurised at 6 MPa. A.) Simulated EDM line length changes. B.) Vertical displacement (Z) of individual points. C.) Radial displacement (R) of individual points.

It can also be inferred that increasingly oblate source shapes cause line length shortening, while prolate shapes cause line lengthening, relative to a spherical source (Figure 3.4). The deformation response at the surface induced by oblate

sources is of a far greater magnitude than that of a prolate source, due to the larger upper surface of the oblate source. This can be observed in both the vertical and radial deformation profiles (Figure 3.4), with the most oblate sources generating vertical deformation of 14 mm directly above the source, and 8 mm at Point E on the edge of the edifice, compared with between 1-2 mm vertical deformation from the most prolate source. The deformation response of oblate sources is predominantly vertical, but there is still a strong radial deformation component, the magnitude of which peaks at Point E on the edge of the edifice with 4.5 mm of deformation. Points B-E on the edifice all display greater radial deformation than the EDM base stations Y and Z with oblate sources, whereas with prolate sources Y and Z deform radially with approximately the same magnitude as the reflectors. Oblate sources result in EDM line lengthening due to the relative radial displacement of reflector and base station, whereby the radial deformation at reflectors is greater than that of the base station. Vertical displacement is greater in magnitude than radial at each point on the edifice, but vertical displacement of the reflector relative to vertical displacement of the base station has a lesser impact on EDM line length change even when the magnitude of the vertical deformation is greater than the radial.

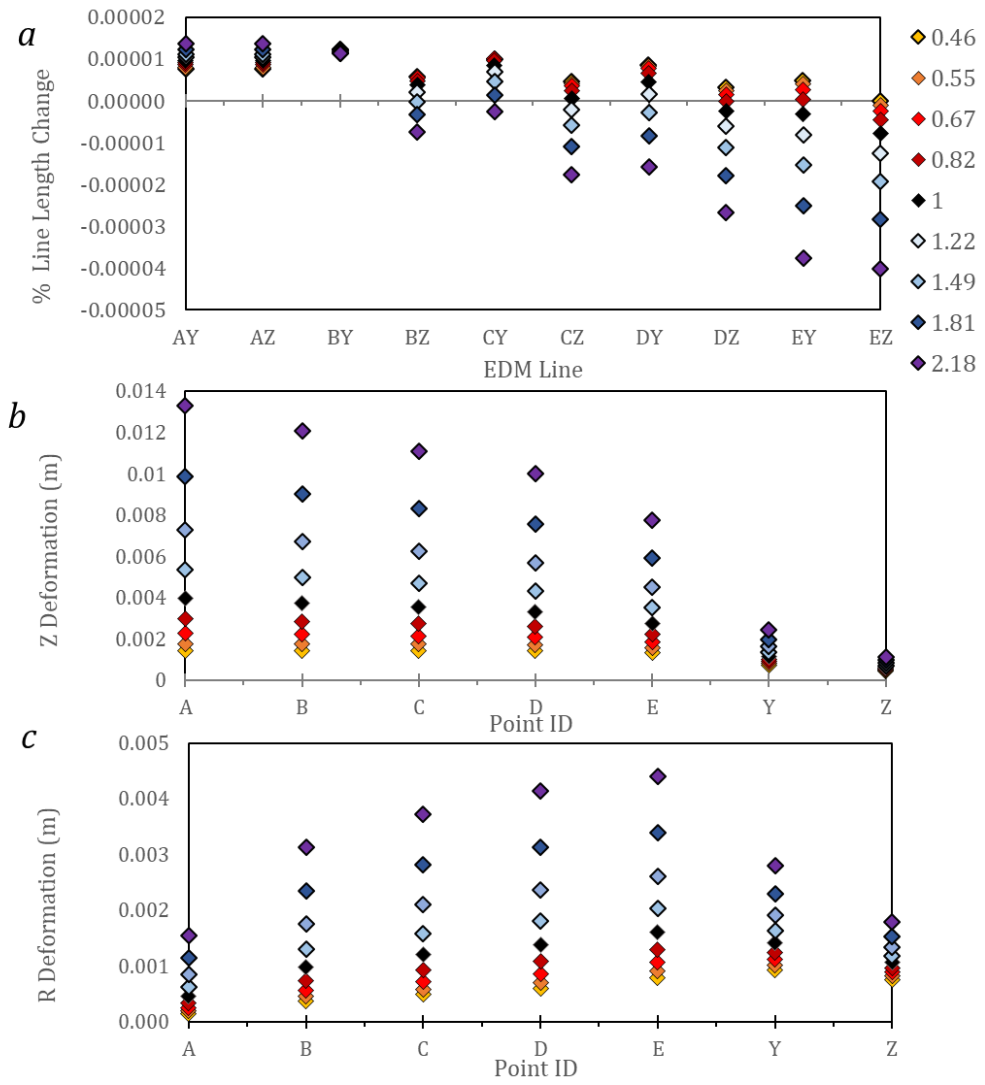

Figure 3.4 – Impact of changing source shape centred at 6000 m depth and pressurised at 6 MPa. The source is pressurised at 6 MPa and centred at a depth of 6000 m. Showing A.) Simulated EDM percentage Line Length Change, B.) Vertical Displacement (Z), and C.) Radial Displacement (R). The ratios used to display source shape are explained in Table 3.2, ratios above 1 represent oblate sources, ratios below 1 represent prolate sources, and a ratio of 1 represents a spherical source.

EDM line lengths change with a linear relationship to increasing or decreasing pressure. Sites closest to the vent experience the most vertical deformation, and radial deformation increases moving away from the vent until it hits a peak at Point E 5 km from the vent (Figure 3.5). Points A-E on the edifice show greater vertical deformation (up to 4 mm at Point A at 10 MPa) than radial deformation (maximum is Point E at 10 MPa, with just under 2 mm of

deformation.) EDM line length changes move from positive to negative as the radial displacement of EDM reflectors increases moving away from the vent.

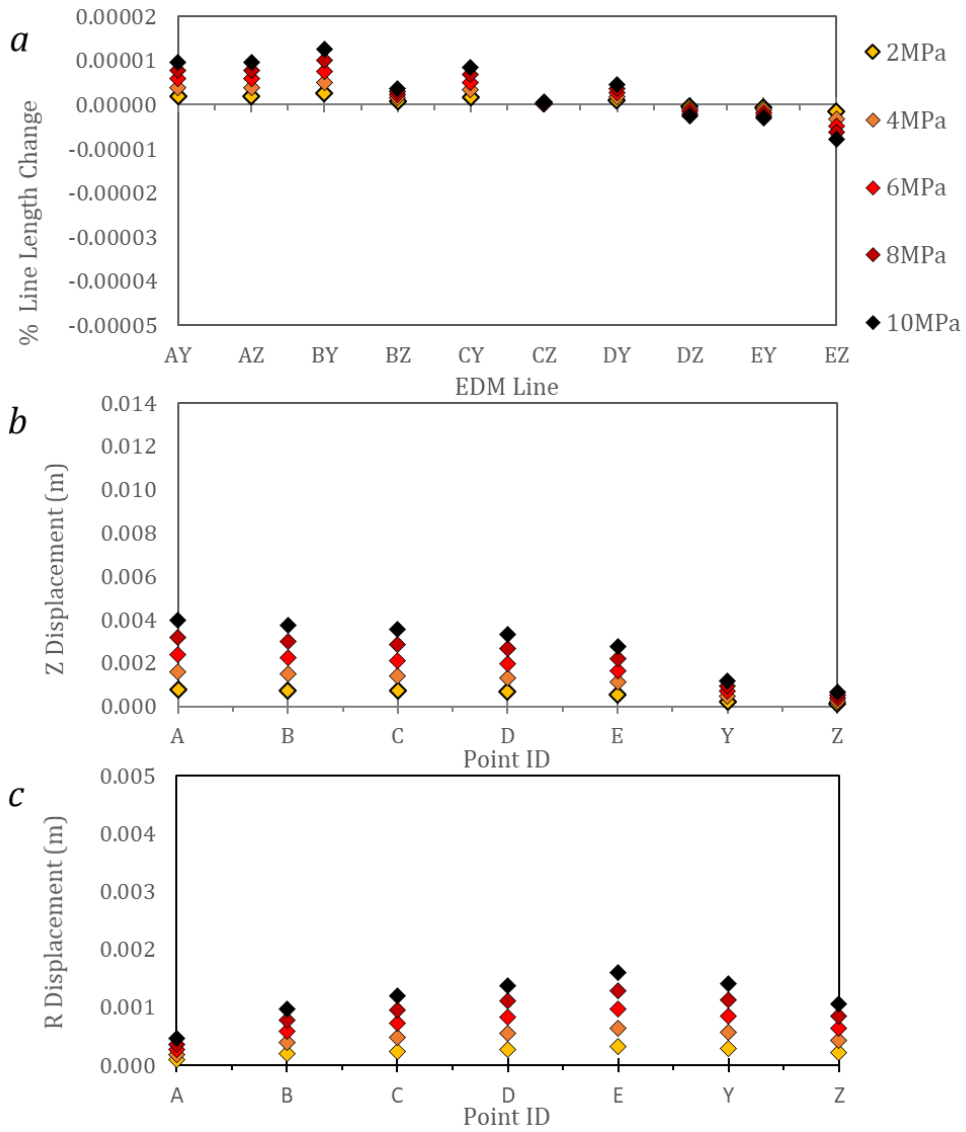

Figure 3.5 – Impact of changing spherical source pressure centred at a depth of 6000m. Results of variation of source pressure in a spherical source centred at 6000 m depth, showing A.) Simulated EDM % Line Length Change, B.) Vertical Displacement (Z), and C.) Radial Displacement (R).

3.4 Discussion

Source depth can impact the sign of an EDM line length change (Figure 3.3). When the source is at shallow depths, the majority of the source deformation acts upon the reflectors close to the vent, and line length shortening occurs. However, the notable exception to this pattern is Point A of the model geometry,

which sits so close to the source that it experiences intense vertical deformation and less radial deformation than other points on the edifice. With source depths greater than 6000 m, the deformation field contains greater radial deformation on the EDM base stations Y and Z than the reflectors, and generates line lengthening as a result.

EDM line shortening with oblate sources is caused by the high magnitude radial deformation experienced by EDM reflectors B-E on the volcanic edifice relative to the radial deformation at EDM base stations Y and Z. Vertical displacements dominates the deformation observed at each point, as expected with oblate sources as they produce strong vertical deformation signals from the larger upper source surface (Figure 3.6). However, the vertical deformation component had far less impact on EDM line length change than the radial deformation component, even when the magnitude of the vertical component was greater than the radial. This is because in right-angled triangles where one side is significantly shorter than the other two (as is the case when calculating EDM line length changes using Pythagoras' Theorem), the length of the hypotenuse is much more sensitive to the changes in the longer side than the shorter one. In the case of most EDM lines, the horizontal distance from reflector to base station is much longer than the vertical distance, hence why the baseline length (the hypotenuse) is more sensitive to radial deformation than vertical. Prolate sources produce less radial deformation across all points, and generally reflectors experience less radial deformation than EDM sites Y and Z, producing relatively minor line lengthening in most cases. Vertical displacement is also subdued compared to oblate sources and decreases moving away from the vent.

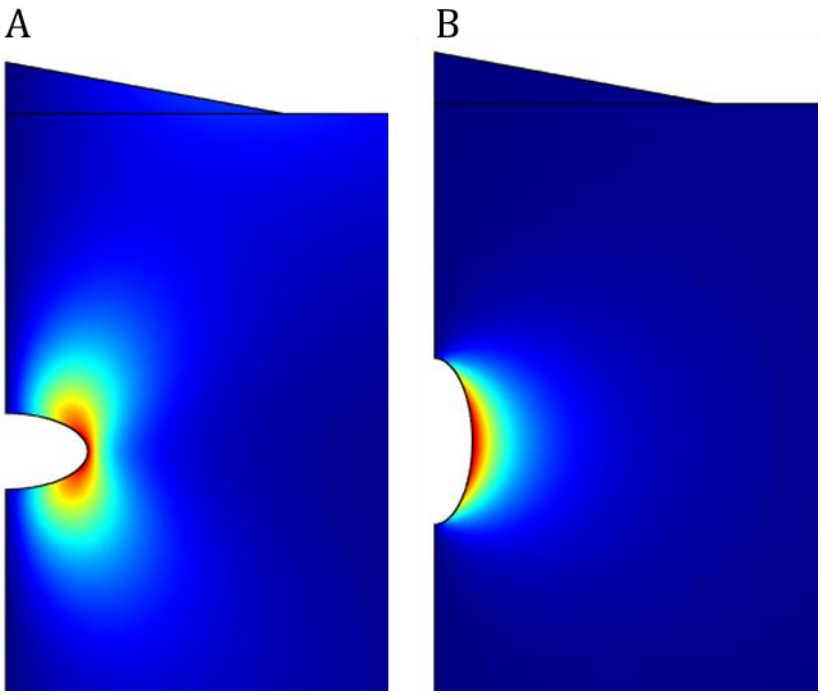

Figure 3.6 – Radial Displacement Cross-Sections. Radial Displacement from A.) An oblate source and B.) A prolate source. The radial displacement produced by oblate sources is transmitted to the surface and results in greater radial deformation than a prolate source as a result.

Varying source pressure had a relatively minor impact on surface deformation compared with source depth or source shape variation. The magnitude of both radial and vertical deformation was low, although this is part due to the pressure range experimented with being fairly narrow and low.

The results of this study suggest that the key controlling factor for EDM line length changes is the relative radial displacement between the EDM base station and reflector. Vertical deformation has a relatively minor impact on EDM line length change, to the extent where the reflector could experience a significant degree of uplift relative to the base station and still display line length shortening with a lower magnitude radial deformation component. The fact they are predominantly controlled by relative radial deformation should be considered when interpreting EDM results. These results also suggest that EDM networks could be sensitive to shallow pressurisation sources, and potentially show line length shortening as magma pressure sources ascends through the crust, especially at depths of less than 6000 m.

This study was limited by the simplified topography, which would fail to take into account the interaction of complex 3D topography and deformation response (Johnson et al, 2019). The magmatic system structures experimented with here are also greatly simplified, with only a single, usually spherical source modelled. The SHV magmatic system has been modelled as either a dual stacked source, or as a single prolate source encompassing the entire mid-crustal system, both connected to the vent by a dyke conduit (Odbert et al, 2014a; Gottsmann et al, 2020).

3.5 Conclusions

1. It is primarily the relative radial deformation between EDM reflector and EDM base station that defines the EDM line length change.

2. Vertical deformation of EDM reflectors and EDM base stations has a relatively minor impact on EDM line length changes compared with radial deformation.

3. An EDM reflector could experience a significant degree of vertical uplift relative to the base station and still display line length shortening with a lower magnitude relative radial deformation component.

4. Shallow sources centred at depths less than 6000 m induce line length shortening due to the high magnitude radial displacement on EDM reflectors on the edifice, except for directly above the source.

5. Oblate sources produce line length shortening to due to the aforementioned importance of relative radial displacement. Oblate sources also produce significantly greater magnitude surface deformation (both vertical and radial) than prolate sources due to their larger upper source surface.

6. EDM line lengths increase linearly in response to increasing pressure.

7. Pressure variation has a relatively minor impact on surface deformation compared with source shape variation and source depth variation.

Chapter 4

RESEARCH PAPER

-

Distinguishing Shallow and Mid-Crustal Magmatic Processes at Soufrière Hills Volcano with Finite Element Modelling and Co-Analysis of EDM and GPS Data

Alexander Johnson [1], James Hickey [1], Karen Pascal [2, 3] Ben Williamson [1], and Raquel Syers [2]

[1]Camborne School of Mines, University of Exeter, Cornwall, TR10 9FE, United Kingdom. aj401@exeter.ac.uk.
[2] Montserrat Volcano Observatory, Montserrat
[3] Seismic Research Centre, University of the West Indies, St. Augustine, Trinidad and Tobago

This is to be submitted to the journal Volcanica.

ABSTRACT

Ground deformation offers vital insight into the activity of volcanoes and associated magmatic systems. We model ground deformation at the Soufrière Hills Volcano (SHV), using data collected by the Montserrat Volcano Observatory. With EDM and GPS data from 2010-19, we investigate the use of EDM in helping to distinguish shallow and mid-crustal magmatic processes and their effect on surface deformation. We find that the EDM network responds predominantly to changes in the shallow magmatic system, while the GPS network primarily responds to changes in the mid-crustal system. Additionally, we show that the behaviour of the EDM network, and of the GPS site HERM which is observed to deform non-radially relative to the vent unlike the broader GPS network, can be explained by under-pressurisation in a shallow dyke conduit orientated NNW-SSE, while the mid-crustal system is still undergoing pressurisation. The modelled dyke conduit may represent magma cooling and contracting from a previous intrusion.

4.1 INTRODUCTION

Volcanic deformation is the inflation or deflation of a volcanic edifice primarily caused by the movement of magma beneath the surface, and is one of the principle volcano monitoring methods alongside seismicity and gas emissions for eruption forecasting [Segall, 2013]. Deformation signals are monitored using a variety of methods, including Electronic Distance Measurement (EDM), Global Position System (GPS), Interferometric Synthetic Aperture Radar (InSAR), tiltmeters, and strainmeters [Odbert et al, 2014; Spaans and Hooper, 2016; Johnson et al, 2016]. Changes in deformation signals may indicate volcanic unrest (a deviation from the background activity of a volcano towards a level of cause for concern), and when used in combination with other monitoring methods provide essential insight into the status of active volcanoes [Gottsmann et al, 2017, Philippson et al, 2013]. Deformation can be caused by both magmatic sources: such as overpressurization of a magma reservoir or chamber [Geirsson et al, 2012], or magma movement such as a sheet intrusion [Biggs and Pritchard, 2017], or non-magmatic sources such as hydrothermal systems [Fournier and Chardot, 2012], the loading of deposits on the volcanic edifice [Odbert et al., 2015], flank collapse/instability [Bonaccorso et al., 2013], or the cooling of magma beneath the surface [Parker et al., 2014]. The intricacies of how magmatic processes produce surface deformation can be examined via the use of models, which require assumptions and simplifications to be made about magma behaviour and crustal mechanics, but can be a useful tool in understanding subsurface processes [Ranalli, 1995; Del Negro et al, 2009; Masterlark, 2007].

Analytical volcanic modelling has been used since the publication of the Mogi model [Mogi, 1958], and can still provide a rapid and simple way of modelling volcanic processes using a spherical ‘point’ source. Analytical models require a significant set of assumptions in order to work: the crustal rheology is usually defined as an isotropic, homogeneous, elastic half space with a flat, free surface. Later analytical models incorporated simple viscoelastic rheologies [Del Negro et al, 2009; Dragoni and Magnanensi, 1989], or source shape variation, such as Fialko et al [2001] modelling a horizontal circular crack, and Yang et al [1988] with a spheroidal reservoir.

Advanced numerical modelling eliminates some of the disadvantages of analytical models by removing or relaxing some of their assumptions. One such numerical modelling method is Finite Element Modelling (FEM), the utility of which has improved considerably in recent years with the increases in computer power readily available. Justification for such additional complexity is afforded through rock mechanics, alongside geophysical, petrological and geological evidence [Cureenti et al, 2007; Masterlark, 2007; Hickey, 2017; Gottsmann and Odbert, 2014; Head et al, 2019; Taylor et al, 2021]. FEM allows for the introduction of complex 3D topography [Hautmann et al, 2009; Hickey at el, 2020], anisotropic continuous heterogeneity [Currenti et al, 2007; Gottsmann et al, 2020; Cabaniss et al, 2020], and viscoelasticity if appropriate [Del Negro et al, 2009; Sigmundsson et al, 2020; Head et al, 2019].

The Soufrière Hills Volcano (SHV) is an andesitic volcano located on the Caribbean island of Montserrat, part of the Lesser Antilles island arc. The SHV is currently in an intra-eruptive pause of an anomalously lengthy eruptive episode, which has been ongoing since 1995 [Odbert et al, 2014; Wadge et al, 2014; Christopher et al, 2014]. Activity at the SHV is typically characterised by phases of eruptions comprised of lava dome growth and collapse, associated pyroclastic flows, and Vulcanian and sub-Plinian explosions [Sparks and Young, 2002].). The volcano possesses a comprehensive monitoring network of GPS sites and EDM baselines (Figure 4.1) as well as strainmeters, occasional gravity monitoring, and, prior to their destruction approximately 20 years ago, tiltmeters. During eruptions, ground deformation is characterised by deflation of the volcanic edifice, with associated subsidence and negative radial deformation (movement towards the vent) [Odbert et al, 2014]. Intra-eruptive pauses are often associated with steady inflation of the edifice, and positive radial deformation (movement away from the vent). However, while the EDM deformation data from the SHV has played a key role in monitoring the SHV during the elongated eruptive episode, it has yet to be utilised in modelling research.

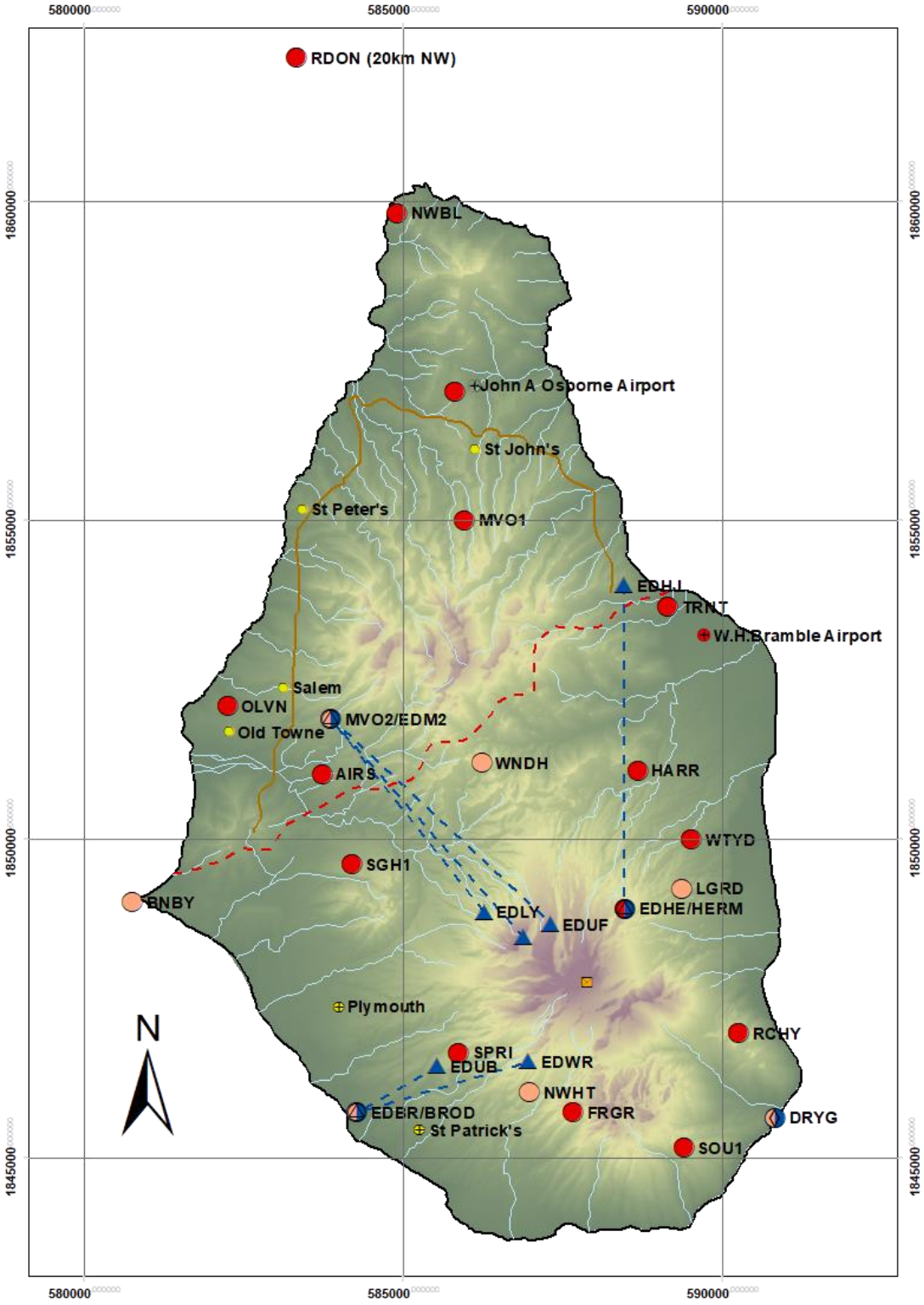

Figure 4.1 - Map of current Montserrat monitoring network. Elements of the geodetic monitoring network on Montserrat used in this study, as indicated in the legend. The EDM network was installed post-2010, and therefore only covers the most recent intra-eruptive pause. There is currently no EDM coverage of the south-eastern flank. The location of the vent has migrated over time, and the location marked is an approximation of the time-averaged position after Odbert et al, [2014]. cGPS = Continuous GPS sites, eGPS = Campaign GPS sites.

The mid-crustal SHV magmatic system has commonly been modelled as two vertically stacked connected magma chambers connected to the surface by a dyke conduit complex [Elsworth et al., 2008; Hautmann et al., 2009; Linde et al., 2010; Mattioli et al., 2010; Gottsmann and Odbert, 2014; Young and Gottsmann, 2015]. However, some studies have shown that the stacked two-chamber system is indistinguishable from a single, large, prolate-shaped reservoir [Voight et al, 2010a, Mattioli et al, 2010], and the most recent modelling studies into the SHV utilise the single prolate-shaped magma system model [Gottsmann and Odbert, 2014; Christopher, 2014; Gottsmann et al, 2020], which acts as a simplified reflection of the trans-crustal magmatic system as a whole [Sparks and Cashman, 2017; Christopher et al, 2014].

Studies into the shallow system of the SHV have modelled the magmatic plumbing as a dyke conduit, extending from approximately 1 km below the vent [Voight et al, 2010a., Costa et al, 2007., Widiwijayanti et al, 2005., Odbert et al, 2014] to a shallow magma source at around 6 km depth [Costa et al, 2007., Mattioli et al, 1998., Hautmann et al, 2009., Linde et al, 2010., Voight et al, 2006., Odbert et al, 2014]. These studies used a combination of GPS and strainmeter data to examine the shallow system, with EDM to date not being used. A strain data-led study into a Vulcanian explosion during in 2004 examined the conduit by modelling a Mogi source and Okada style dyke model [Linde et al, 2010]. The results correspond with previous GPS-based models of Mattioli et al [1998] and Hautmann et al [2009] of a roughly north west-south east orientated dyke conduit, and thereby help to support the overall picture built up of the shallower dyke conduit part of the system. A further study by Young and Gottsmann [2015] examined volumetric strain data from the July 2008 Vulcanian explosion using a heterogeneous elastic finite element model, and found the conduit had a radius of approx. 40 m, and extended to a depth of approx. 1500 m from the vent, where it connected to a 2 m thick dyke which extended to the mid-crustal magmatic system.

A historical stumbling block for GPS-led modelling studies into the SHV has been the continuous GPS site HERM, situated on the north-eastern flank, and closer to the vent than any other GPS site currently in the monitoring network (Figure

4.1). The deformation recorded at this site is often anomalous, behaving out of sync to the rest of the GPS network [Odbert et al, 2014] which has led it to be excluded from some GPS-led modelling studies [Mattioli et al, 2010; Gottsmann et al, 2020]. During the early stages of the eruptive episode at SHV, HERM displayed high magnitude radial deformation compared to the rest of the GPS network during both eruptions and intra-eruptive pauses, with spikes in radial deformation occurring towards the end of eruptions in March 2001, June 2002, and July 2003 and immediately before eruptions in August 2005 and October 2009 [Odbert et al, 2014, Wadge et al, 2014]. The behaviour of HERM has previously been hypothesised as the emplacement of a secondary non-feeder dyke on the North East side of the edifice between HERM and the vent, creating a decoupled wedge of land between two valleys [McPherson, 2013] on the basis of short term deformation patterns from data collected between 1998-2010. Using the additional context of the EDM data in modelling the magmatic system, we are able to present another potential explanation for the behaviour of HERM and a discussion on the insight this GPS site can offer into the post-2010 behaviour of the magmatic system at SHV.

4.2 Methods and Data

4.2.1. GPS and EDM Data

We use GPS (Figure 4.2) and EDM (Figure 4.3) derived surface displacements from the 2010-2019 period, collected by the Montserrat Volcano Observatory (MVO). The geodetic network at SHV has been steadily developed since the eruption began in 1995, and now includes a comprehensive GPS network using both campaign and continuous GPS sites, as well as a set of EDM baselines first established in the initial stages of the eruptive episode (Figure 4.1). During the current extended intra-eruptive pause, the GPS network as a whole recorded outward radial deformation due to steady inflation of the edifice and pressurisation of the magmatic system. The GPS site HERM has deformed to the east south east, with positive vertical deformation (Figure 4.2). HERM is also sensitive to significant VT events, such as the March 2012 VT event where HERM underwent significant outward radial deformation compared with the rest of the GPS network [Stinton et al, MVO OFR 20-05].

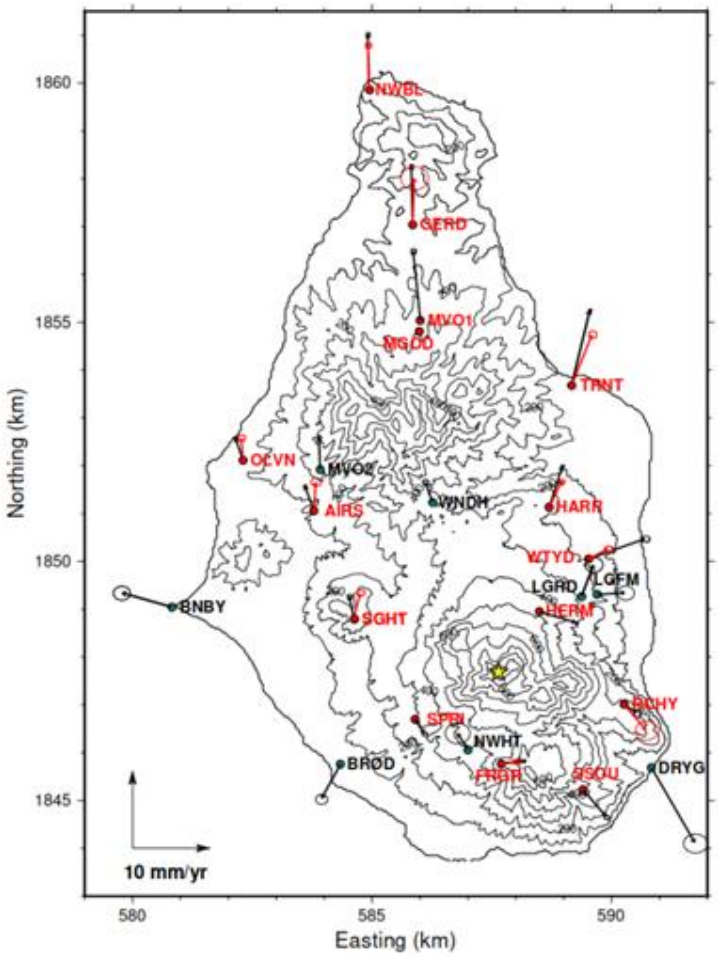

Figure 4.2 - 2010-2019 horizontal GPS velocities. Horizontal GPS velocities observed by MVO from 2010-2019, calculated relative to the Caribbean tectonic plate velocity model. The vent is marked with a yellow star, Black arrows show the average velocities for the full time-period (2010-2019). Red arrows show velocity vectors for the October 2018-March 2020 period. The length of the arrow is an indicator of the scale of deformation, and the size of the circle represents the 95% error. Continuous and campaign GPS sites are marked in red and black respectively. [Stinton et al, 2020].

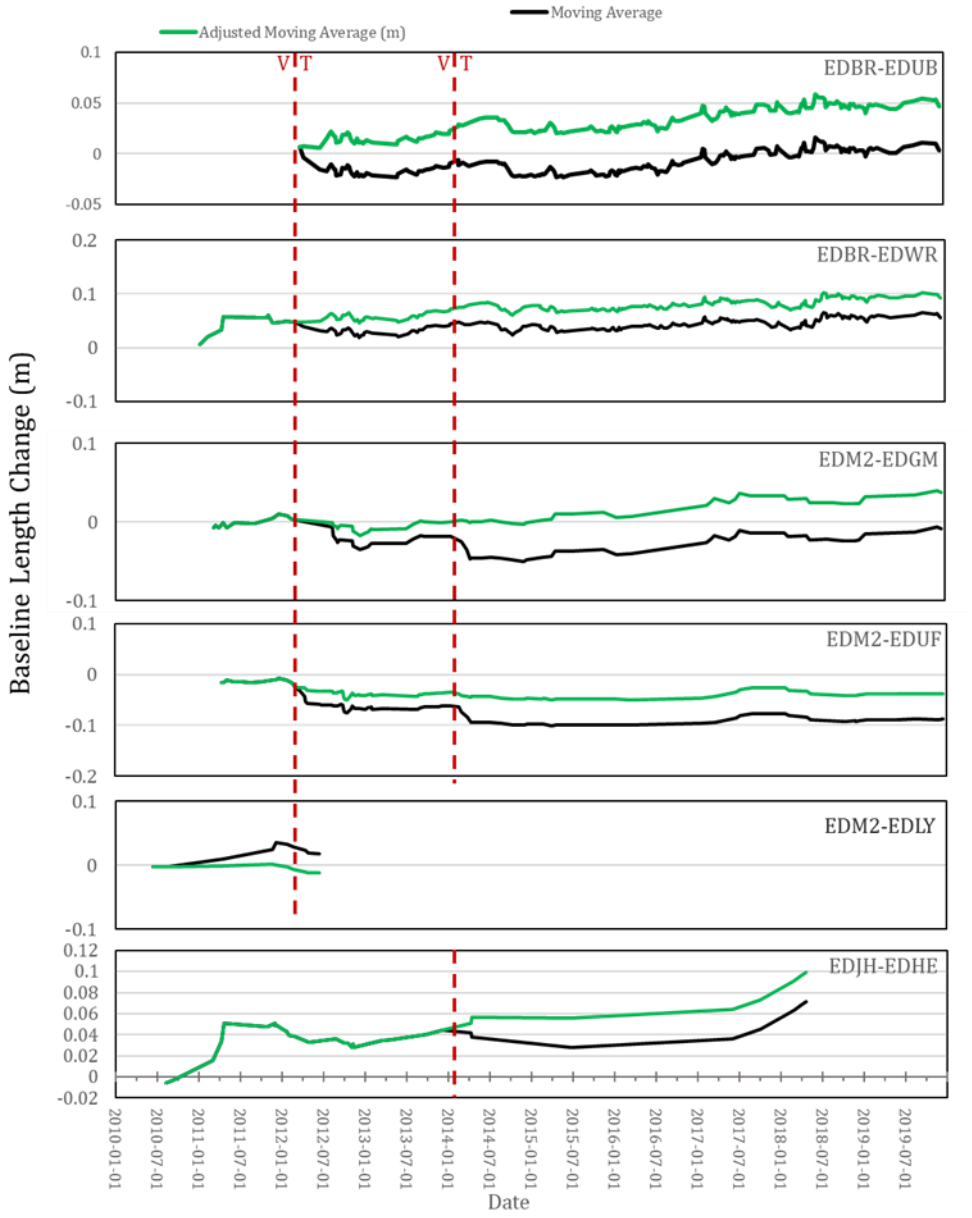

Figure 4.3 - Observed EDM baseline changes between 2010 and 2019. Red dashed lines mark the points of significant volcanotectonic (VT) events that were corrected for in the EDM measurements (March 2012 and March 2014). The 3-point moving average for the raw length change is shown in black, and the 3-point moving average for the adjusted data is shown in green.

The raw EDM data were smoothed using a 3-point rolling average to minimize the impact of noise inherent to EDM measurements. The data still showed large step-changes in line length associated with significant discrete volcanotectonic (VT) events that occurred in March 2012 (which involved ash venting and the creation of two small craters), and March 2014. To isolate and remove the effect of the VT events, the EDM data were corrected for by assuming zero line length

change over the VT event (Figure 4.3), achieved by calculating the line length change between the length change before the VT event, and the length immediately after, creating an offset from the observed deformation trend.

4.2.2 Model Setup

We use Finite Element Modelling (FEM) with COMSOL Multiphysics v5.5 to simulate the magmatic system at SHV, using voids in the model space as proxies for magma bodies and pressurising their exterior surfaces (Figure 4.4). A full 3D model geometry is used, implementing a 2014 Digital Elevation Model (DEM) of the island [Stinton et al, 2015]. We use prolate cavities, or in the case of the shallow dyke, a rectangular cuboid cavity, to simulate deformation sources. To represent the mid-crustal magmatic system, we use a single large prolate source with an x-axis of 2000 m, y-axis of 2000 m, z-Axis of 4000 m, and centred at a depth of 9500 m [Gottsmann et al, 2020]. The model domain is large enough to avoid boundary effects (60 km x 60 km x 30 km), and an infinite element domain also surrounds the model geometry to further aid this. A tetrahedral mesh is used, as a tetrahedral mesh better represents 3D curved edges than a cuboid mesh, with higher mesh density surrounding the sources and volcanic edifice. A roller boundary surrounds the model, and the base of the model is fixed [Hickey et al, 2014]. Elastic behaviour is assumed for the rheology, to focus our efforts on the spatial deformation pattern rather than time-dependent phenomena. The position change of GPS and EDM points placed into the model geometry were recorded, and for EDM lines the relative changes of each end of a baseline were used to calculate the modelled line length change.

4.2.3 Modelling Approach

We utilise the prolate source model proposed by Gottsmann et al [2020] as a proxy for the mid-crustal magmatic system (Figure 4.4, Table 4.1). Using a series of forward models, we experiment with the further addition of a shallow prolate source or dyke, in order to explore differences in how the island's EDM and GPS monitoring networks record changes to pressurisation in different parts of the magmatic system. To do this we investigated three main scenarios.

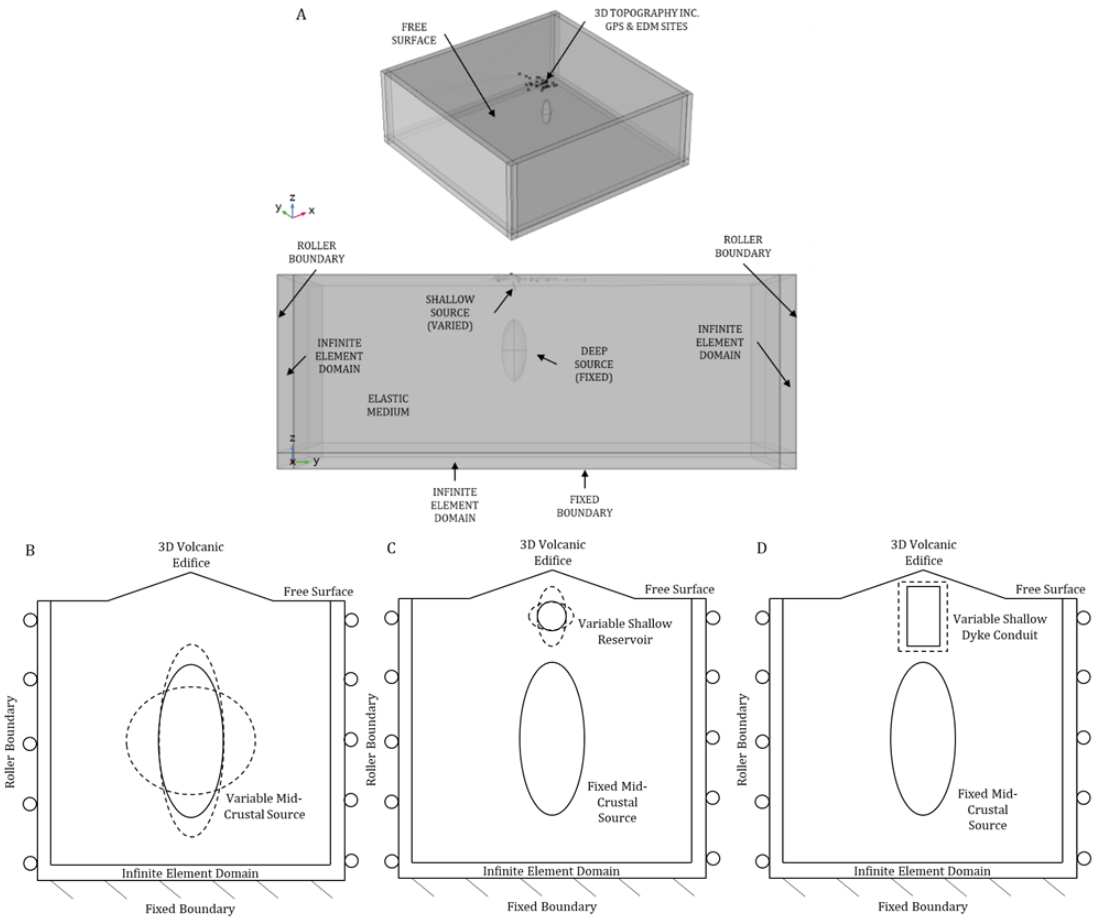

Figure 4.4 - Schematic diagrams of 3D Finite Element Model setup. The model is 3D in order to include the 3D topography of the island and non-axisymmetric deformation sources. The model size is 60 km x 60 km x 30 km, and an infinite element domain incorporated, to prevent boundary conditions from interfereing with interior results. The mesh was refined on the magma bodies and island topography. The domain is elastic. The base of the model is a fixed boundary, with roller boundaries on the edges and a free surface on top. A.) 3D view of the model geometry with 3D topography. B.) Sketch of model geometry for variation of mid-crustal reservoir (Table 4.1). C.) Sketch of model geometry for variation of a shallow reservoir (Table 4.2). D.) Sketch of model geometry for variation of a shallow dyke conduit (Table 4.3).

Firstly, in step one, we modelled the mid-crustal reservoir in isolation and conducted sensitivity tests on each source parameter independently (Table 4.1) to observe the mid-crustal magmatic system's effect on the surface deformation footprint. The source parameters employed were optimised on GPS data from 2003 [Gottsmann et al, 2020], so we also compared our modelled results to the recorded 2010-2019 GPS and EDM data to derive a slightly modified optimum

set of source parameters for this more recent deformation period. The updated mid-crustal reservoir parameters are also used in steps two and three.

Table 4.1 - 3D Model Source Parameters, Mid-Crustal Reservoir.

Source Parameters (Mid-Crustal Reservoir)				
Parameter	Low Margin	Default	High Margin	Step
Depth (m)	7000	9500	12000	500
X-Location	583500	588500	593500	1000
Y-Location	1843280	1848280	1853280	1000
a (x)-axis (m)	1840	1890	1940	50
b (y)-axis (m)	1960	2010	2060	50
c (z)-axis (m)	4960	5010	5060	50
Source Rotation (°)	-6.2	-1.2	3.8	1
Source Dip (°)	0	9	14	1
Source Heading (°)	118	128	138	5
Pressure (MPa)	1	11	21	1

Table 4.2 - 3D Model Source Parameters, Shallow Reservoir.

Source Parameters (Shallow Reservoir)					
Parameter	Mid-Crustal Source	Shallow Source			Step
		Low Margin	Default	High Margin	
Depth (m)	9500	500	1500	2500	100
X-Location	588500	583500	588500	593500	1000
Y-Location	1848280	1843280	1848280	1853280	1000
a (x)-axis (m)	2000	100	500	1000	100
b (y)-axis (m)	2000	100	500	1000	100
c (z)-axis (m)	4000	100	500	1000	100
Source Rotation (°)	0	0	180	330	30
Source Dip (°)	0	0	180	330	30
Source Heading (°)	0	0	180	330	30
Pressure (MPa)	10	-25	20	25	1

Table 4.3. 3D Model Source Parameters: Dyke Conduit Source. A.) Preliminary sensitivity test parameters. B.) Co-parameter variation.

A.) Source Parameters (Dyke Conduit Sensitivity Tests)

Parameter	Mid-Crustal Source	Dyke Conduit (Rectangular Cuboid)			Step
		Low Margin	Default	High Margin	
Depth (midpoint) (m)	9500	2500	3500	5000	100
X-Location	588500	583500	588500	593500	1000
Y-Location	1848280	1843280	1848280	1853280	1000
a (x)-axis (m)	2000	100	500	1100	100
b (y)-axis (m)	2000	N/A	5000	N/A	N/A
c (z)-axis (m)	4000	N/A	50	N/A	N/A
Source Rotation (°)	0	0	90	180	30
Source Dip (°)	0	-30	0	30	10
Source Heading (°)	0	0	0	180	30
Pressure (MPa)	10	-30	6	30	3

B.) Source Parameters (Dyke Conduit Co-Parameter Test)

Parameter	Mid-Crustal Source	Dyke Conduit (Rectangular Cuboid)			Step
		Low Margin	Default	High Margin	
Depth (midpoint) (m)	9500	N/A	2500	N/A	100
X-Location	588500	N/A	588500	N/A	1000
Y-Location	1848280	N/A	1848280	N/A	1000
a (x)-axis (m)	2000	N/A	500	N/A	100
b (y)-axis (m)	2000	N/A	5000	N/A	100
c (z)-axis (m)	4000	N/A	50	N/A	100
Source Rotation (°)	0	N/A	0	N/A	30
Source Dip (°)	0	N/A	0	N/A	30
Source Heading (°)	0	20	N/A	80	10
Pressure (MPa)	10	-30	N/A	30	3

In step two, we add a second, smaller, shallow, prolate reservoir between the top of the mid-crustal magmatic system and the edifice. The mid-crustal magmatic system is kept fixed, and sensitivity tests are conducted on the parameters defining the shallow source (Table 4.2). The shallow prolate source parameters are approximately based on the findings of studies into a shallow reservoir as part of a dual reservoir stacked magmatic system [Mattioli et al, 1998; Voight et al, 2006; Wadge et al, 2006; Elsworth et al, 2008; Hautmann et al, 2013]. Finally, in step three, we replace the shallow prolate source with a dyke conduit and conduct

further sensitivity tests (Table 4.3). To simulate the shallow magmatic system as a dyke conduit, a single rectangular cuboid source 500 m wide and 50 m thick was used [Costa et al, 2007; Mattioli et al, 1998; Hautmann et al, 2009; Linde et al, 2010] and extends from approximately 200 m below sea level (1.2 km below the vent) to a depth of 4.5 km below sea level. However, we use a thicker dyke (50 m) compared to previous estimates (2 m) to reduce the computational cost of our approach; a 2 m thick dyke in a 60 km wide model geometry required a computational mesh that was too dense for the efficient building and solving of the numerical model with available computer power and time. To confirm our modification would not produce erroneous results, we computed a simple comparison of a 2 m and a 50 m wide dyke using a 2D Finite Element model, and found that the increase in dyke thickness when applying a uniform pressure increase made no significant difference to the surface deformation response (Appendix A). Within step 3, a preliminary sensitivity test (step 3a) was undertaken for all parameters, which found that pressure and orientation were the two most important factors. The preliminary sensitivity tests also found that a better fit to the observed data was achieved with a shallower dyke depth, so for subsequent models the dyke conduit extended from 0.5 km above sea level to 3.5 km below sea level, approximately 500 m shallower than previous studies. The dyke was also made shorter by 1.2 km so as not to intersect with the mid-crustal source and to avoid mesh-building issues. Following the results of the preliminary sensitivity tests finding pressure and orientation to be the two most significant parameters, we ran a co-parametric test (step 3b) of pressure and orientation simultaneously with the updated dyke geometry, including negative overpressures to simulate magma cooling/withdrawal scenarios (Table 4.3). Conditions for the mid-crustal magmatic system were kept constant at 10 MPa with no rotation or tilt of the prolate source for both shallow source experiments (steps two and three), and results were again compared to the recorded 2010-2019 EDM and GPS data.

We compare our model results to the GPS and EDM datasets using a misfit function adapted from Hickey et al [2015b] to numerically evaluate how changes to the magmatic system affect the overall fit to the geodetic data. The misfit function, J, is defined as:

$$J = \sqrt{\sum f_i} \quad (1)$$

$$f_i = [(M_i - D_i) \times W_i]^2 \quad (2)$$

$$W_i = \frac{a_i}{\sum a_i} \quad (3)$$

$$a_i = \left|\frac{D_i}{E_i}\right| \quad (4)$$

where *M* corresponds to the modelled deformation, *D* corresponds to the observed deformation, *E* corresponds to the error, *W* corresponds to the weighting, and *i* is the index for each individual EDM baseline or GPS vector. The misfit function value was calculated for both GPS and EDM for each model iteration. The lower the misfit function value, the better the fit of the model to the observed data; and the greater the variation in the misfit function values for a given sensitivity test, the greater role that source parameter plays in dictating the surface deformation response.

Following the findings of the dyke conduit study, we further experimented with two new prospective EDM lines by adding a new EDM reflector (ENEW1) site on the south-eastern flank relatively close to the vent with an EDM baseline extending down to the pre-existing GPS site DRYG (DRYG-ENEW1), and a new EDM base station (ENEW2) on the southern coastline with a baseline extending up to the pre-existing reflector EDWR (ENEW2-EDWR). These sites were chosen to explore the deformation response on a part of the island with no present EDM coverage, and to see if the pattern of EDM line behaviour seen on the north and west of the vent is mirrored.

4.3. Results and Discussion

4.3.1 Mid-Crustal Magmatic System

Varying the parameters of a single, large, prolate source could not explain the pattern of observed EDM deformation alone (Figure 4.5), consistently either overestimating line length change on EDM2-EDLY/EDUF/EDGM on the north-western flank, or underestimating line length change on EDJH-EDHE (north-eastern flank), and to a lesser extent, underestimating line length change on EDBR-EDWR/EDUB (south-western flank). This pattern was repeated for all parameters tested, with the mid-crustal source producing a symmetrical deformation field which could not account for the asymmetric EDM line length changes observed. The GPS response to mid-crustal source parameter variation is broadly in line with observed data, with sites placed far from the vent experiencing more radial deformation than sites close to the vent. Notably, this model also could not account for the observed movement of HERM.

Naturally, the misfit function results for the GPS network provided a closer fit to the observed values than the EDM network (Figure 4.6), as the mid-crustal magmatic system geometry was optimised on GPS data from 2003 [Gottsmann et al, 2020]. Varying the depth of the source also shows that EDM is unresponsive to changes in a mid-crustal source when compared to the sensitivity of the GPS data, and only began to show a significant response at depths of less than 10,000 m. The closest fit to the GPS data was obtained by a mid-crustal prolate source with a midpoint at 9500 m pressurised at 10 or 11 MPa (Figure 4.6), with other parameter results provided in Table 1 as the mid-crustal source values for steps two and three. These results combined imply that there is a shallower aspect to the magmatic system that is at least partially dictating the line length changes seen on EDJH-EDHE, and the behaviour of the EDM network as a whole, as the EDM network is more sensitive to shallower pressurisation.

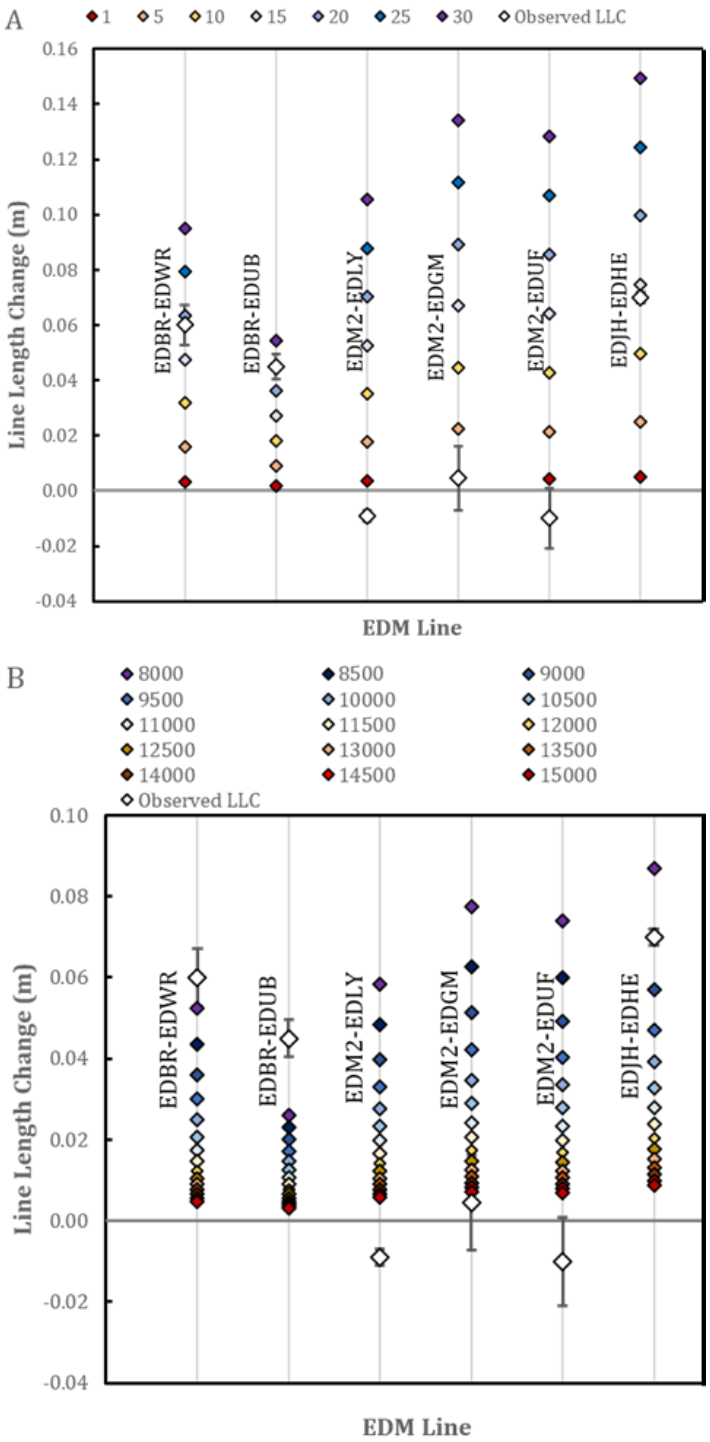

Figure 4.5 - Mid-crustal source variation EDM results. Sensitivity test results of varying the; A.) Pressure (MPa), and B.) Depth (m), of a single prolate mid-crustal source compared against recorded EDM data. Variation of the mid-crustal source alone produces a broadly symmetrical deformation pattern across all EDM lines, which fails to account for the far greater magnitude of deformation observed on EDJH-EDHE relative to other EDM lines (observed data shown in white).

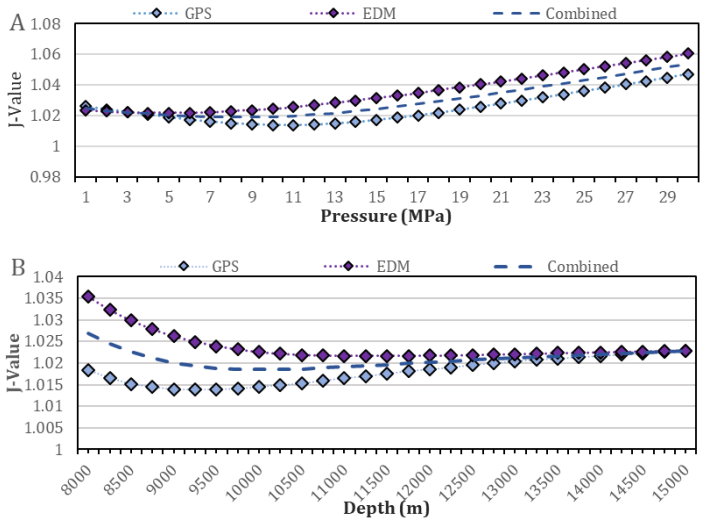

Figure 4.6 - Mid-crustal source sensitivity test results. Misfit (J) values with variation of; A.) Pressure and B.) Depth, of a md-crustal prolate source. The lower the misfit the better the fit of the model to the observed data. The model produces a closer fit to the GPS data than the EDM data, with different optimum pressures (EDM – 4 MPa; GPS – 10 or 11 MPa) and depths (EDM – 11500 m; GPS – 9250 m) for the two datasets when observed independently. Other sensitivity test results are available in appendix B.

4.3.2 Incorporation of Shallow Pressure Sources

The effect of pressure changes in a shallow source is expected to primarily effect the area closest to vent, and be relatively minor in amplitude compared to the impact of the mid-crustal magmatic system [Hautmann et al, 2009]. As the deformation signal of a shallow source would likely be confined to the area closest to then vent, the EDM network should theoretically be better placed to detect changes than the GPS sites, as EDM reflectors are located closest to the vent (Figure 1). We test this assumption using a shallow magma reservoir or a shallow dyke as an additional deformation source, in tandem with the mid-crustal source.

4.3.2.1 Addition of a Shallow Prolate Source

Firstly, a second, shallow prolate magma reservoir source was added, above the mid-crustal magma reservoir (Table 4.2). Sensitivity tests of the parameters defining the second prolate source showed that changes to a shallow deformation source of this type produce negligible variation in the modelled surface deformation patterns (Figure 4.7). The lack of deformation response in both GPS and EDM measurements suggests that the deformation signal from the mid-crustal source overprints the effect of any shallow reservoir-style source (Figure

4.7). The only parameter variations that induced measurable EDM line length changes were variations to the X and Y axes of the shallow source (Figure 4.7) likely due to the asymmetrical near-field deformation this begins to produce in contrast to the symmetrical deformation field of the 'default' shallow source or the fixed mid-crustal source (Table 4.2). The GPS network was also largely unresponsive to changes in the shallow source, although it did result in some minor movement at HERM and LGRD, both situated closest to the vent, and therefore to the source itself (Appendix C).

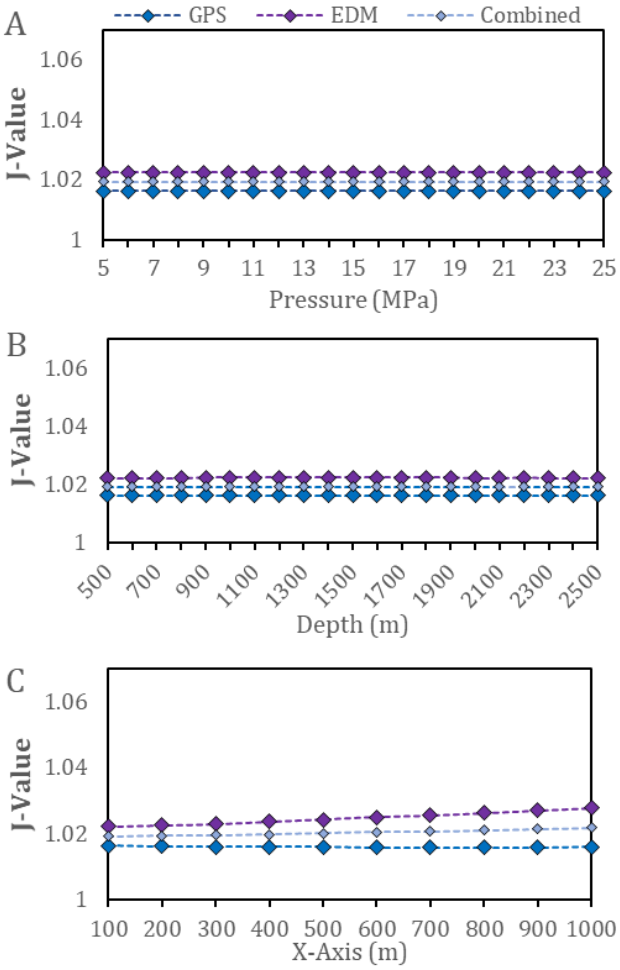

Figure 4.7 - Shallow reservoir sensitivity test results. Changes to misfit (J) value with; A.) Pressure variation of a shallow reservoir style source and a fixed mid-crustal source. B.) Depth variation of a shallow reservoir source and a fixed mid-crustal source; and C.) X-Axis variation of the shallow source with a fixed mid-crustal source. There is no change to the fit of the model with variation of the shallow source pressure or depth, but there is some minor impact on fit to the EDM data alone when the horizontal axes of the shallow source are changed. The modelled GPS network did not detect any deformation changes from X-Axis variation. Other sensitivity test results are available in appendix B.

From these results, we can infer that that when the deformation signal produced by the shallow source is symmetrical, it cannot be distinguished from that of the mid-crustal magmatic system. However, asymmetric deformation fields produced by the shallow source, such as when the horizontal axes of the shallow source were non-equal, can have a measurable effect on the EDM monitoring network. The fact that the near-vent asymmetric deformation effects are not picked up by the GPS network, HERM and LGRD aside, suggests the deformation effect produced by the shallow source only effects the area closest to the vent, an area of the volcanic edifice the EDM network has far greater coverage of compared to the GPS network.

4.3.2.2 Addition of a Shallow Dyke Source

Our preliminary sensitivity tests of a shallow dyke conduit source showed that variation in certain source parameters had a significant impact on the fit to EDM data, far more so than that of GPS, and that the asymmetric deformation field produced was measurable above that produced by the mid-crustal magmatic system (Figure 4.8). The two parameters that produced the most significant changes to misfit values were pressure and rotation, with misfit values indicating the optimal dyke orientation is approximately north west-south east (Figure 8). Therefore, we also undertook a further co-parametric sensitivity test of pressure and orientation in tandem, with a more focused orientation parameter range than the original sensitivity tests (Table 4.3).

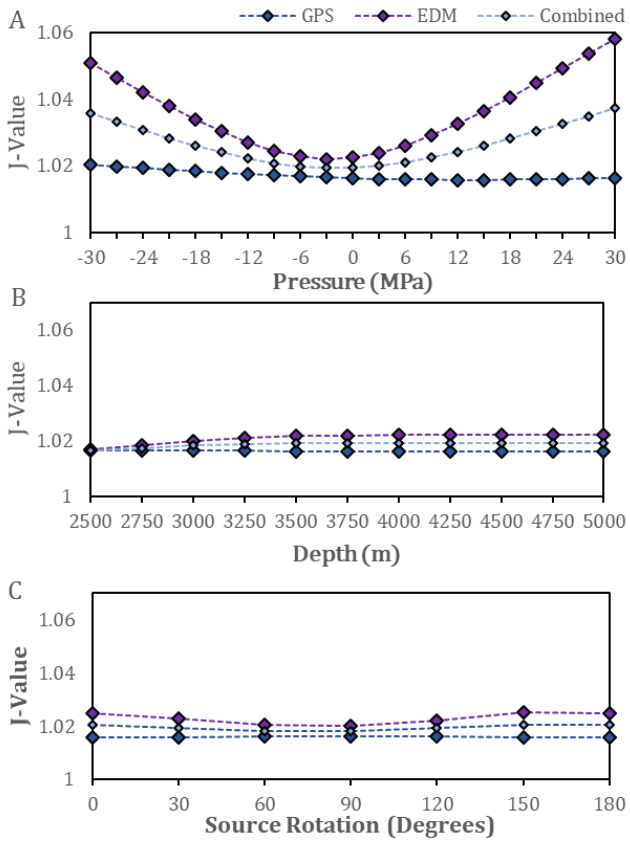

Figure 4.8 - Shallow dyke conduit sensitivity test results. Changes to misfit (J) value with results of sensitivity tests for A.) Pressure in a shallow dyke conduit. B.) Depth of shallow dyke conduit; and C.) Rotation of shallow dyke conduit. Pressure was the parameter results were most sensitive to, followed by source rotation. Both EDM and GPS networks were largely unresponsive to depth changes, except for EDM at depths shallower than 3000 m, with the closest fit obtained at 2500 m. Other parameter variations largely failed to produce meaningful deformation responses, although other parameters that changed the symmetry of the deformation field produced by the shallow source such as source heading, x-location, and y-location, did have a minor effect. The GPS response to all parameter variation was negligible, with pressure being the exception, and this was extremely minor when compared to the response to pressure recorded by EDM. Other sensitivity test results are available in appendix B.

We found that the closest fit to the observed EDM data was achieved by a shallow dyke orientated 60° anti-clockwise from north (NNW-SSE) and a pressure of -12 MPa (Figure 4.9). This dyke orientation is consistent with the tectonic stress field and fault structures surrounding Montserrat [Feuillet et al, 2010] and previous modelling studies into the shallow magmatic system [Mattioli et al, 1998; Costa et al, 2007; Hautmann et al, 2009; Linde et al, 2010]. The deformation field produced by the dyke was small, and only affected a local area of the edifice

close to the vent; further away from the vent the dyke-derived deformation field weakened until it was overwritten by that from the mid-crustal magmatic system. The overwhelming majority of the GPS network is situated too far away from the vent to detect the deformation field changes controlled by a shallow dyke conduit source, with the only exception being HERM (and possibly LGRD). However, EDM reflectors are situated close enough to the vent to respond to these shallow source changes.

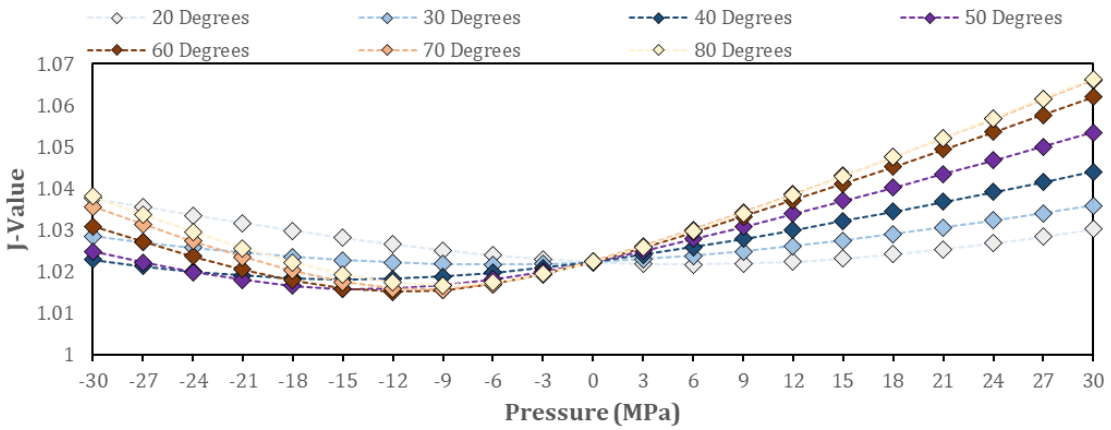

Figure 4.9 - Co-Parameter variation misfit results. Misfit 'J' value results from co-parameter variation of pressure and orientation of a shallow dyke source above a fixed mid-crustal source. The closest fits were obtained by negative pressures in the shallow system. The best overall fit was in a dyke orientated at 60° rotation (NNW-SSE) and a pressure of -12MPa.

Negative pressure changes in the dyke source produced line lengthening on all EDM lines (Figure 4.10), with EDJH-EDHE the most responsive. This pattern is generated due to EDM reflectors close to the vent showing negative radial deformation (movement towards the vent) in response to negative shallow pressurisation. In contrast, the deformation response of EDM stations further from the vent are determined by the positive pressurisation of the mid-crustal magmatic system, resulting in positive radial deformation (movement away from the vent) (Figure 4.11). The opposite movement of both ends of the EDM baselines produces positive EDM line lengthening, as the mid-crustal system pressurises (possibly through magma supply) and the shallow system depressurises, indicating volume contraction, possibly through cooling and contraction or magma withdrawal.

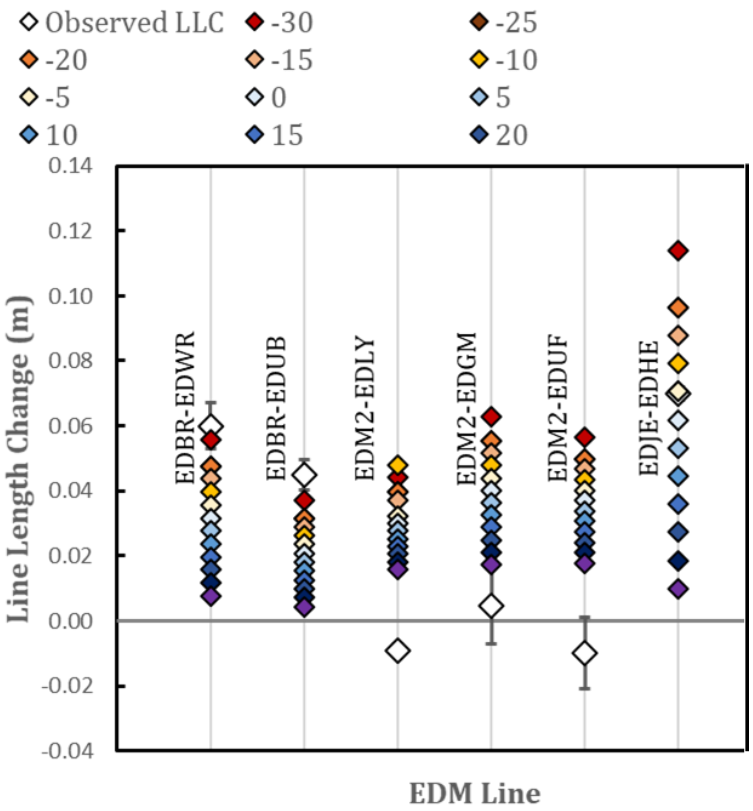

Figure 4.10 - Co-Parameter variation EDM results. EDM line responses to pressure variation of a dyke source (placed above a mid-crustal magmatic system pressurised at 10 MPa) at a rotation of 60° from north (angled NNW-SSE) Different coloured symbols represent results of different source pressurisation (MPa). The increased sensitivity of the north-eastern flank (specifically reflector site EDHE) to pressure changes in a dyke source is seen here, with negative pressurisation generating greater line length extension.

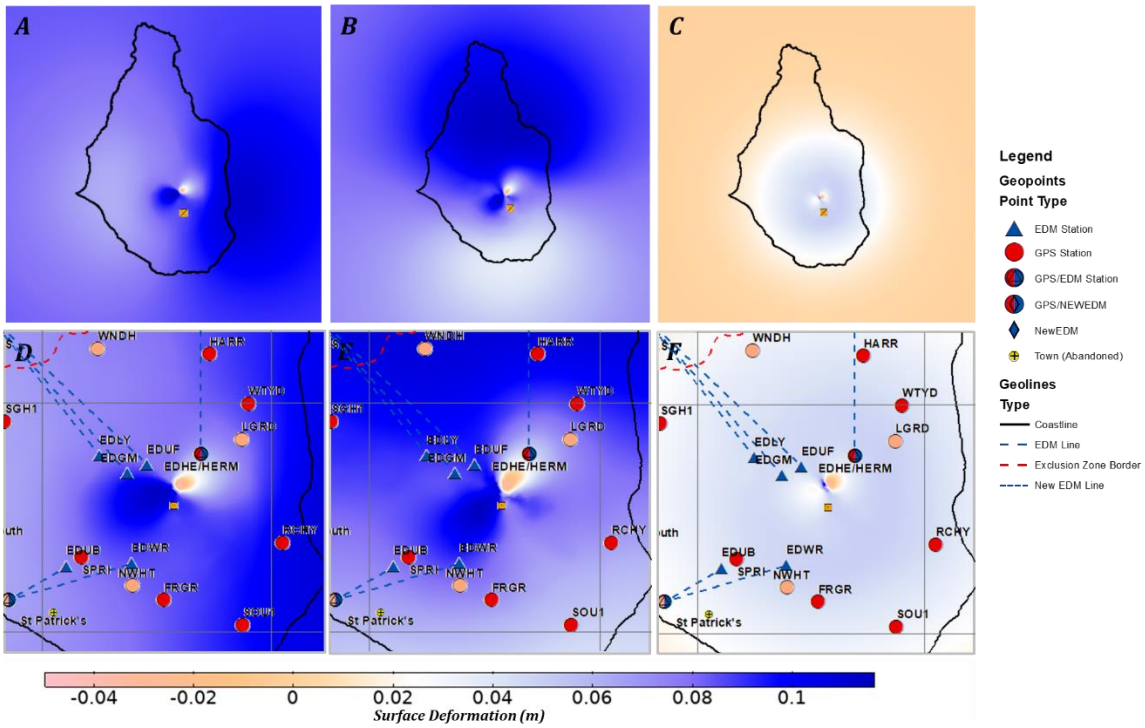

Figure 4.11 - Surface deformation maps, cropped from the full model domain. Plot of modelled surface deformation, with a mid-crustal source pressurised at 10 MPa, and a shallow dyke orientated at 60° from north and pressurised at -12 MPa. The top row shows the full view of Montserrat with deformation patterns predominantly caused by the mid-crustal magmatic system; A.) East-west Deformation; B.) North-south Deformation; and C.) Vertical Deformation. The bottom row shows zoomed-in near the vent, better highlighting the deformation field produced by the dyke: D.) East-west Deformation; E.) North-south deformation;, and F.) Vertical Deformation. All maps are orientated with north at the top.

The deformation generated by our best-fitting shallow dyke conduit, orientated NNW-SSE and pressurised at -12 MPa is perpendicular to the strike of the dyke (i.e., ENE-SWS). The interaction of the shallow dyke-derived deformation and surface topography means that only a small area of significant deformation is produced that overprints the more dominant deformation signal of the mid-crustal system (Figure 4.11). This area encompasses the GPS site HERM, and could be a possible explanation for the behaviour of HERM with regards to its velocity vectors often in contrast to the pattern of most other GPS sites.

Seismic data indicates that over the course of the 2010-2019 period earthquake activity has decreased, and the average depth of volcanotectonic (VT) quakes has changed [Cole et al, MVO OFR 11-02; Stinton et al, MVO OFR 20-05,]. In

2011 the average hypocentre depth was around 1 km below sea level, with a number of quakes above sea level within the edifice itself. By contrast, the average hypocentre depth of earthquakes under the SHV in late 2019/early 2020 was 2 km, with only very few VT quakes at a depth of less than 1 km below sea level (Appendix D).This suggests that the upper part of the dyke conduit system is possibly showing less movement of magma, and that cooling and/or contraction could be occurring in this part of the dyke conduit system [White and McCausland, 2016].

4.3.3 Prospective New EDM Lines

In our tests with two new prospective EDM lines (Figure 4.12) the modelled results show that on the south-eastern flank DRYG-ENEW1 was relatively unresponsive to pressure changes in the shallow dyke conduit (Figure 4.13). This is partly due to the shorter starting line length when compared with EDM baselines on the northern flank, as points further away from the vent experience a greater radial deformation effect from the pressurisation of the mid-crustal magmatic system. The relative unresponsiveness of DRYG-ENEW1 is also to some extent a mirror of the reduced line length change seen on EDM2-EDLY/EDGM/EDUF on the north-western flank (when compared with EDJH-EDHE). However, unlike the line length behaviour of EDM2-EDLY/EDGM/EDUF, DRYG-ENEW1 shows increased line lengthening with increasing pressure, the inverse of the modelled behaviour of all other EDM lines in response to the over- or under-pressurisation of a dyke conduit source.

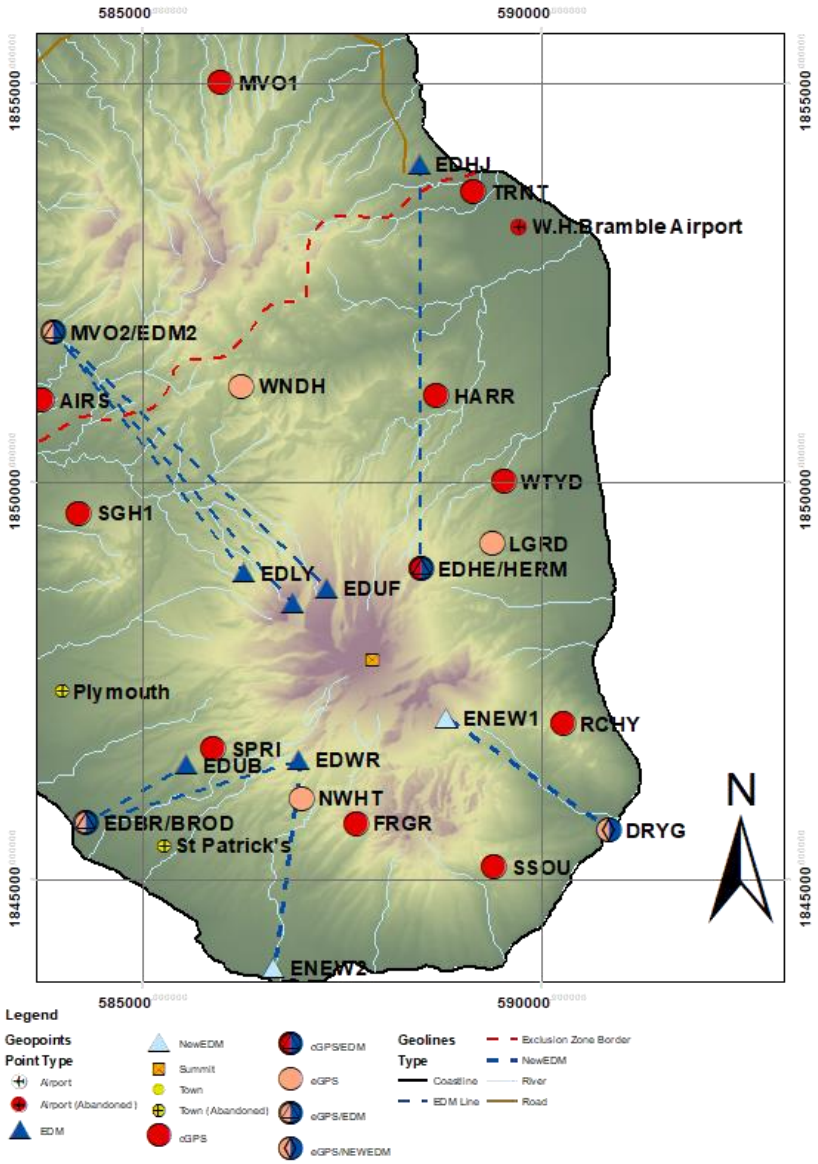

Figure 4.12 - EDM monitoring network map. Map of the EDM monitoring network this study draws data from on Montserrat, with 2 additional theoretical EDM line locations shown which were experimented with in this study. These two prospective EDM lines were incorporated to infer deformation behaviour on the southern and south-eastern flanks, which currently lack EDM monitoring capability.

ENEW2-EDWR behaves more in line with other EDM baselines, and produces very similar results to EDBR-EDWR due to sharing a reflector. The reflector EDWR on the south-western flank is responding to the pressurisation of the dyke conduit in a similar manner to EDHE on the north-eastern flank (Figures 10 and 13). While the prospective EDM baseline ENEW2-EDWR does not provide much insight above and beyond what EDBR-EDWR can offer, it does help to illustrate

that it is the reflector, not the base station, which defines the line length behaviour in relation to shallow source pressurisation.

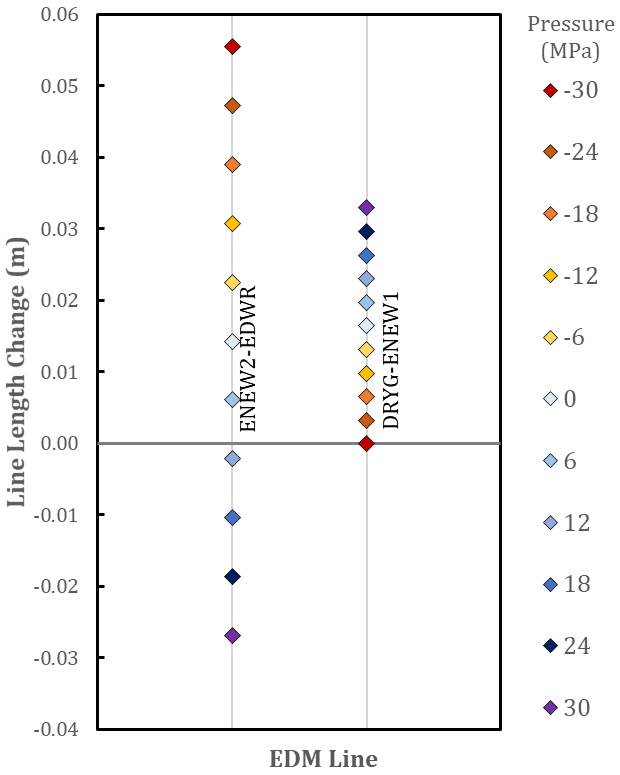

Figure 4.13 - Prospective EDM line modelling results. Predicted line length changes due to pressure variation in a shallow dyke source orientated 60° from north (north-north west-south south east) on the two prospective new EDM lines.

In summary, a new EDM line on the south-eastern flank of the volcano (DRYG-ENEW1) would likely not be optimally placed to respond to pressure changes in the shallow magmatic system despite filling a geographical gap in the spatial coverage of the EDM network, as well as being potentially difficult to access due to its position in the island's exclusion zone. On the other hand, while ENEW2-EDWR on the south-western flank is sensitive to shallow source pressurisation, it likely only serves to duplicate the results of EDBR-EDWR, which when combined with the difficulty in accessing the base station site in the exclusion zone means it may not provide good cost-benefit trade-offs.

4.3.4 Implications

The GPS network on Montserrat is well placed to monitor changes to the mid-crustal magmatic system. However, our results suggest that changes in the

shallow system would likely not be detected by the GPS network. The surface deformation footprint of the shallow system is small, partially overprinted by that of the mid-crustal source and highly asymmetrical, and as a result displays significant local variation. The only GPS site situated within the predicted area of effect of the shallow dyke source is HERM, which potentially explains why its behaviour is different to that of the rest of the GPS network. The placement of HERM and EDHE within the deformation footprint (Figure 4.11) of our modelled shallow dyke source is potentially significant, as the east-west, north-south, and vertical deformation components of the shallow dyke source have different relative amplitudes. The co-location of HERM and EDHE is in an area which our model predicts responds strongly to the north-south displacement component of the shallow dyke's deformation field, weakly to the east-west displacement component, and insignificantly to the vertical displacement component. This has the effect of HERM/EDHE's north-south displacement being controlled primarily by the shallow dyke conduit, resulting in southward movement as the dyke contracts. However, the east-west displacement and vertical displacement of the site would be controlled by the behaviour of the mid-crustal source, causing the uplift and eastward component of the migration of the site observed between 2010-2019. There could also be an element of edifice decoupling causing the ridge upon which HERM and EDHE are situated to deform in a different way to the rest of the edifice [McPherson, 2013].

EDM reflectors are generally situated much closer to the vent than GPS stations on Montserrat, and as a result are better placed to respond to changes in the shallow system. Interpretation of EDM line length changes should consider that each end of the line is responding to different parts of the magmatic system. EDM stations away from the vent respond to changes in the mid-crustal magmatic system similar to the GPS network, whereas the EDM reflectors close to the vent respond predominantly to changes in the shallow system. However, the exact location of the EDM reflectors is vital due to the substantial local variation in surface deformation behaviour close to the vent produced by topographical effects and the likely asymmetry of the deformation field associated with the shallow dyke. EDM line EDJH-EDHE is best placed to detect changes in the shallow system at the SHV, as the EDM reflector EDHE is within the deformation

footprint of the shallow dyke conduit (Figure 4.11), as is the GPS station HERM. The EDM lines EDBR/EDUB-EDWR are also well placed to detect changes in the shallow dyke conduit.

From our results showing best fits to negative pressurisation in the shallow system, and the behaviour of HERM and EDJH-EDHE, we can interpret that the current shallow system behaviour is one of cooling and contraction, or magma withdrawal. The results from the GPS network suggest the mid-crustal magmatic system is still being pressurised at about 10 MPa between 2010-2019, assuming the deformation source is magmatic, but it is not causing any reactivation in the shallow system at present. The overpressure of the mid-crustal magmatic system would likely drop during an eruptive phase as magma moves up through the system, positively pressurising the shallow dyke conduit. The likely pattern of pressurisation in the immediate build-up to eruptive activity, would have the predicted effect of flipping the pattern of behaviour in both EDM and GPS compared to the current pause state being, with GPS sites distal to the vent moving inwards, HERM showing increased radial deformation and northward migration, EDJH-EDHE, EDBR-EDWR, and EDBR-EDUB showing significant shortening, and EDM2-EDLY, EDM2-EDGM, and EDM2-EDUF relatively unresponsive. For future monitoring of the island, this could mean that over-pressurisation of the shallow conduit would present as outward radial deformation and northward movement of HERM, and line length shortening of EDJH-EDHE, as these would be the best indicators of shallow system behaviour.

For application to other volcanoes, we suggest that EDM provides a cheaper and safer way of effectively monitoring the shallow magmatic system than GPS as reflectors can be set up quickly, measurements taken from a safe distance, and equipment can be replaced at much cheaper costs if destroyed. Covering multiple flanks to find possible dyke conduit orientations and monitor shallow system behaviour is important, as half the area close to the vent may still be relatively unresponsive to a dyke source pressurisation. Installing multiple GPS monitoring sites close to the vent may be impossible for many volcano observatories, either due to financial or safety restraints, leading to limited and incomplete coverage of shallow system processes. For installing new sites, priority should be given to

the flanks perpendicular to the likely dyke orientation as determined by the regional stress field, as the areas perpendicular to the strike of the dyke are going to be the most responsive to pressurisation of the dyke.

4.3.5 Limitations

The model uses a simple homogenous elastic domain, which does not consider the effects of viscoelasticity [Del Negro et al, 2009; Sigmundsson et al, 2020; Head et al, 2019] or temperature variation [Gudmundsson, 2011] on rheological behaviour. A temperature dependent viscoelastic medium would likely result in lower overpressure requirements for the mid-crustal source due to thermal weakening of the Young's modulus and enhanced deformation from the viscous component [Foroozan et al, 2010; Head et al, 2021].The pressure value of the shallow dyke source is unlikely to be affected, as the colder shallow crust is more likely to behave in an elastic manner. The shape of the dyke is a simplified rectangular cuboid, with a thickness of 50 m, to reduce mesh density and RAM requirements. Previous investigations into the dyke found a dyke conduit width as narrow as 2 m [Costa et al, 2007; Hautmann et al, 2009]. To quantify the effect of the increased dyke thickness imposed upon our study, we ran a comparison of a 2 m wide dyke and a 50 m wide dyke with equal pressure and geometry in a 2D elastic medium. There is no significant difference to the surface deformation response caused by the increase in dyke thickness (Appendix A), and therefore this limitation does not have a significant impact on our deformation results. However, future work should endeavour to use a 2 m wide dyke as suggested by previous work. This improvement may allow for an investigation into possible volume contraction rates to compare against thermal models in order to potentially distinguish between magma withdrawal and magma cooling and contraction as the physical mechanism driving the under-pressurisation of the dyke source.

4.4 CONCLUSIONS

1. The pattern of EDM line length changes recorded at SHV between 2010 and 2019 cannot be solely explained by the effects of a mid-crustal deformation source, the proxy of the mid-crustal magmatic system. The radial deformation produced by the mid-crustal source is too symmetrical to fit the observed data. The modelled deformation produced by a singular mid-crustal source provides a closer fit to the GPS data, excluding the site HERM, as the GPS network is better placed to respond to a mid-crustal focused deformation source than the EDM network.

2. A shallow magma reservoir-style prolate source (in addition to the mid-crustal source) also cannot explain the pattern of EDM line length changes observed, and variations to such a source has a negligible impact on EDM and GPS networks alike. This is due to the deformation field produced by such a source being symmetrical, and therefore is easily overprinted by the deformation field produced by the mid-crustal magmatic system.

3. The modelled spatial deformation field is sensitive to variations of a dyke conduit-style shallow source, with pressure and orientation parameters being the most important. However, the spatial extent of the deformation field produced by the shallow source is limited, and only effects a small area of the edifice close to the vent; further away it weakens until it is overwritten by the mid-crustal magmatic system. The overwhelming majority of the GPS network is situated too far from the vent to detect the deformation field changes controlled by a shallow dyke conduit source, with the only exception being HERM. However, EDM reflectors are situated close enough to the vent to respond to these shallow source changes.

4. Varying the orientation and pressure of a shallow dyke conduit source simultaneously found that the closest fit to the observed EDM data was for a dyke orientated NNW-SSE (60° from north) with a pressure of -12 MPa. Negative pressure values consistently produced closer fits to the observed data than positive pressure values. This could be explained by cooling and contraction, or magma withdrawal, while the mid-crustal magmatic system is still being pressurised (to 10 MPa), possibly due to magma supply from depth.

5. At our dyke orientation of best fit, negative pressurisation of the dyke causes a small area of the edifice on the north-eastern flank of the vent to deform to the south-west. This area includes the GPS site HERM and the EDM reflector EDHE. We conclude that the behaviour of HERM is potentially due to HERM responding to a combination of pressure changes in the shallow dyke conduit and mid-crustal system, while the rest of the GPS network responds to pressure changes in the mid-crustal system only.

6. For future monitoring purposes, the behaviour of HERM and the EDM network, (especially EDJH-EDHE) are likely indicative of pressure changes in the shallow system. Outward radial deformation and northward migration of HERM, or line length shortening of EDJH-EDHE, and EDBR-EDUB/EDWR, could indicate pressurisation of the shallow magmatic system and magma migration upwards from the mid-crustal system.

7. The mid-crustal magmatic system is still being pressurised, possibly by magma supply from depth. However, the shallow magmatic system is possibly undergoing cooling and contraction or magma withdrawal, and is not currently being recharged by the mid-crustal system. This is supported by the changing nature of volcanotectonic seismic activity indicating the average depth of earthquake hypocentres has moved deeper between 2010 and 2019.

8. EDM provides a safer, quicker, and cheaper way of effectively monitoring shallow system processes than GPS, as coverage of multiple flanks close (within 1 km) to the vent is vital to understanding the behaviour of dyke conduit-shaped shallow magmatic system processes, as they produce highly asymmetrical deformation fields. When choosing monitoring sites targeting the shallow system, preference should be given to sites perpendicular to the expected dyke orientation as determined by the regional stress field, as these areas are more sensitive to deformation changes from the expected geometry of the shallow magmatic system.

AUTHOR CONTRIBUTIONS

A.J, J.H, and K.P derived the lines of investigation. Primary data collection was undertaken by K.P. and R.S. Data post-processing, modelling, and analysis of results was done by A.J. Manuscript drafting was undertaken by A.J, with all authors contributing to the final version.

ACKNOWLEDGEMENTS

The authors have no acknowledgements to make at this time.

SUBMISSION INFORMATION

This paper will be submitted to the journal Volcanica.

REFERENCES

Biggs, J., and Pritchard, M. E. (2017). Global Volcano Monitoring: What Does It Mean When Volcanoes Deform? Elements, 13(1), 17–22. https://doi.org/10.2113/gselements.13.1.17

Bonaccorso, A., Currenti, G., and del Negro, C. (2013). Interaction of volcano-tectonic fault with magma storage, intrusion and flank instability: A thirty years study at Mt. Etna volcano. Journal of Volcanology and Geothermal Research, 251, 127–136. https://doi.org/10.1016/j.jvolgeores.2012.06.002

Cabaniss, H. E., P. M. Gregg, S. L. Nooner, and W. W. Chadwick Jr. (2020). Triggering of eruptions at Axial Seamount, Juan de Fuca Ridge, Scientific Reports, pp. 1–11, doi:10.1038/s41598-020-67043-0.

Christopher, T. E., Humphreys, M. C. S., Barclay, J., Genareau, K., de Angelis, S. M. H., Plail, M., and Donovan, A. (2014). Chapter 17 Petrological and geochemical variation during the Soufrière Hills eruption, 1995 to 2010. Geological Society, London, Memoirs, 39(1), 317–342. https://doi.org/10.1144/m39.17

Currenti, G., Del Negro. C and Ganci. G. (2007). Modelling of ground deformation and gravity fields using finite element method: An application to Etna volcano, Geophysical Journal International, 169(2), 775–786, doi:10.1111/j.1365-246X.2007.03380.x.

del Negro, C., Currenti, G., and Scandura, D. (2009). Temperature-dependent viscoelastic modeling of ground deformation: Application to Etna volcano during the 1993–1997 inflation period. Physics of the Earth and Planetary Interiors, 172(3–4), 299–309. https://doi.org/10.1016/j.pepi.2008.10.019

Dragoni, M., and Magnanensi, C. (1989). Displacement and stress produced by a pressurized, spherical magma chamber, surrounded by a viscoelastic shell.

Physics of the Earth and Planetary Interiors, 56(3–4), 316–328. https://doi.org/10.1016/0031-9201(89)90166-0

Elsworth, D., Mattioli, G., Taron, J., Voight, B., and Herd, R. (2008). Implications of Magma Transfer Between Multiple Reservoirs on Eruption Cycling. Science, 322(5899), 246–248. https://doi.org/10.1126/science.1161297

Feuillet, N., Leclerc, F., Tapponnier, P., Beauducel, F., Boudon, G., le Friant, A., Deplus, C., Lebrun, J. F., Nercessian, A., Saurel, J. M., and Clément, V. (2010). Active faulting induced by slip partitioning in Montserrat and link with volcanic activity: New insights from the 2009 GWADASEIS marine cruise data. Geophysical Research Letters, 37(19), n/a. https://doi.org/10.1029/2010gl042556

Fialko, Y., Khazan, Y., and Simons, M. (2001). Deformation due to a pressurized horizontal circular crack in an elastic half-space, with applications to volcano geodesy. Geophysical Journal International, 146(1), 181–190. https://doi.org/10.1046/j.1365-246x.2001.00452.x

Fournier, N., and Chardot, L. (2012). Understanding volcano hydrothermal unrest from geodetic observations: Insights from numerical modeling and application to White Island volcano, New Zealand. Journal of Geophysical Research: Solid Earth, 117(B11), n/a. https://doi.org/10.1029/2012jb009469

Geirsson, H., LaFemina, P., ÁRnadóttir, T., Sturkell, E., Sigmundsson, F., Travis, M., Schmidt, P., Lund, B., Hreinsdóttir, S., and Bennett, R. (2012). Volcano deformation at active plate boundaries: Deep magma accumulation at Hekla volcano and plate boundary deformation in south Iceland. Journal of Geophysical Research: Solid Earth, 117(B11), n/a. https://doi.org/10.1029/2012jb009400

Gottsmann, J., and Odbert, H. (2014). The effects of thermomechanical heterogeneities in island arc crust on time-dependent preeruptive stresses and the failure of an andesitic reservoir. Journal of Geophysical Research: Solid Earth, 119(6), 4626–4639. https://doi.org/10.1002/2014jb011079

Gottsmann, J., Flynn, M., and Hickey, J. (2020). The Transcrustal Magma Reservoir Beneath Soufrière Hills Volcano, Montserrat: Insights From 3-D Geodetic Inversions. Geophysical Research Letters, 47(20). https://doi.org/10.1029/2020gl089239

Gottsmann, J., Komorowski, J. and Barclay, J. (2017). Volcanic Unrest and Pre-eruptive processes: A Hazard and Risk perspective. Advs in Volcanology (2019), pp.1-21.

Gudmundsson, A. (2011). Rock Fractures in Geological Processes (1st ed.). Cambridge University Press.

Hautmann, S., Gottsmann, J., Sparks, R. S. J., Costa, A., Melnik, O., and Voight, B. (2009). Modelling ground deformation caused by oscillating overpressure in a dyke conduit at Soufrière Hills Volcano, Montserrat. Tectonophysics, 471(1–2), 87–95. https://doi.org/10.1016/j.tecto.2008.10.021

Hautmann, S., Hidayat, D., Fournier, N., Linde, A. T., Sacks, I. S., and Williams, C. P. (2013). Pressure changes in the magmatic system during the December 2008/January 2009 extrusion event at Soufrière Hills Volcano, Montserrat (W.I.), derived from strain data analysis. Journal of Volcanology and Geothermal Research, 250, 34–41. https://doi.org/10.1016/j.jvolgeores.2012.10.006

Hickey, J. (2015). Constraining Volcanic Unrest with Integrated Geodetic Modelling. Ph.D. University of Bristol.

Hickey, J., Gottsmann, J., Mothes, P., Odbert, H., Prutkin, I., and Vajda, P. (2017). The Ups and Downs of Volcanic Unrest: Insights from Integrated Geodesy and Numerical Modelling. Advances in Volcanology, 203–219. https://doi.org/10.1007/11157_2017_13

Hickey, J., Gottsmann, J., Nakamichi, H., and Iguchi, M. (2016). Thermomechanical controls on magma supply and volcanic deformation:

application to Aira caldera, Japan. Scientific Reports, 6(1). https://doi.org/10.1038/srep32691

Hickey, J., Lloyd, R., Biggs, J., Arnold, D., Mothes, P., and Muller, C. (2020). Rapid localized flank inflation and implications for potential slope instability at Tungurahua volcano, Ecuador. Earth and Planetary Science Letters, 534, 116104. https://doi.org/10.1016/j.epsl.2020.116104

Johnson, J. H., Poland, M. P., Anderson, K. R., and Biggs, J. (2019). A Cautionary Tale of Topography and Tilt from Kīlauea Caldera. Geophysical Research Letters, 46(8), 4221–4229. https://doi.org/10.1029/2018gl081757

Linde, A. T., Sacks, S., Hidayat, D., Voight, B., Clarke, A., Elsworth, D., Mattioli, G., Malin, P., Shalev, E., Sparks, S., and Widiwijayanti, C. (2010). Vulcanian explosion at Soufrière Hills Volcano, Montserrat on March 2004 as revealed by strain data. Geophysical Research Letters, 37(19), n/a. https://doi.org/10.1029/2009gl041988

Masterlark, T. (2007). Magma intrusion and deformation predictions: Sensitivities to the Mogi assumptions. Journal of Geophysical Research, 112(B6). https://doi.org/10.1029/2006jb004860

Mattioli, G. S., Dixon, T. H., Farina, F., Howell, E. S., Jansma, P. E., and Smith, A. L. (1998). GPS measurement of surface deformation around Soufriere Hills Volcano, Montserrat from October 1995 to July 1996. Geophysical Research Letters, 25(18), 3417–3420. https://doi.org/10.1029/98gl00931

Mattioli, G. S., Herd, R. A., Strutt, M. H., Ryan, G., Widiwijayanti, C., and Voight, B. (2010). Long term surface deformation of Soufrière Hills Volcano, Montserrat from GPS geodesy: Inferences from simple elastic inverse models. Geophysical Research Letters, 37(19), n/a. https://doi.org/10.1029/2009gl042268

McPherson, E. E. (2013, August). A model of short term surface deformation of Soufriere Hills Volcano, Montserrat constrained by GPS geodesy.

https://rc.library.uta.edu/uta-ir/bitstream/handle/10106/23910/McPherson_uta_2502M_12371.pdf?sequence=1&isAllowed=y

Mogi, K. (1958), Relations between the eruptions of various volcanoes and the deformations of the ground surfaces around them, Bulletin of the Earthquake Research Institute, 36, 99–134.

Stinton, A. J. Montserrat Volcano Observatory. (2015, July). A new Digital Elevation Model of the Soufrière Hills Volcano, Montserrat. http://www.mvo.ms/pub/Open_File_Reports/MVO_OFR_15_01-New_Soufriere_Hills_DEM.pdf

Cole, P., Bass, V., Christopher, T., Murrell, C., Odbert, H., Smith, P., Stewart, R., Stinton, A., Syers, R., Williams, P. Montserrat Volcano Observatory. (2011, February). MVO scientific report for volcanic activity between 1 May 2011 and 31 October 2011 prepared for the sixteenth meeting of the Scientific Advisory Committee 14 – 16 November 2011. http://www.mvo.ms/pub/Open_File_Reports/MVO_OFR_11_02-MVO_Report_to_SAC_16.pdf

Stinton, A.J., Bass, V., Christopher, T., Fergus, M., Miller, V., Pascal, K., Rostant, K., Ryan, G.A., Stewart, R., Syers, R., Wade, V., Williams, P. Montserrat Volcano Observatory. (2020, May). MVO Scientific Report for Volcanic Activity between 1 April and 30 September 2020. http://www.mvo.ms/pub/Open_File_Reports/MVO_OFR_20_05-Six_Monthly_Report.pdf

Odbert, H. M., Ryan, G. A., Mattioli, G. S., Hautmann, S., Gottsmann, J., Fournier, N., and Herd, R. A. (2014). Chapter 11 Volcano geodesy at the Soufrière Hills Volcano, Montserrat: a review. Geological Society, London, Memoirs, 39(1), 195–217. https://doi.org/10.1144/m39.11

Odbert, H., Taisne, B., and Gottsmann, J. (2015). Deposit loading and its effect on co-eruptive volcano deformation. Earth and Planetary Science Letters, 413, 186–196. https://doi.org/10.1016/j.epsl.2015.01.005

Parker, A. L., Biggs, J., and Lu, Z. (2014). Investigating long-term subsidence at Medicine Lake Volcano, CA, using multitemporal InSAR. Geophysical Journal International, 199(2), 844–859. https://doi.org/10.1093/gji/ggu304

Phillipson, G., Sobradelo, R., and Gottsmann, J. (2013). Global volcanic unrest in the 21st century: An analysis of the first decade. Journal of Volcanology and Geothermal Research, 264, 183–196. https://doi.org/10.1016/j.jvolgeores.2013.08.004

Ranalli, G. (1995). Rheology of the Earth, 434 pp., Chapman and Hall, London.

Sigmundsson, F., Pinel. V, Grapenthin. R, Hooper. A, Halldorsson. S.A, P. Einarsson, Ófeigsson, B.G., Heimisson, E.R, Jónsdóttir, K, Gudmundsson, M.T Vogfjórd, K, Parks, M Li,S., Drouin, V., Geirsson, H., Dumont, S., Fridriksdottir, H.M., Gudmundsson, G.B., Wright, T.J., and Yamasaki, T. (2020). Unexpected large eruptions from buoyant magma bodies within viscoelastic crust, Nature Communications, 11(2403), 1–11, doi:10.1038/s41467-020-16054-6.

Spaans, K., and Hooper, A. (2016). InSAR processing for volcano monitoring and other near-real time applications. Journal of Geophysical Research: Solid Earth, 121(4), 2947–2960. https://doi.org/10.1002/2015jb012752

Sparks, R. S. J., and Cashman, K. V. (2017). Dynamic Magma Systems: Implications for Forecasting Volcanic Activity. Elements, 13(1), 35–40. https://doi.org/10.2113/gselements.13.1.35

Sparks, R. S. J., and Young, S. R. (2002). The eruption of Soufrière Hills Volcano, Montserrat (1995–1999): overview of scientific results. Geological Society, London, Memoirs, 21(1), 45–69. https://doi.org/10.1144/gsl.mem.2002.021.01.03

Voight, B., Linde, A. T., Sacks, I. S., Mattioli, G. S., Sparks, R. S. J., Elsworth, D., Hidayat, D., Malin, P. E., Shalev, E., Widiwijayanti, C., Young, S. R., Bass, V., Clarke, A., Dunkley, P., Johnston, W., McWhorter, N., Neuberg, J., and Williams, P. (2006). Unprecedented pressure increase in deep magma reservoir triggered by lava-dome collapse. Geophysical Research Letters, 33(3). https://doi.org/10.1029/2005gl024870

Wadge, G., Mattioli, G., and Herd, R. (2006). Ground deformation at Soufrière Hills Volcano, Montserrat during 1998–2000 measured by radar interferometry and GPS. Journal of Volcanology and Geothermal Research, 152(1–2), 157–173. https://doi.org/10.1016/j.jvolgeores.2005.11.007

Wadge, G., Voight, B., Sparks, R. S. J., Cole, P. D., Loughlin, S. C., and Robertson, R. E. A. (2014). Chapter 1 An overview of the eruption of Soufrière Hills Volcano, Montserrat from 2000 to 2010. Geological Society, London, Memoirs, 39(1), 1.1-40. https://doi.org/10.1144/m39.1

Yang, X. M., Davis, P. M., and Dieterich, J. H. (1988). Deformation from inflation of a dipping finite prolate spheroid in an elastic half-space as a model for volcanic stressing. Journal of Geophysical Research: Solid Earth, 93(B5), 4249–4257. https://doi.org/10.1029/jb093ib05p04249

Young, N. K., and Gottsmann, J. (2015). Shallow crustal mechanics from volumetric strain data: Insights from Soufrière Hills Volcano, Montserrat. Journal of Geophysical Research: Solid Earth, 120(3), 1559–1571. https://doi.org/10.1002/2014jb011551

Chapter 5

CONCLUSIONS AND IMPLICATIONS

-

The primary objective of this project was to examine how EDM and GPS can be used in conjunction to model the magmatic system of the SHV, alongside producing models to help understand surface deformation patterns at the SHV between 2010 and 2019. These models were constructed using Finite Element Modelling in order to incorporate detailed 3D topography, vital for accurate modelling of the EDM network due to the interaction of topography and deformation footprints (Johnson et al, 2019).

To begin to address the overall project objective, Chapter 3 examines how EDM and GPS jointly record deformation in response to changing deformation source pressure, depth, and shape. This preliminary study utilises a 2D axisymmetric model with a simplified volcanic edifice as a proxy for the SHV. Upon the edifice were 5 points, each simulating a GPS site and EDM reflector. 2 more points were placed beyond the extent of the edifice, simulating GPS points and EDM base stations. The vertical and horizontal deformation components were calculated for each point, giving synthetic GPS results. The distances between each proxy reflector and proxy base station were calculated before and after the application of pressure to the source, giving synthetic EDM results.

It was observed through the synthetic GPS results that radial displacement increases away from the vent to a peak at the edge of the edifice, although the placement of the peak varied slightly with source depth. Vertical deformation peaked over the vent in all cases, with a higher magnitude of deformation observed in cases with shallow sources, oblate sources, and higher source pressures. Variations to synthetic EDM baseline lengths suggest that it is primarily the relative radial deformation between the EDM reflector and EDM base station that defines the overall EDM line length change. Vertical deformation of EDM reflectors and EDM base stations has a relatively minor

impact on EDM line length changes compared with radial deformation. This meant that an EDM reflector could experience a significant degree of uplift relative to the base station and still display line length shortening with a relative radial deformation component lower in magnitude than the relative vertical deformation. Shallow sources centred at depths less than 6000 m induce line length shortening due to the high magnitude radial displacement pushing EDM reflectors on the edifice closer to the EDM base stations.

Oblate sources had a complex effect on the deformation responses of GPS and EDM in this study. Oblate sources produce significantly greater magnitudes of surface deformation than prolate sources due to their larger upper source surface, and produce a much stronger vertical deformation component than radial (Fialko et al, 2001), and this pattern of deformation is reflected in the synthetic GPS results. However, due to the aforementioned importance of relative radial deformation over relative vertical deformation in determining EDM baseline length changes, oblate sources led to synthetic EDM line length shortening, as the proxy reflectors on the edifice experienced greater radial deformation than the proxy base stations. The fact that the proxy reflectors experienced greater vertical deformation than the proxy base stations (which would result in expected line lengthening) was of far less significance to baseline length changes than the difference in radial deformation. In practical application, oblate sources would not necessarily generate EDM line length shortening, as it would be dependent on the extent of the radial deformation footprint and the placement of EDM reflector and base stations. In this synthetic example, the base station is situated outside of the radial deformation peak, whereas the reflectors are situated close to the peak. It is possible, and indeed highly likely, that in practical settings with deeper magmatic systems and shorter EDM baselines, that the base station would be situated closer to the peak radial deformation footprint and as a result induce increased line lengthening from oblate sources.

EDM line lengths increase linearly in response to increasing pressure, and pressure variation has a relatively minor impact on surface deformation compared with source shape variation and source depth variation.

Chapter 4 applies the principles of how EDM and GPS respond to deformation established in Chapter 3 to more complex and realistic models of the SHV and its associated magmatic system. An initial magmatic system model of a single prolate deformation source (as a proxy for a magma reservoir) could not solely explain the pattern of EDM line length changes recorded at SHV between 2010 and 2019. The radial deformation produced by the mid-crustal source was too symmetrical to fit the observed data. The modelled deformation produced by a singular mid-crustal source provides a closer fit to the GPS data, excluding the site HERM, as the GPS network as a whole is better placed to respond to a deeper focused deformation source than the EDM network. A shallow magma reservoir-style prolate source (in addition to the mid-crustal source) also fails to explain the pattern of EDM line length changes observed, and variations to such a source had a negligible impact on EDM and GPS networks alike. This is due to the deformation field produced by such a source being symmetrical, and therefore the deformation field produced by the mid-crustal magmatic system overprints it.

The modelled spatial deformation field was sensitive to variations of a dyke conduit-style shallow deformation source when in combination with the mid-crustal reservoir-style source; the pressure and orientation parameters produced the greatest magnitude changes to the surface deformation response. However, the spatial extent of the deformation field produced by the shallow source was limited, and only effected a small area of the edifice close to the vent (a radius of ~1.5 km); further away it weakened until it was overwritten by the mid-crustal magmatic system. The overwhelming majority of the GPS network is situated too far from the vent to detect the deformation field changes controlled by a shallow dyke conduit source, with the only exception being the continuous GPS site HERM. However, EDM reflectors are situated close enough to the vent to respond to these shallow source changes. When the orientation and pressure of the dyke conduit was varied simultaneously, a closest fit to the observed EDM data was found for a dyke orientated NNW-SSE (60° from north) with a pressure of -12 MPa. The dyke orientation is in line with previous studies into the dyke conduit system at Montserrat (Mattioli et al, 1998; Costa et al, 2007; Hautmann et al, 2009; Linde et al, 2010) and with the regional tectonic stress field (Feuillet et al, 2010). Negative pressure values

consistently produced closer fits to the observed data than positive pressure values. This suggests that the shallow system of the SHV is in a state of cooling and contraction or magma withdrawal, while the mid-crustal magmatic system is still being pressurised (to ~10 MPa), possibly due to magma supply at depth. The inferred pressure values here may be an overestimate due to the elastic medium used in this study, but mid-crustal pressure values are in line with previous studies (Gottsmann et al, 2020).

At the dyke orientation of best fit for the parameters tested, negative pressurisation of the dyke causes a small area of the edifice on the North East flank of the vent to deform to the south west. This area includes the GPS site HERM and the EDM reflector EDHE. The placement of HERM and EDHE within the deformation footprint of the inferred shallow dyke source is potentially significant, as the east-west, north-south, and vertical deformation components of the shallow dyke source have different relative amplitudes. The co-location of HERM and EDHE is in an area which is predicted to respond strongly to the north-south deformation component of the inferred shallow dyke's deformation field, weakly to the east-west deformation component, and insignificantly to the vertical deformation component. This has the effect of HERM/EDHE's north-south deformation being controlled primarily by the shallow dyke conduit, resulting in southward movement as the dyke contracts. However, the east-west deformation and vertical deformation of the site would be controlled by the behaviour of the mid-crustal source, causing the uplift and eastward component of the migration of the site observed between 2010-2019. The deformation behaviour of HERM compared with the rest of the GPS network is therefore likely due to HERM responding to a combination of pressure changes in the shallow dyke conduit and mid-crustal system, while the rest of the GPS network responds to pressure changes in the mid-crustal system alone. There may also be an element of edifice decoupling as proposed by McPherson (2013). This makes it difficult to incorporate into future modelling studies into the mid-crustal system, but investigations into the magmatic system of the SHV which include shallow system processes should take the deformation response of HERM into account alongside the EDM network.

For future monitoring purposes at the SHV, the deformation response of HERM and of the EDM network as a whole are good indicators of shallow system

behaviour. In particular, the EDM lines EDJH-EDHE, EDBR-EDUB, and EDBR-EDWR are good indicators of pressure changes in the shallow system. North-east movement of HERM, or line length shortening of EDJH-EDHE, EDBR-EDUB, and EDBR-EDWR, could indicate pressurisation of the shallow magmatic system and magma migration upwards from the mid-crustal system. At greater distances from the vent, GPS sites remain an effective and accurate means of measuring the deformation response to mid-crustal processes. Consequently, when modelling the mid-crustal system of the SHV, best fit to GPS data should be preferred to EDM, whereas when modelling shallow processes, EDM data is a better reflection of the shallow magmatic system. Installing new EDM lines to monitor the south-eastern flank would likely not be worthwhile despite filling a geographical gap in the spatial coverage of the EDM network. A site on this flank would not be optimally placed to respond to pressure changes in the shallow magmatic system as well as being potentially difficult to access due to its position in the island's exclusion zone.

For application to other volcanoes, we suggest that placement of monitoring sites, whether they are EDM or GPS, close to the vent is vital to effectively monitor any shallow magmatic system, as the deformation footprint of shallow dyke conduits and other small-volume magmatic components are spatially-restricted. Covering multiple flanks to find possible dyke conduit orientations is important, as half the area close to the vent may still be relatively unresponsive to dyke-shaped source pressurisation given the predominant deformation field from such a source is perpendicular to its strike. For the installation of new sites, priority should be given to the flanks perpendicular to the likely dyke orientation as determined by the regional stress field. EDM provides a safer, quicker, and cheaper way of effectively monitoring shallow system processes than GPS once the reflectors are installed, as coverage of multiple flanks close (within 1 km) to the vent is vital to understanding the behaviour of dyke conduit-shaped shallow magmatic system processes, as they produce highly asymmetrical deformation fields. When modelling other volcanoes, the placement of monitoring sites from which data has been collected to measure the fit of the model should be taken into account. The part of the magmatic system the monitoring site is responding to should be reflected in the choice of which data to compare model results to where possible. In addition,

incorporating analysis of additional monitoring techniques such as EDM into modelling studies in order to provide more complete geographical data coverage allows for better constrained results.

BIBLIOGRAPHY

-

Albino, F., Biggs, J. and Syahbana, D. (2019). Dyke intrusion between neighbouring arc volcanoes responsible for 2017 pre-eruptive seismic swarm at Agung. Nature Communications, 10(1).

Amelung, F., Galloway, D., Bell, J., Zebker, H. and Laczniak, R. (1999). Sensing the ups and downs of Las Vegas: InSAR reveals structural control of land subsidence and aquifer-system deformation. Geology, 27(6), p.483.

Barclay, J., Rutherford, M., Carroll, M., Murphy, M., Devine, J., Gardner, J. and Sparks, R. (1998). Experimental phase equilibria constraints on pre-eruptive storage conditions of the Soufriere Hills magma. Geophysical Research Letters, 25(18), pp.3437-3440.

Battaglia, M., Cervelli, P. and Murray, J. (2013). dMODELS: A MATLAB software package for modeling crustal deformation near active faults and volcanic centers. Journal of Volcanology and Geothermal Research, 254, pp.1-4.

Battaglia, M., Alpala, J., Alpala, R., Angarita, M., Arcos, D., Euillades, L., Euillades, P., Muller, C., and Narváez, L. (2019). Monitoring Volcanic Deformation. Reference Module in Earth Systems and Environmental Sciences. Published. https://doi.org/10.1016/b978-0-12-409548-9.10902-9

Biggs, J. and Pritchard, M. (2017). Global Volcano Monitoring: What Does It Mean When Volcanoes Deform?. Elements, 13(1), pp.17-22.

Bonaccorso, A., Cianetti, S., Giunchi, C., Trasatti, E., Bonafede, M., and Boschi, E. (2005). Analytical and 3-D numerical modelling of MT. Etna (Italy) Volcano inflation. Geophysical Journal International, 163(2), 852–862. https://doi.org/10.1111/j.1365-246x.2005.02777.x

Bonaccorso, A., Currenti, G, and Del Negro, C. (2013), Interaction of volcano-tectonic fault with magma storage, intrusion and flank instability: A thirty years

study at Mt. Etna volcano, Journal of Volcanology and Geothermal Research, 251, 127–136. doi:10.1016/j.jvolgeores.2012.06.002.

Bonafede, M., and Ferrari, C. (2009). Analytical models of deformation and residual gravity changes due to a Mogi source in a viscoelastic medium. Tectonophysics, 471(1-2), 4–13. https://doi.org/10.1016/j.tecto.2008.10.006

Cabaniss, H. E., Gregg, P.M, S. Nooner, L. and Chadwick Jr, W.W. (2020). Triggering of eruptions at Axial Seamount, Juan de Fuca Ridge, Scientific Reports, pp. 1–11, doi:10.1038/s41598-020-67043-0.

Carmo, J. S. A. D. (2020). Numerical modelling and its physical modelling support in Civil Engineering. Research, Society and Development, 9(10), e5019108409. https://doi.org/10.33448/rsd-v9i10.8409

Cayol, V. and Cornet, F. (1998). Effects of topography on the interpretation of the deformation field of prominent volcanoes-Application to Etna. Geophysical Research Letters, 25(11), pp.1979-1982.

Chen, C., Huang, H., Hautmann, S., Sacks, I., Linde, A. and Taira, T. (2018). Resonance oscillations of the Soufrière Hills Volcano (Montserrat, W.I.) magmatic system induced by forced magma flow from the reservoir into the upper plumbing dike. Journal of Volcanology and Geothermal Research, 350, pp.7-17.

Christensen, R. M. (1982). Theory of viscoelasticity: An introduction. New York: Dover Publications.

Christopher, T., Humphreys, M., Barclay, J., Genareau, K., De Angelis, S., Plail, M., and Donovan, A. (2014). Chapter 17 Petrological and geochemical variation during the Soufrière Hills eruption, 1995 to 2010. Geological Society, London, Memoirs, 39(1), 317-342. https://doi.org/10.1144/m39.17

Cimarelli, C., Costa, A., Mueller, S. and Mader, H. (2011). Rheology of magmas with bimodal crystal size and shape distributions: Insights from analog experiments. Geochemistry, Geophysics, Geosystems, 12(7)

Cole, P., Calder, E., Druitt, T., Hoblitt, R., Robertson, R., Sparks, R. and Young, S. (1998). Pyroclastic flows generated by gravitational instability of the 1996-97

Lava Dome of Soufriere Hills Volcano, Montserrat. Geophysical Research Letters, 25(18), pp.3425-3428.

Cole, P., Bass, V., Christopher, T., Murrell, C., Odbert, H., Smith, P., Stewart, R., Stinton, A., Syers, R., Williams, P. Montserrat Volcano Observatory. (2011, February). MVO scientific report for volcanic activity between 1 May 2011 and 31 October 2011 prepared for the sixteenth meeting of the Scientific Advisory Committee 14 – 16 November 2011. http://www.mvo.ms/pub/Open_File_Reports/MVO_OFR_11_02-MVO_Report_to_SAC_16.pdf

Costa, A., Melnik, O., Sparks, R. and Voight, B. (2007). Control of magma flow in dykes on cyclic lava dome extrusion. Geophysical Research Letters, 34(2).

Crawford, R. J. (1998). Plastics engineering. Oxford: Butterworth-Heinemann.

Currenti, G., Del Negro, C, and Ganci, G. (2007). Modelling of ground deformation and gravity fields using finite element method: An application to Etna volcano, Geophysical Journal International, 169(2), 775–786, doi:10.1111/j.1365-246X.2007.03380.x.

De Natale, G., Petrazzuoli, S. M., and Pingue, F. (1997). The effect of collapse structures on ground deformations in calderas. Geophysical Research Letters, 24(13), 1555–1558. https://doi.org/10.1029/97gl01600

Del Negro, C., Currenti, G., and Scandura, D. (2009), Temperature-dependent viscoelastic modelling of ground deformation: Application to Etna volcano during the 1993 - 1997 inflation period, Physics of the Earth and Planetary Interiors, 172(3-4), 299–309.

Delgado, F., Pritchard, M., Samsonov, S., and Córdova, L. (2018). Renewed posteruptive uplift following the 2011–2012 rhyolitic eruption of Cordón Caulle (Southern Andes, Chile): Evidence for transient episodes of magma reservoir recharge during 2012–2018. Journal of Geophysical Research: Solid Earth, 123(11), 9407–9429.

Dragoni, M. and Magnanensi, C. (1989). Displacement and stress produced by a pressurized, spherical magma chamber, surrounded by a viscoelastic shell. Physics of the Earth and Planetary Interiors, 56(3-4), pp.316-328.

Dzurisin, D. (2003). A comprehensive approach to monitoring volcano deformation as a window on the eruption cycle. Reviews of Geophysics, 41(1). https://doi.org/10.1029/2001rg000107

Dzurisin, D. (2007). Volcano Deformation. SPRINGER.

Elsworth, D., Mattioli, G., Taron, J., Voight, B. and Herd, R. (2008). Implications of magma transfer between multiple reservoirs on eruption cycling. Science, 322, 246 – 248.

Elsworth, D., Foroozan, R., Taron, J., Mattioli, G. S. and Voight, B. (2014). Geodetic imaging of magma migration at Soufriere Hills Volcano 1995 to 2008. Geological Society, London, Memoirs, 39(1), pp.219-227.

Feuillet, N., Leclerc, F., Tapponnier, P., Beauducel, F., Boudon, G., and Le Friant, A. et al. (2010). Active faulting induced by slip partitioning in Montserrat and link with volcanic activity: New insights from the 2009 GWADASEIS marine cruise data. Geophysical Research Letters, 37(19). https://doi.org/10.1029/2010gl042556

Fialko, Y., Khazan, Y., and Simons, M. (2001), Deformation due to a pressurized horizontal circular crack in an elastic half-space, with applications to volcano geodesy, Geophysical Journal International, 146(1), 181–190.

Folch, A., and Gottsmann, J. (2006). Faults and ground uplift at active calderas, Geological Society Special Publication, 269, 109–120. doi:10.1144/GSL.SP.2006.269.01.07.

Foroozan, R., Elsworth, D., Voight, B. and Mattioli, G. S. (2010). Dual reservoir structure at Soufrière Hills Volcano inferred from continuous GPS observations and heterogeneous elastic modeling. Geophysical Research Letters, 37, L00E12, http://dx.doi.org/10.1029/2010GL042511

Fournier, N., and Chardot, L. (2012), Understanding volcano hydrothermal unrest from geodetic observations: Insights from numerical modeling and application to White Island volcano, New Zealand, Journal of Geophysical Research, 117(B11), B11,208.

Galgana, G. A., Newman, A. V., Hamburger, M. W., and Solidum, R. U. (2014). Geodetic observations and modeling of time-varying deformation at

Taal Volcano, Philippines. Journal of Volcanology and Geothermal Research, 271, 11–23.

Gambino, S., Falzone, G., Ferro, A. and Laudani, G. (2014). Volcanic processes detected by tiltmeters: A review of experience on Sicilian volcanoes. Journal of Volcanology and Geothermal Research, 271, pp.43-54.

Geirsson, H., LaFemina, P., Árnadóttir, T., Sturkell, E., Sigmundsson, F., Travis, M., Schmidt, P., Lund, B., Hreinsdóttir, S. and Bennett, R. (2012). Volcano deformation at active plate boundaries: Deep magma accumulation at Hekla volcano and plate boundary deformation in south Iceland. Journal of Geophysical Research: Solid Earth, 117(B11)

Geyer, A., and Martí, J. (2009). Stress fields controlling the formation of nested and overlapping calderas: Implications for the understanding of caldera unrest, Journal of Volcanology and Geothermal Research, 181(3-4), 185–195. doi:10.1016/j.jvolgeores.2009.01.018.

Geyer, A., and Gottsmann, J. (2010). The influence of mechanical stiffness on Caldera deformation and implications for THE 1971–1984 RABAUL uplift (Papua New Guinea). Tectonophysics, 483(3-4), 399–412. https://doi.org/10.1016/j.tecto.2009.10.029

Gottsmann, J. and Odbert, H. (2014). The effects of thermomechanical heterogeneities in island arc crust on time-dependent preeruptive stresses and the failure of an andesitic reservoir. Journal of Geophysical Research: Solid Earth, 119(6), pp.4626-4639.

Gottsmann, J., Komorowski, J. and Barclay, J. (2017). Volcanic Unrest and Pre-eruptive processes: A Hazard and Risk perspective. Advs in Volcanology (2019), pp.1-21.

Gottsmann, J., Flynn, M. and Hickey, J. (2020). The Transcrustal Magma Reservoir Beneath Soufrière Hills Volcano, Montserrat: Insights From 3-D Geodetic Inversions. Geophysical Research Letters, 47(20).

Gudmundsson, A. (2006). How local stresses control magma-chamber ruptures, dyke injections, and eruptions in composite volcanoes. Earth-Science Reviews, 79(1-2), pp.1-31.

Gudmundsson, A. (2011). Rock Fractures in Geological Processes (1st ed.). Cambridge University Press.

Harnett, C., Kendrick, J., Lamur, A., Thomas, M., Stinton, A., Wallace, P., Utley, J., Murphy, W., Neuberg, J. and Lavallée, Y. (2019). Evolution of Mechanical Properties of Lava Dome Rocks Across the 1995–2010 Eruption of Soufrière Hills Volcano, Montserrat. Frontiers in Earth Science, 7.

Hatter, S. J., Palmer, M. R., Gernon, T. M., Taylor, R. N., Cole, P. D., Barfod, D. N., and Coussens, M. (2018). The Evolution of the Silver Hills Volcanic Center, and Revised40Ar/39Ar Geochronology of Montserrat, Lesser Antilles, With Implications for Island Arc Volcanism. Geochemistry, Geophysics, Geosystems, 19(2), 427–452. https://doi.org/10.1002/2017gc007053

Hautmann, S., Gottsmann, J., Sparks, R. S. J., Costa, A., Melnik, O. and Voight, B. (2009). Modelling ground deformation caused by oscillating overpressure in a dyke conduit at Soufrière Hills Volcano, Montserrat. Tectonophysics, 471, 87 –95.

Hautmann, S., Gottsmann, J., Sparks, R. S. J., Mattioli, G. S., Sacks, I. S. and Strutt, M. H. (2010). The effect of mechanical heterogeneity in arc crust on volcano deformation with application to Soufrière Hills Volcano, Montserrat (W.I.). Journal of Geophysical Research, 115, B09203, http://dx.doi.org/10.1029/2009JB006909

Hautmann, S., Hidayat, D., Fournier, N., Linde, A. T., Sacks, I. S. and Williams, C. P. (2013). Pressure changes in the magmatic system during the December 2008/January 2009 extrusion event at Soufrière Hills Volcano, Montserrat (W.I.), derived from strain data analysis. Journal of Volcanology and Geothermal Research, 250, 34 – 41.

Hautmann, S., Witham, F., Christopher, T., Cole, P., Linde, A. T., Sacks, I. S., and Sparks, R. S. J. (2014). Strain field analysis on Montserrat (W.I.) as tool for assessing permeable flow paths in the magmatic system of Soufrière Hills Volcano. Geochemistry, Geophysics, Geosystems, 15(3), 676–690. https://doi.org/10.1002/2013gc005087

Herd, R., Edmonds, M. and Bass, V. (2005). Catastrophic lava dome failure at Soufrière Hills Volcano, Montserrat, 12–13 July 2003. Journal of Volcanology and Geothermal Research, 148(3-4), pp.234-252.

Hickey, J. and Gottsmann, J. (2014). Benchmarking and developing numerical Finite Element models of volcanic deformation. Journal of Volcanology and Geothermal Research, 280, pp.126-130.

Hickey, J., 2015(a). Constraining Volcanic Unrest with Integrated Geodetic Modelling. Ph.D. University of Bristol.

Hickey, J., Gottsmann, J. and Mothes, P., 2015(b). Estimating volcanic deformation source parameters with a finite element inversion: The 2001–2002 unrest at Cotopaxi volcano, Ecuador. Journal of Geophysical Research: Solid Earth, 120(3), pp.1473-1486.

Hickey, J., Gottsmann, J., Nakamichi, H. and Iguchi, M. (2016). Thermomechanical controls on magma supply and volcanic deformation: application to Aira caldera, Japan. Scientific Reports, 6(1).

Hickey, J., Gottsmann, J., Mothes, P., Odbert, H., Prutkin, I. and Vajda. P (2017). The Ups and Downs of Volcanic Unrest: Insights from Integrated Geodesy and Numerical Modelling. Advs in Volcanology (2019) 203–219, DOI 10.1007/11157_2017_13

Hickey, J., Lloyd, R., Biggs, J., Arnold, D., Mothes, P. and Muller, C. (2020). Rapid localized flank inflation and implications for potential slope instability at Tungurahua volcano, Ecuador. Earth and Planetary Science Letters, 534, p.116104.

Holden, L., R. Cas, N. Fournier, and L. Ailleres. (2017), Modelling ground deformation patterns associated with volcanic processes at the Okataina Volcanic Centre, Journal of Volcanology and Geothermal Research, 344, 65–78, doi:10.1016/j.jvolgeores.2017.04.014.

Hurwitz, S., Christiansen, L. and Hsieh, P. (2007). Hydrothermal fluid flow and deformation in large calderas: Inferences from numerical simulations. Journal of Geophysical Research, 112(B2).

Johnson, J., Poland, M., Anderson, K. and Biggs, J. (2019). A Cautionary Tale of Topography and Tilt from Kīlauea Caldera. Geophysical Research Letters, 46(8), pp.4221-4229.

Kavanagh, J. L., Engwell, S. L., and Martin, S. A. (2018). A review of laboratory and numerical modelling in volcanology. Solid Earth, 9(2), 531–571. https://doi.org/10.5194/se-9-531-2018

Komorowski, J., Legendre, Y., Christopher, T., Bernstein, M., Stewart, R., Joseph, E., Fournier, N., Chardot, L., Finizola, A., Wadge, G., Syers, R., Williams, C. and Bass, V. (2010). Insights into processes and deposits of hazardous vulcanian explosions at Soufrière Hills Volcano during 2008 and 2009 (Montserrat, West Indies). Geophysical Research Letters, 37(19).

Le Friant, A., Lock, E. J., Hart, M. B., Boudon, G., Sparks, R. S. J., Leng, M. J., Smart, C. W., Komorowski, J. C., Deplus, C., and; Fisher, J. K. (2008). Late Pleistocene Tephrochronology of marine Sediments adjacent to Montserrat, Lesser Antilles volcanic arc. Journal of the Geological Society, 165(1), 279–289. https://doi.org/10.1144/0016-76492007-019

Linde, A. and Sacks, S. (1995). Continuous Monitoring of Volcanoes with Borehole Strainmeters. Mauna Loa Revealed: Structure, Composition, History, and Hazards. Geophys. Monogr. Ser., vol. 92, edited by J. M. Rhodes and J. P. Lockwood, pp. 171-185, AGU, Washington, D. C.

Linde, A., Sacks, S., Hidayat, D., Voight, B., Clarke, A., Elsworth, D., Mattioli, G., Malin, P., Shalev, E., Sparks, S. and Widiwijayanti, C. (2010). Vulcanian explosion at Soufrière Hills Volcano, Montserrat on March 2004 as revealed by strain data. Geophysical Research Letters, 37(19).

Lisowski M. (2007) Analytical volcano deformation source models. In: Volcano Deformation. Springer Praxis Books. Springer, Berlin, Heidelberg. https://doi.org/10.1007/978-3-540-49302-0_8

Loughlin, S., Baptie, B. et al. (2006). Report to the Scientific Advisory Committee. Montserrat Volcano Observatory, Open File Report, 06/07. Montserrat Volcano Observatory, Flemmings, Montserrat.

Loughlin, S., Luckett, R., Ryan, G., Christopher, T., Hards, V., De Angelis, S., Jones, L. and Strutt, M. (2010). An overview of lava dome evolution, dome collapse and cyclicity at Soufrière Hills Volcano, Montserrat, 2005-2007. Geophysical Research Letters, 37(19)

Magee, C., Stevenson, C.T.E., Ebmeier, S.K., Keir, D., Hammond, J., Gottsmann, J.H., Whaler, K., Schofield, N., Jackson, C., Petronis, M, O'Driscoll B., Morgan, J., Cruden, A., Vollgger, S., Dering, G., Micklethwaite, S., Jackson, M. (2018). Magma Plumbing Systems: A Geophysical Perspective, Journal of Petrology, Volume 59, Issue 6, June 2018, Pages 1217–1251, https://doi.org/10.1093/petrology/egy064

Manconi, A., Walter, T. R., Amelung, F. (2007). Effects of mechanical layering on volcano deformation. Geophysical Journal International, 170(2), 952–958. https://doi.org/10.1111/j.1365-246x.2007.03449.x

Masterlark, T. (2007). Magma intrusion and deformation predictions: Sensitivities to the Mogi assumptions. Journal of Geophysical Research, 112(B6).

Masterlark, T., Feigl, K., Haney, M., Stone, J., Thurber, C. and Ronchin, E. (2012). Nonlinear estimation of geometric parameters in FEMs of volcano deformation: Integrating tomography models and geodetic data for Okmok volcano, Alaska. Journal of Geophysical Research: Solid Earth, 117(B2)

Mattioli, G., Dixon, T., Farina, F., Howell, E., Jansma, P. and Smith, A. (1998). GPS measurement of surface deformation around Soufriere Hills Volcano, Montserrat from October 1995 to July 1996. Geophysical Research Letters, 25(18), pp.3417-3420.

Mattioli, G. S, Herd, R. Seismol. Res. Lett. 74, 230 (2003). In: Elsworth, D., Mattioli, G., Taron, J., Voight, B. and Herd, R. (2008). Implications of magma transfer between multiple reservoirs on eruption cycling. Science, 322, 246 – 248.

Mattioli, G. S., Herd, R. A., Strutt, M. H., Ryan, G., Widiwijayanti, C. and Voight, B. (2010). Long term surface deformation of Soufrière Hills Volcano, Montserrat from GPS geodesy: inferences from simple elastic inverse models. Geophysical Research Letters, 37, L00E13, http://dx.doi.org/10.1029/2009GL042268

McPherson, E. E. (2013). A model of short term surface deformation of Soufriere Hills Volcano, Montserrat constrained by GPS geodesy. https://rc.library.uta.edu/uta-ir/bitstream/handle/10106/23910/McPherson_uta_2502M_12371.pdf?sequence=1&isAllowed=y

McTigue, D. F. (1987). Elastic stress and deformation near a finite spherical magma body: Resolution of the point source paradox. Journal of Geophysical Research, 92(B12), 12931. https://doi.org/10.1029/jb092ib12p12931

Melnik, O. and Sparks, R. (2002). Dynamics of magma ascent and lava extrusion at Soufrière Hills Volcano, Montserrat. Geological Society, London, Memoirs, 21(1), pp.153-171.

Mogi, K. (1958), Relations between the eruptions of various volcanoes and the deformations of the ground surfaces around them, Bulletin of the Earthquake Research Institute, 36, 99–134.

Newman, A. V., Dixon, T. H., Ofoegbu, G. I., and Dixon, J. E. (2001). Geodetic and seismic constraints on recent activity at Long Valley Caldera, California: Evidence for viscoelastic rheology. Journal of Volcanology and Geothermal Research, 105, 183–206.

Odbert, H., Ryan, G., Mattioli, G., Hautmann, S., Gottsmann, J., Fournier, N. and Herd, R. (2014a). Chapter 11 Volcano geodesy at the Soufrière Hills Volcano, Montserrat: a review. Geological Society, London, Memoirs, 39(1), pp.195-217.

Odbert, H., Stewart, R. and Wadge, G. (2014b). Cyclic phenomena at the Soufrière Hills Volcano, Montserrat. Geological Society, London, Memoirs, 39(1), pp.41-60.

Odbert, H., Taisne, B., and Gottsmann, J. (2015). Deposit loading and its effect on co-eruptive volcano deformation. Earth and Planetary Science Letters, 413, 186–196. https://doi.org/10.1016/j.epsl.2015.01.005

Okada, Y. (1985). Surface deformation due to shear and tensile faults in a half-space. Bulletin of the Seismological Society of America, 75(4), pp.1135-1154.

Parker, A. L., J. Biggs, and Z. Lu. (2014). Investigating long-term subsidence at Medicine Lake volcano, CA, using multitemporal InSAR, Geophysical Journal International, 199(2), 844–859.

Pascal, K. (2013). Interaction between deformation sources & implications for numerical modelling of magma storage. Ph.D. University of Leeds.

Phillipson, G., Sobradelo, R. and Gottsmann, J. (2013). Global volcanic unrest in the 21st century: An analysis of the first decade. Journal of Volcanology and Geothermal Research, 264, pp.183-196.

R.S.J. Sparks. (2003). Forecasting volcanic eruptions, Earth and Planetary Science Letters, Volume 210, Issues 1–2, Pages 1-15, ISSN 0012-821X, https://doi.org/10.1016/S0012-821X(03)00124-9.

Ramírez-Ruiz, J., Santiago-Jiménez, H., Alatorre-Chávez, E. and Bretón-González, M. (2002). EDM deformation monitoring of the 1997–2000 activity at Volcán de Colima. Journal of Volcanology and Geothermal Research, 117(1-2), pp.61-67.

Ranalli, G. (1995). Rheology of the Earth, 434 pp., Chapman and Hall, London.

Ranalli, G. and Rybach, L. (2005). Heat flow, heat transfer and lithosphere rheology in geothermal areas: Features and examples. Journal of Volcanology and Geothermal Research, 148(1-2), pp.3-19.

Roobol, M. and Smith, A. (1998). Pyroclastic stratigraphy of the Soufriere Hills Volcano, Montserrat - Implications for the present eruption. Geophysical Research Letters, 25(18), pp.3393-3396.

Ryan, G., Loughlin, S., James, M., Jones, L., Calder, E., Christopher, T., Strutt, M. and Wadge, G. (2010). Growth of the lava dome and extrusion rates at Soufrière Hills Volcano, Montserrat, West Indies: 2005-2008. Geophysical Research Letters, 37(19).

Segall, P. (2013). Volcano deformation and eruption forecasting. Geological Society, London, Special Publications, 380(1), pp.85-106.

Segall, P. (2019). Magma chambers: What we can, and cannot, learn from volcano geodesy. Philosophical Transactions of the Royal Society A: Mathematical, Physical & Engineering Sciences, 377(2139), 20180158.

Shepherd, J., Herd, R., Jackson, P. and Watts, R. (1998). Ground deformation measurements at the Soufriere Hills Volcano, Montserrat: II: Rapid static GPS measurements June 1996-June 1997. Geophysical Research Letters, 25(18), pp.3413-3416.

Sigmundsson, F., V. Pinel, R. Grapenthin, A. Hooper, S. A. Halldorsson, P. Einarsson, B. G. Ófeigsson, E. R. Heimisson, K. Jónsdóttir, M. T. Gudmundsson, K. Vogfjórd, M. Parks, S. Li, ¨ V. Drouin, H. Geirsson, S. Dumont, H. M. Fridriksdottir, G. B. Gudmundsson, T. J. Wright, and T. Yamasaki. (2020), Unexpected large eruptions from buoyant magma bodies within viscoelastic crust, Nature Communications, 11(2403), 1–11, doi:10.1038/s41467-020-16054-6.

Šindija, D., Neuberg, J. and Smith, P. (2021). The complex, static displacement of a very long period seismic signal observed at Soufrière Hills volcano, Montserrat, WI. Journal of Volcanology and Geothermal Research, 413, p.107209.

Smith, A. L., Roobol, M. J., Schellekens, J. H., Mattioli, G. S. (2007). Prehistoric stratigraphy of the Soufriere Hills–south Soufrière hills volcanic Complex, Montserrat, West Indies. The Journal of Geology, 115(1), 115–127. https://doi.org/10.1086/509271

Spaans, K. and Hooper, A. (2016). InSAR processing for volcano monitoring and other near-real time applications. Journal of Geophysical Research: Solid Earth, 121(4), pp.2947-2960.

Stinton, A.J. (2015). A new Digital Elevation Model of the Soufrière Hills Volcano, Montserrat. Open File Report OFR, pp.15-01.

Stinton, A.J., Bass, V., Christopher, T., Fergus, M., Miller, V., Pascal, K., Rostant, K., Ryan, G.A., Stewart, R., Syers, R., Wade, V., Williams, P. Montserrat Volcano Observatory. (2020, May). MVO Scientific Report for Volcanic Activity between 1 April and 30 September 2020. http://www.mvo.ms/pub/Open_File_Reports/MVO_OFR_20_05-Six_Monthly_Report.pdf

T.E. Sheldrake, W.P. Aspinall, H.M. Odbert, G. Wadge, R.S.J. Sparks. (2017). Understanding causality and uncertainty in volcanic observations: An example of forecasting eruptive activity on Soufrière Hills Volcano, Montserrat. Journal of Volcanology and Geothermal Research, 341 (287-300)

Tammaro, U., Riccardi, U., Romano, V., Meo, M., and Capuano, P. (2021). Topography and Structural Heterogeneities in surface Ground deformation: A simulation test for Somma-vesuvius volcano. Advances in Geosciences, 52, 145–152. https://doi.org/10.5194/adgeo-52-145-2021

Taylor, N., Johnson, J. and Herd, R. (2021). Making the most of the Mogi model: Size matters. Journal of Volcanology and Geothermal Research, 419, p.107380.

Trasatti, E., Giunchi, C. and Bonafede, M. (2003). Effects of topography and rheological layering on ground deformation in volcanic regions. Journal of Volcanology and Geothermal Research, 122(1-2), pp.89-110.

Voight, B., Hoblitt, R., Clarke, A., Lockhart, A., Miller, A., Lynch, L. and McMahon, J. (1998). Remarkable cyclic ground deformation monitored in real-time on Montserrat, and its use in eruption forecasting. Geophysical Research Letters, 25(18), pp.3405-3408.

Voight, B. (1999). Magma Flow Instability and Cyclic Activity at Soufriere Hills Volcano, Montserrat, British West Indies. Science, 283(5405), pp.1138-1142.

Voight, B., Linde, A., Sacks, I., Mattioli, G., Sparks, R., Elsworth, D., Hidayat, D., Malin, P., Shalev, E., Widiwijayanti, C., Young, S., Bass, V., Clarke, A., Dunkley, P., Johnston, W., McWhorter, N., Neuberg, J. and Williams, P. (2006). Unprecedented pressure increase in deep magma reservoir triggered by lava-dome collapse. Geophysical Research Letters, 33(3).

Voight, B., Hidayat, D., Sacks, S., Linde, A., Chardot, L., Clarke, A., Elsworth, D., Foroozan, R., Malin, P., Mattioli, G., McWhorter, N., Shalev, E., Sparks, R., Widiwijayanti, C. and Young, S. (2010a). Unique strainmeter observations of Vulcanian explosions, Soufrière Hills Volcano, Montserrat, July 2003. Geophysical Research Letters, 37(19).

Voight, B., Widiwijayanti, C., Mattioli, G., Elsworth, D., Hidayat, D. and Strutt, M. (2010b). Magma-sponge hypothesis and stratovolcanoes: Case for a compressible reservoir and quasisteady deep influx at Soufrière Hills Volcano, Montserrat. Geophysical Research Letters, 37, L00E05, http://dx.doi.org/10.1029/2009GL041732

Wadge, G., Mattioli, G. and Herd, R. (2006). Ground deformation at Soufrière Hills Volcano, Montserrat during 1998–2000 measured by radar interferometry and GPS. Journal of Volcanology and Geothermal Research, 152(1-2), pp.157-173.

Wadge, G., Voight, B., Sparks, R., Cole, P., Loughlin, S. and Robertson, R. (2014). Chapter 1 An overview of the eruption of Soufrière Hills Volcano, Montserrat from 2000 to 2010. Geological Society, London, Memoirs, 39(1), pp.1.1-40.

White, R. and McCausland, W. (2016). Volcano-tectonic earthquakes: A new tool for estimating intrusive volumes and forecasting eruptions. Journal of Volcanology and Geothermal Research, 309, pp.139-155.

Widiwijayanti, C. (2005). Geodetic constraints on the shallow magma system at Soufrière Hills Volcano, Montserrat. Geophysical Research Letters, 32(11).

Williams, C. and Wadge, G. (2000). An accurate and efficient method for including the effects of topography in three-dimensional elastic models of ground deformation with applications to radar interferometry. Journal of Geophysical Research: Solid Earth, 105(B4), pp.8103-8120.

Yang, X., Davis, P. and Dieterich, J. (1988). Deformation from inflation of a dipping finite prolate spheroid in an elastic half-space as a model for volcanic stressing. Journal of Geophysical Research: Solid Earth, 93(B5), pp.4249-4257.

Young, S., Sparks, R., Aspinall, W., Lynch, L., Miller, A., Robertson, R. and Shepherd, J. (1998). Overview of the eruption of Soufriere Hills Volcano, Montserrat, 18 July 1995 to December 1997. Geophysical Research Letters, 25(18), pp.3389-3392.

Young, S., Voight, B. and Duffell, H. (2003). Magma extrusion dynamics revealed by high-frequency gas monitoring at Soufrière Hills volcano,

Montserrat. Geological Society, London, Special Publications, 213(1), pp.219-230.

Zhan, Y., P. M. Gregg, H. Le Mevel, C. A. Miller, and C. Cardona. (2019), Integrating Reservoir Dynamics, Crustal Stress, and Geophysical Observations of the Laguna del Maule Magmatic System by FEM Models and Data Assimilation, Journal of Geophysical Research: Solid Earth, 124, doi:10.1029/2019JB018681.

Appendix A. Dyke Thickness Comparison

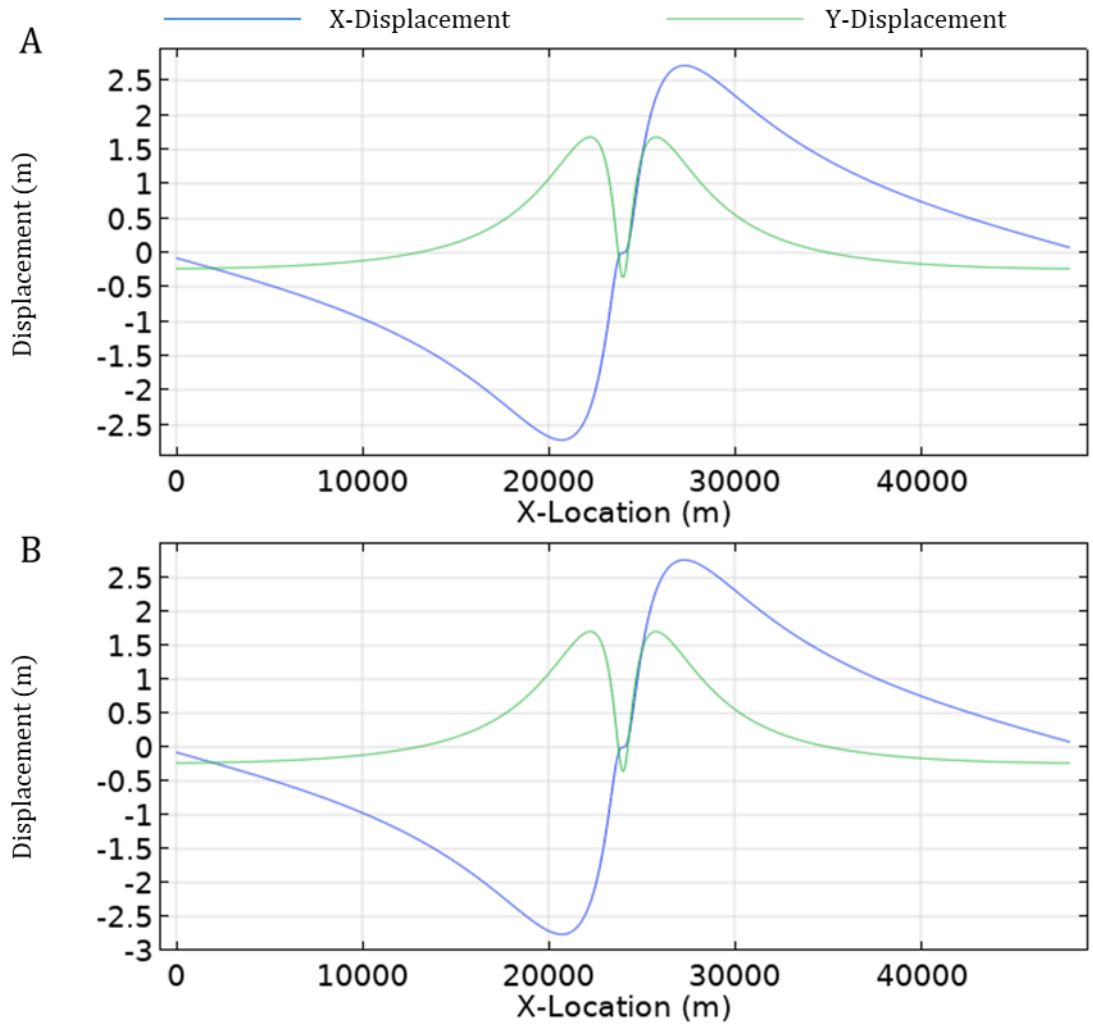

Figure A1. Comparison of deformation responses of differing dyke thicknesses. Previous literature estimated the thickness of the dyke conduit at the SHV at 2 m [Costa et al, 2007; Hautmann et al, 2009], but mesh density limitations meant the dyke used in our modelling was 50 m thick. We therefore set out to quantify the difference the increased dyke thickness would make using a simple 2D FEM with a linear elastic medium. X-Displacement is shown in blue, and Y-Displacement in green. A.) Deformation response of a 2 m wide dyke extending from 500 m below the free surface to 4500 m, pressurised at 10 MPa. B.) Deformation response of a 50 m wide dyke extending from 500 m below the free surface to a depth of 4500 m, pressurised at 10 MPa. There is no substantial difference in deformation response from increasing the dyke thickness alone.

Appendix B. Sensitivity Test Results

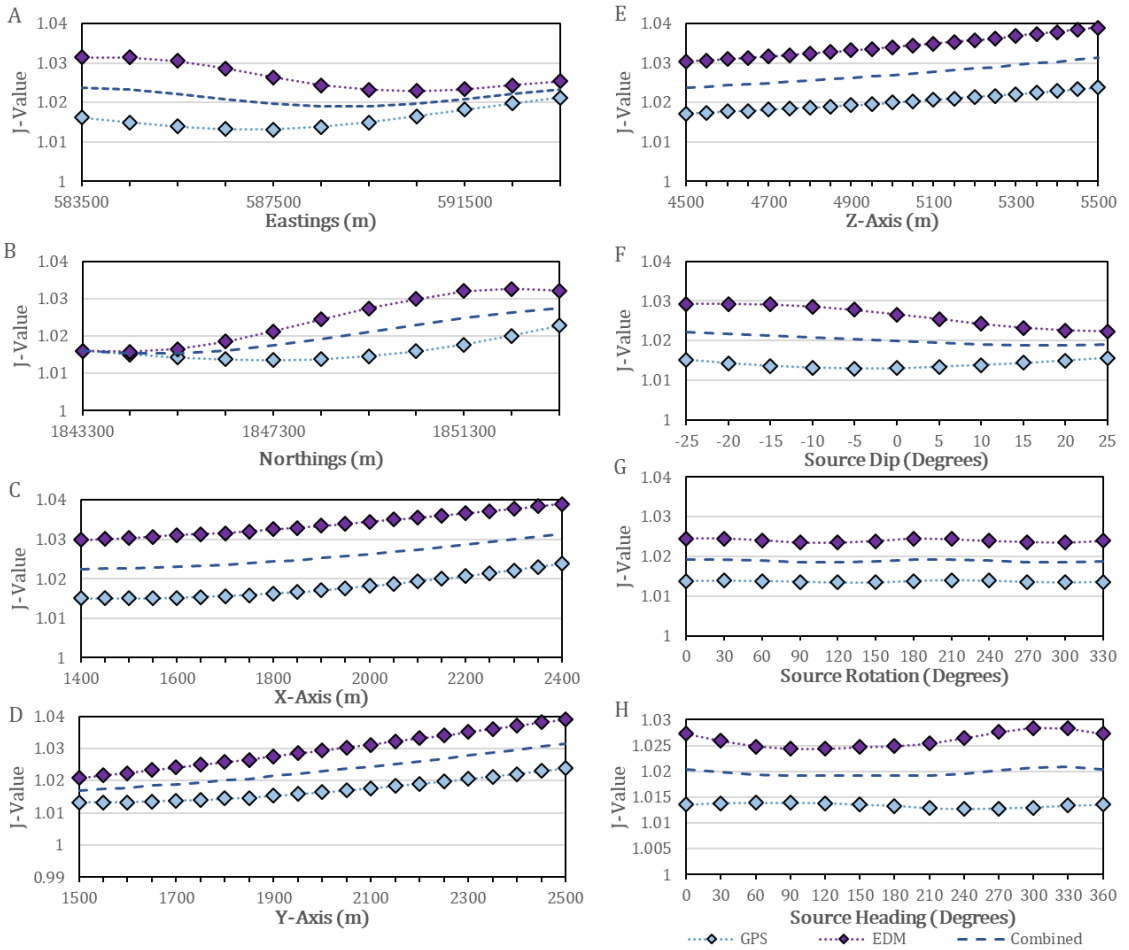

Figure B1. Remaining mid-crustal source variation sensitivity test results. Remaining results of sensitivity tests of parameter variation of a mid-crustal prolate source based on the findings of Gottsmann et al, [2020]. A.) X-Position of source. B.) Y-Position of Source. C.) X-Axis of Source. D.) Y-Axis of Source. E.) Z-Axis of Source. F.) Source Dip. G.) Source Rotation. H.) Source Heading. Source pressurisation and depth are presented in Figure 6 of the paper.

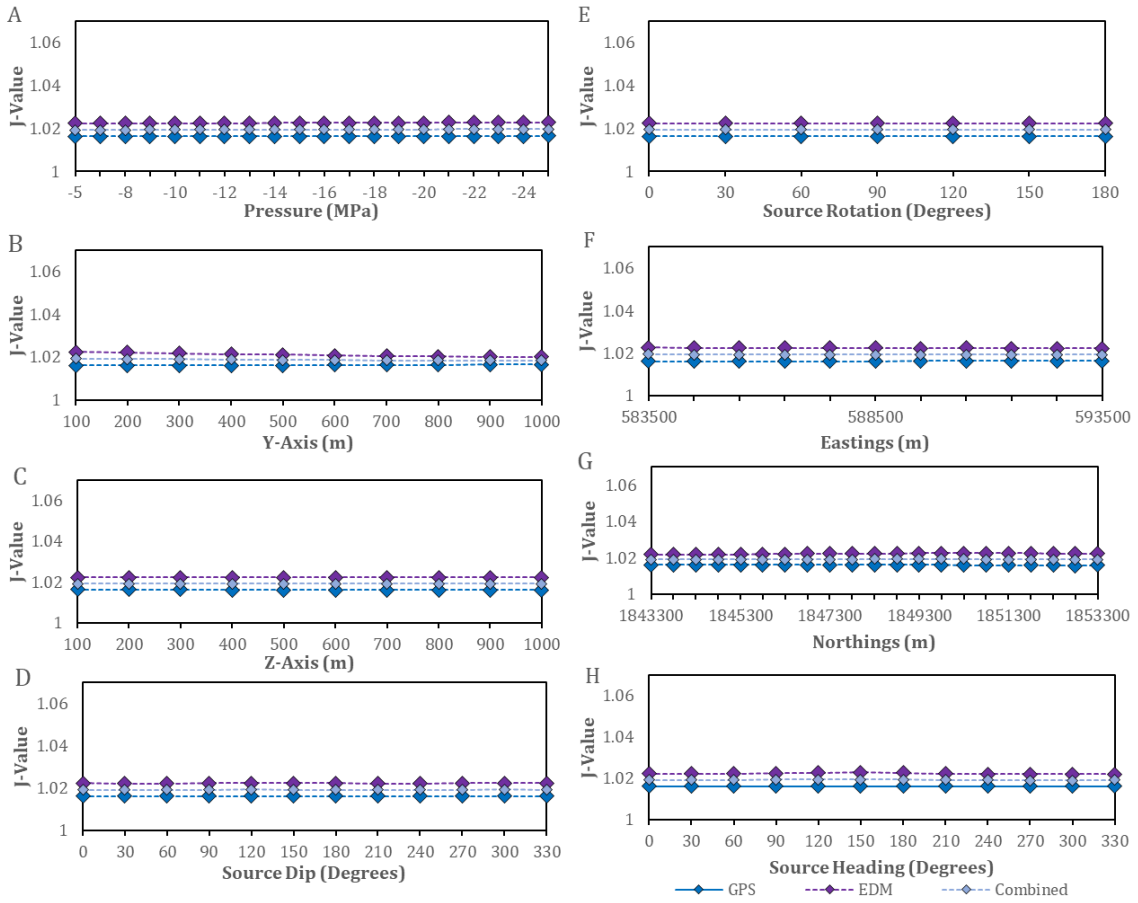

Figure B2. Remaining shallow reservoir sensitivity test results. Remaining results of sensitivity tests of parameter variation of a shallow reservoir source, in conjunction with a fixed prolate deep source. A.) Negative Pressurisation. B.) Y-Axis of source. C.) Z-Axis of source (where Z-Axis > 500 m = Oblate, Z-Axis = 500 m = Spherical, Z-Axis < 500 m = Prolate). D.) Source Dip. E.) Source Rotation. F.) X-Location. G.) Y-Location. H.) Source Heading. Results for positive pressurisation, depth variation, and X-Axis variation are presented in Figure 7 in the paper.

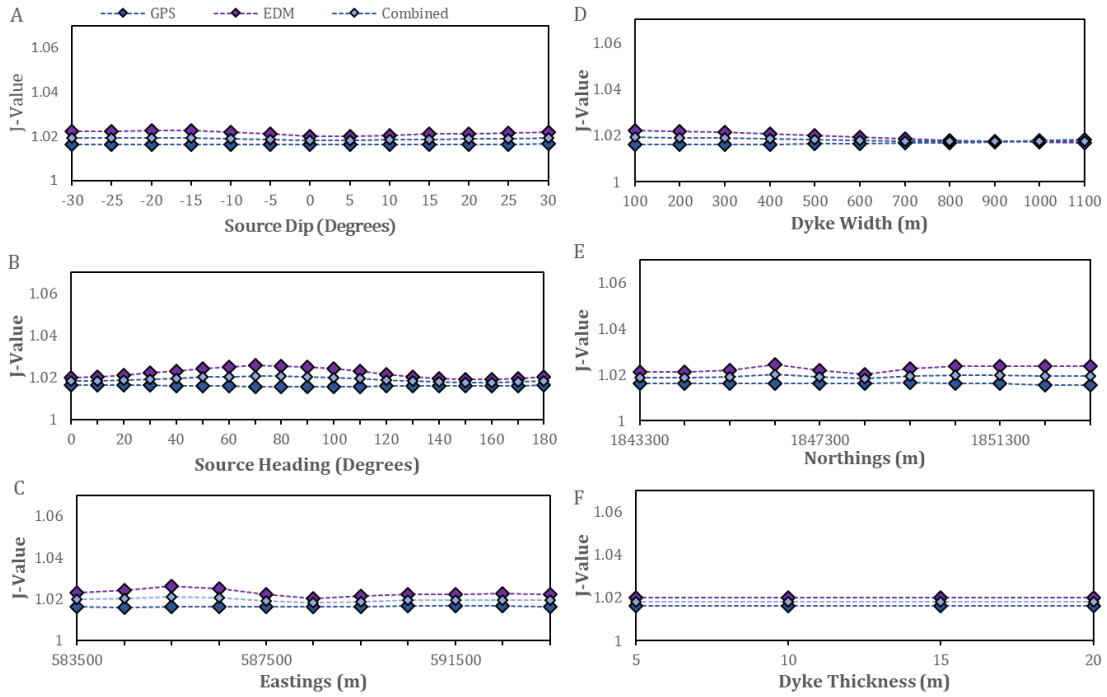

Figure B3. Remaining shallow dyke conduit sensitivity test results. Remaining results of sensitivity tests of parameter variation of a shallow dyke conduit source, in conjunction with a fixed prolate deep source. A.) Source Dip. B.) Source Heading. C.) X-Position of Source. D.) Dyke Width. E.) Y-Location of Source. F.) Dyke Thickness. Results for source pressurisation, depth variation, and source rotation are presented in Figure 8 in the paper.

Appendix C. Shallow Reservoir Variation GPS Results

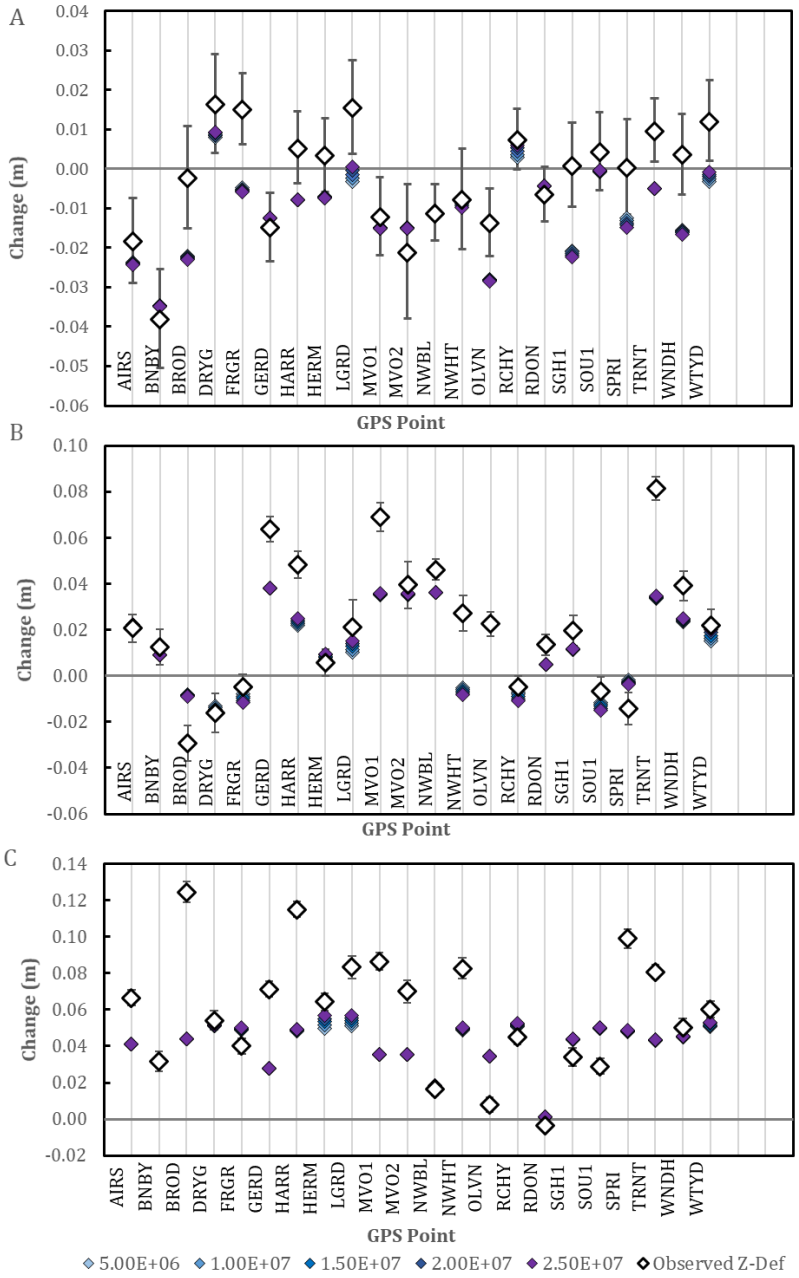

Figure C1. Variation of pressure in a shallow reservoir GPS results. GPS results for pressure variation in a shallow spherical reservoir centred at a depth of 1500 m, with a fixed deep prolate source centred at a depth of 9500 m and pressurised at 10 MPa incorporated into the model. Showing A.) Modelled X-Deformation of GPS sites. B.) Y-Deformation. C.) Z-Deformation. The GPS network is almost entirely unresponsive to not only pressure changes, but all parameter changes, in a shallow reservoir source. The only two sites to show measurable deformation responses are HERM and LGRD, the two GPS sites situated closest to the vent. These results suggest the GPS network is not well-placed to respond to changes in a shallow reservoir source.

Appendix D. VT Earthquake Hypocentres

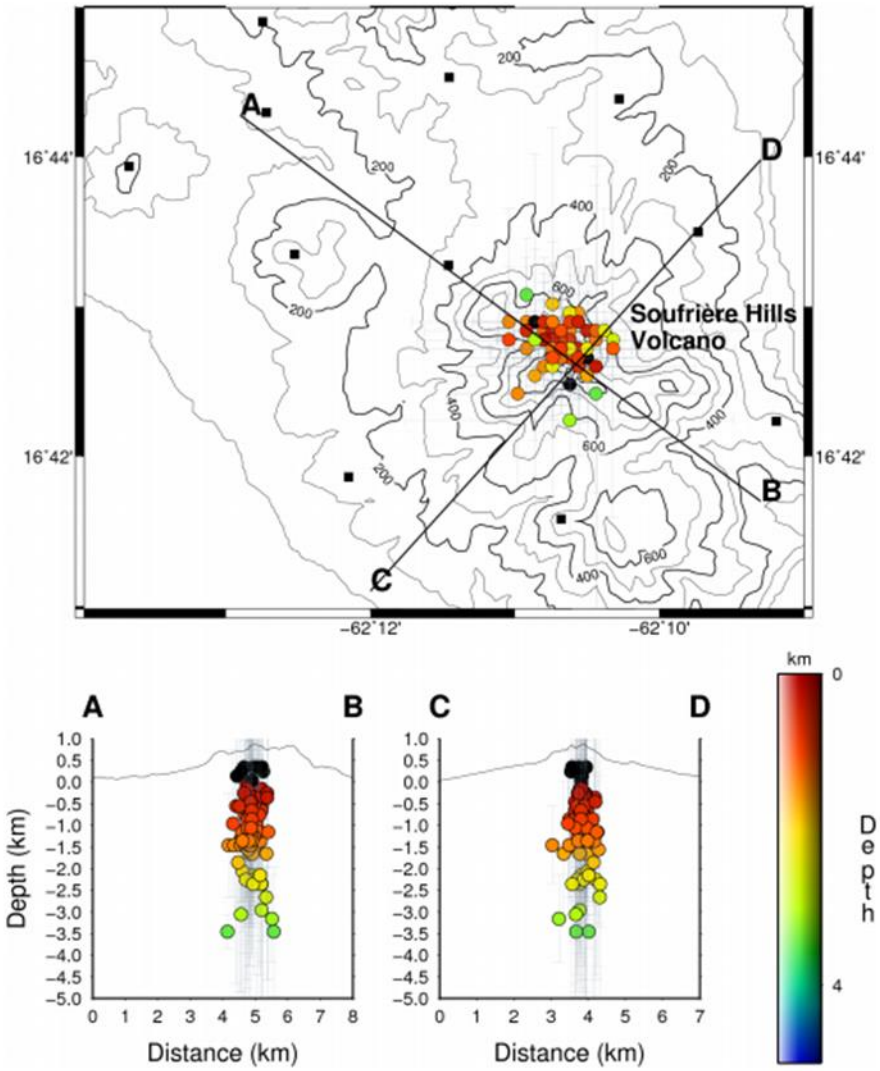

Figure D1. SHV 2011 VT earthquake hypocentres. Hypocentres of located VT earthquakes recorded on the MVO seismic network between 01 May 2011 and 31 October 2011 (153 in total). Error bars indicate the error estimates in hypocentre latitude, longitude, and depth. [Cole et al, 2011].

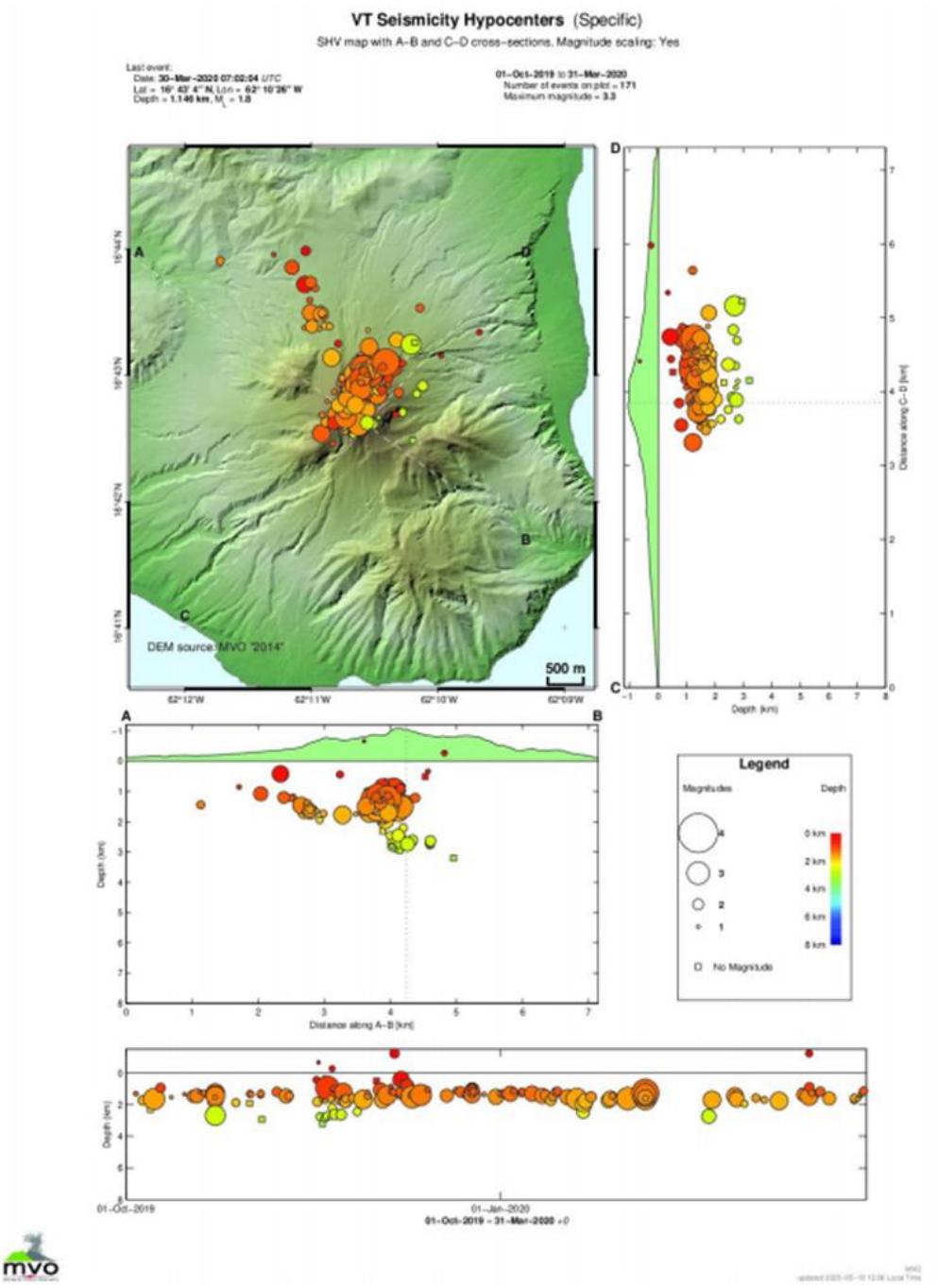

Figure D2. SHV 2019/2020 VT earthquake hypocentres. Hypocentres of located VT earthquakes recorded by the MVO seismic network between 01 October 2019 and 31 March 2020. The size of each circle is a function of earthquake magnitude. The lower panel displays the depths as a function of time. [Stinton et al, 2020].

Appendix E. GPS Radial Deformation 2010-2020

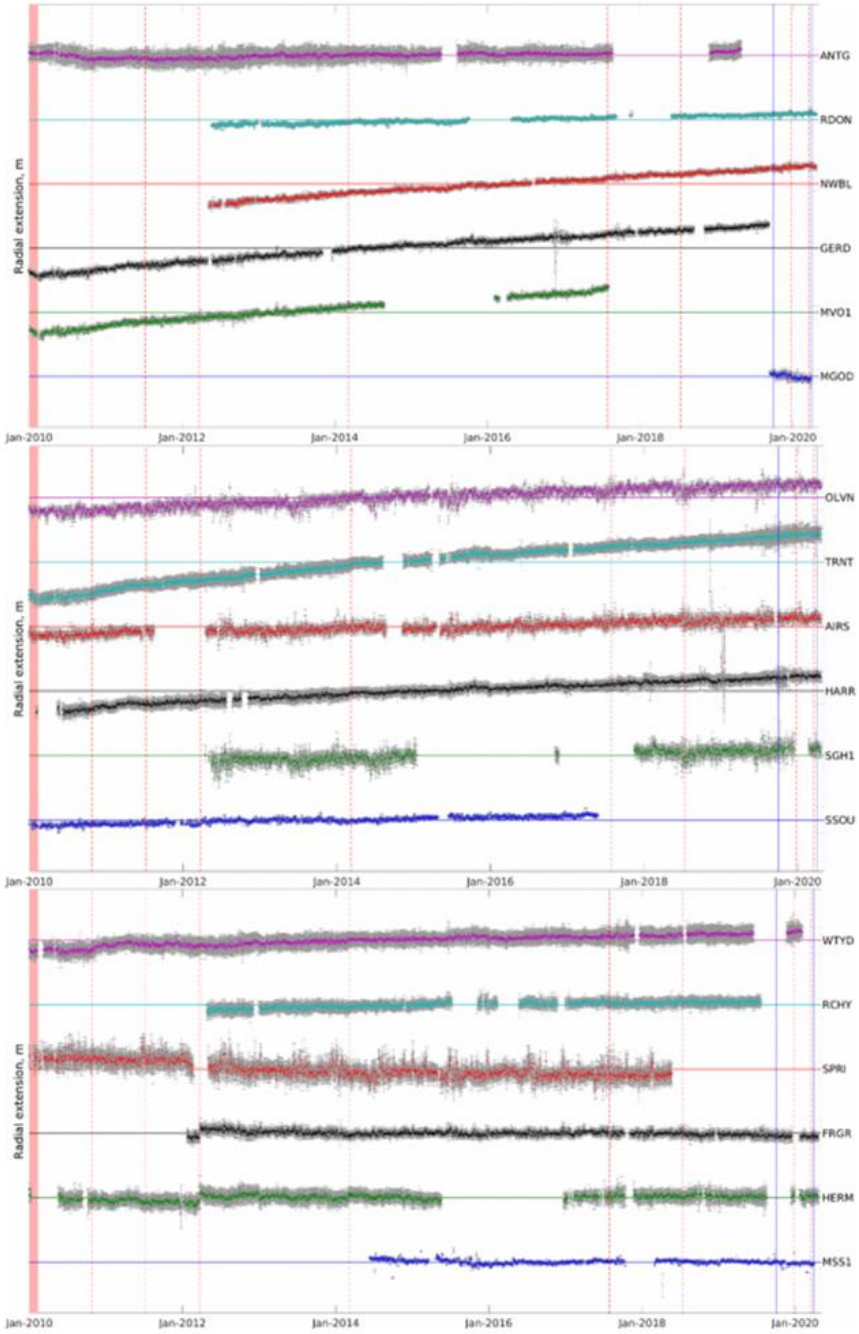

Figure E1. SHV GPS radial deformation 2010-2020. Radial extension relative to the volcanic vent for Pause 5 (February 2010-March 2020). The reporting period is bounded by the two blue lines. The distance station-volcanic vent increases from bottom to top of figure. The background Caribbean plate velocity was removed from the data. Displacements due to antenna changes have been corrected. The strongest VT events have been highlighted (red dashed lines). The distance separating each gridline is equal to 1 cm of deformation. [Stinton et al, 2020].